Utrecht University

Graduate school of natural sciences

Institute for theoretical physics

Modelling the Tidal Disruption Frequency for Neutron Star-Black Hole Binary Systems

Ima Meijer

July 2022

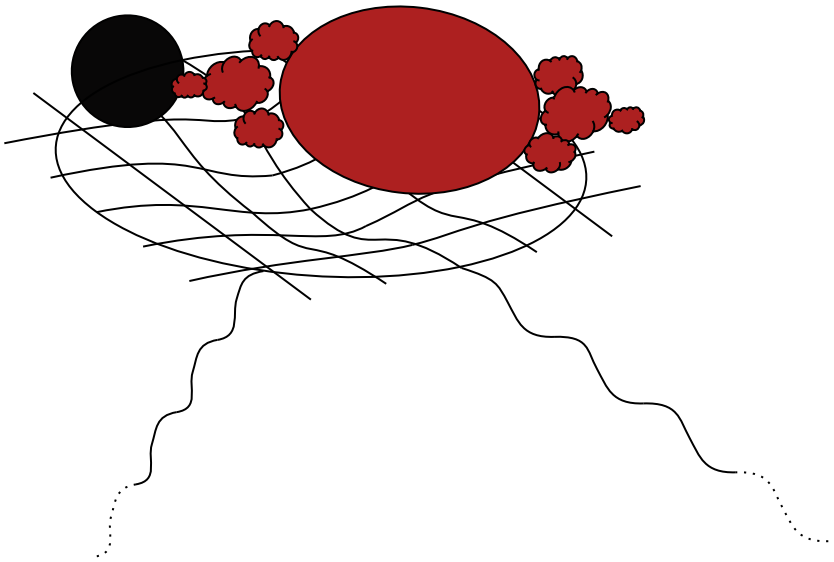

Master's thesis

under the supervision of

Dr. Tanja Hinderer

Utrecht University

Acknowledgements

Over the last year, I have been guided by Dr. Tanja Hinderer in the long process of writing my master's thesis. From the beginning, she gave me space to figure out things independently, which gave me a feeling of trust. Towards the end, when the research became more interesting, she was always there to discuss the interesting topics which became part of my master's thesis, sometimes several times a week. I am extremely thankful for this style of guidance that suited me very well, and I can truly say that I could not have wished for a better supervisor.

Gratitude should also go to the gravitational wave group meetings and the cosmology journal clubs, which forced me to investigate topics I would have otherwise never investigated, of which parts eventually did reach a discussion of some form in my thesis.

I am also grateful to my colleagues on the seventh floor of the BBG, who were always there for informal coffee meetings and interesting discussions. In particular, I am thankful to Maarten Rottier, who has motivated me most to work hard and stay disciplined over the course of my studies.

Finally, I would like to thank Sacha de Wind for doing a project with me in our first year of the bachelor's degree, which led to a manuscript where section 2.2 is now based on. Since then, Sacha has always remained a great friend who morally supported me during my time as a student.

Abstract

Gravitational waves (GWs) from neutron star-black hole binary systems (NSBHs) are a promising probe of the neutron star equation of state. One needs to model these waveforms accurately to gain information from NSBH waveform signals. A unique feature of NSBHs is that the merger can happen in a disruptive manner, i.e. the neutron star can get tidally disrupted before it merges with the black hole for a certain parameter subspace of the system. This unique feature has a distinct imprint on the GWs an NSBH produces. Understanding the tidal disruption of the neutron star by a companion black hole plays a vital role in accurately modelling waveforms. We construct an effective action considering dynamical tidal effects and aligned spin interactions in our work. We can use the action to set up an energy balance from which we can compute the orbital frequency at which the neutron star tidally disrupts. The parameter region of validity is given by $\Lambda_2 \in [1, 5000]$, $Q \in [1, 10]$, $\chi_{\rm NS}$ and $\chi_{\rm BH} \in [-0.5, 0.5]$. It is shown that this novel model agrees with numerical relativity (NR) results and significantly outperforms the merger frequencies obtained from the current waveform model PhenomNSBH. Furthermore, recommendations are made for further NR simulations to verify the model such that it can be used to generate accurate gravitational waveforms.

Contents

Introduction

Gravitational waves (GWs) were predicted by Einstein over a hundred years ago as a consequence of the theory of general relativity (GR). On September 14th, 2015, GWs were finally observed by GW-detectors on earth, and the theory of Einstein was once again validated. The LIGO and VIRGO collaboration announced the detection several months later, on February 11th, 2016, after the data was processed [1]. The signal originated from a binary black hole (BBH) system. Later on, the GWs of binary neutron star (BNS) [2] and binary neutron star-black hole (NSBH) [3] systems have also been detected. The first detection gave a boost to the subfield of physics called GW astronomy.

With the first detection of GWs, the need for accurate waveform models arose. To extract information from observed GWs, accurate waveform templates need to be modelled. Nowadays, numerical simulations exist that can produce accurate waveforms for a given set of system parameters [4, 5, 6]. It is not possible yet however, to cover the entire parameter space with numerical relativity (NR) waveforms, where NR simulations generate waveforms with code that simulates matter subject to Einstein's equations. This is because one NR simulation for a given set of system parameters can take up to months of simulation time on supercomputer clusters. Therefore, the need for more simple, easy-to-generate waveform models remains. This work aims to contribute to the family of easy-to-generate NSBH waveform models. Such a waveform model can be used to extract information about the equation of state (EOS) of the neutron star. The strong gravitational compression inside a neutron star pushes its matter densities well above normal nuclear matter densities. It is yet unknown what the composition of this extremely dense matter is, and its properties are also unknown, i.e. we do not yet know what the EOS of a neutron star should be. GWs could therefore be of essential use in discovering this EOS, and an accurate NSBH waveform model could thus contribute to new physics being discovered.

In chapter 1 we revisit the calculations of Einstein leading to the proposition of GWs to give the reader a full historical perspective. Furthermore, we use this theory together with Newtonian theory to qualitatively discuss the first detection of GWs. We are able to find rough estimates for the chirp mass - for now, think of it as a composite parameter containing both the component masses - and are also able to conclude that the signal must have been from a BBH. Furthermore, we will discuss the first detection of GWs from an NSBH and conclude that a qualitative analysis becomes more difficult in this regard. We will therefore continue with a more in-depth analysis.

The unique feature of an NSBH system is that the companion black hole can tidally disrupt the neutron star before it merges into the black hole. i.e. the tidal effects due to the external tidal field of the black hole can become so strong that they can disrupt the neutron star. In a BNS system the gravity is not strong enough to completely disrupt either of the neutron stars. Furthermore, all the matter effects in an NSBH system can be attributed to the neutron star alone, whereas a BNS has complex matter interactions of the different stars that have complex imprints on the GWs. The disruption of the neutron star is a dynamic process which will be discussed in chapter 2. Parts of chapter 2 carry over to the more general

description of a binary system of any two compact objects. We will construct an effective action which takes these dynamical tidal effects into account, where by dynamical we mean that we allow for fast evolution of the orbital scale of the system compared to the internal scale of the system. We will also take spin interactions into account. We can assign four different angular momenta to the NSBH system, the neutron star and black hole angular momenta, the orbital angular momentum and a tidal bulge angular momentum. The latter represents the spin of the tidal bulge, i.e. the deformed mass bulge due to tidal effects, of the neutron star. These four different spins can interact in different ways, which will all be discussed. The final effective action can be used to calculate a tidal energy.

We will consider the point where the tidal energy exceeds the self-gravitational energy as the point of tidal disruption. Equating the tidal energy with the self-gravitational energy gives us an energy balance which in turn can be used to calculate a tidal disruption frequency. This will be outlined in chapter 3. The final merger frequency of the NSBH is modelled by the tidal disruption frequency in the disruptive regime, i.e. the regime where the neutron star is tidally disrupted before it merges with the black hole. The final merger frequency of the NSBH is modelled by the merger frequency as if the two bodies were black holes in the non-disruptive regime, i.e. the regime where the neutron star plunges into the black hole before being disrupted. Subsequently, we will compare our model to NR simulations. The NR simulations parameter space region is given by [4, 5, 6]: $\Lambda_2 \in [288, 2324]$, $Q \in [2, 7]$, $\chi_{\rm NS} \in [-0.2, 0.0]$ and $\chi_{\rm BH} \in [0, 0.9]$. Where Λ_2 is the dimensionless tidal deformability parameter, Q the mass ratio between the black hole and the neutron star and $\chi_{\rm NS}$ and $\chi_{\rm BH}$ are the dimensionless spin parameters of the neutron star and the black hole. We find an average absolute relative error of 4.8%. To put this into perspective, comparing the PhenomNSBH model [7] to the NR data gives a 46% average absolute relative error. We are therefore confident to pose a region of validity of our model that goes beyond the verification against the NR simulations of $\Lambda_2 \in [1, 5000]$, $Q \in [1, 10]$, $\chi_{\rm NS}$ and $\chi_{\rm BH} \in [-0.5, 0.5]$. We included spin interactions up to linear order in the black hole spin in our model. For higher black hole spins we see that our model starts to slightly diverge from the NR data, which can be directly attributed to this truncation. For the neutron star, we do not have any NR data to check its behaviour for higher spins. Therefore, we do not include dimensionless spin above 0.5 for both the neutron star and the black hole spin. Naturally, the parameter space region of validity can be improved by taking higher order spin interactions into account. We also recommend, from a model verification point of view, for NR simulations to be done in the non-zero neutron star spin regime to check whether higher order neutron star spin interactions should be included.

An independent merger frequency model for an NSBH is a key ingredient in subsequently constructing a waveform model. Our model does not require the introduction of free fit parameters, while the existing waveform models in the literature do [7, 8]. This makes these models less robust to changes of parameters. These models also do not consider the merger frequency of an NSBH system as a benchmark to model the peak amplitude of the gravitational waveform. In contrast, our model is based on physical considerations and first-principles calculations, which can pinpoint the clear peak amplitude of the gravitational waveform by making use of the merger frequency. No fitting to the NR data is needed to find already an excellent dependence on the different parameters in a vast parameter regime. In chapter 4 we discuss these findings and conclude that we see promising signs to use our merger frequency model for future NSBH waveform models.

We will use the convention that latin indices denote spatial indices which run over 1,2,3 while greek indices denote spacetime indices which run over 0,1,2,3 or t, x, y, z. We will use the Einstein summation convention, i.e. repeated indices will be summed over. We will use the $(-,+,+,+)$ metric signature. Derivatives will be denoted by $\partial_\mu = \frac{\partial}{\partial x^\mu}$. The d'Alembertian or box operator is given by $\partial_\mu \partial^\mu = \Box$. For convenience we will also work in geometric units where $G = c = 1$. Where needed we can easily recover SI-units by dimensional analysis.

A reader with only a general physics background can read the introduction at the beginning of every chapter until the first section starts together with the sections with a * denoted next to the title. The other chapters go into more technical details that can be skipped to still get a taste of the bigger picture.

Chapter 0

Preliminaries

Before introducing GWs we will introduce several quantities and concepts from GR which will be used later in this thesis. We will however assume that the reader is familiar with basic concepts of GR. For an introduction to GR the reader is referred to [9]. To summarise: space and time are connected through the metric tensor $g_{\mu\nu}$ which denotes the curvature of four-dimensional spacetime (one time and three spatial dimensions). The metric determines an invariant spacetime interval according to:

$$ds^2 = g_{\mu\nu} dx^\mu dx^\nu, \tag{0.1}$$

where dx^μ represents the difference between the coordinates x^μ that label points in spacetime. The vectors dx^μ and x^μ are four-dimensional vectors with one time and three spatial dimensions and are called four-vectors, $g_{\mu\nu}$ is a symmetric spacetime tensor and therefore naturally has ten independent components. Locally, i.e. in special relativity, spacetime is flat and is given by the Minkowski metric:

$$\eta_{\mu\nu} = \text{diag}(-1, +1, +1, +1). \tag{0.2}$$

In GR however, spacetime is curved, the geometry becomes dynamical and is described by the field $g_{\mu\nu}$. This means that every point in space and time has a metric value associated with it. The dynamics of spacetime are described by the Einstein equation, which without a cosmological constant is given by:

$$G_{\mu\nu} = R_{\mu\nu} - \frac{1}{2} R g_{\mu\nu} = 8\pi T_{\mu\nu}. \tag{0.3}$$

Here $G_{\mu\nu}$ is the Einstein tensor which is defined in terms of $R_{\mu\nu}$, R and $g_{\mu\nu}$, quantities that all depend on the metric only and are different measures of the curvature of spacetime. The Ricci tensor $R_{\mu\nu}$ can be computed from the Riemann tensor as $R_{\sigma\nu} = R^\rho_{\sigma\rho\nu}$, where the Riemann curvature tensor is given by:

$$R^\rho_{\sigma\mu\nu} = \partial_\mu \Gamma^\rho_{\nu\sigma} - \partial_\nu \Gamma^\rho_{\mu\sigma} + \Gamma^\rho_{\mu\lambda} \Gamma^\lambda_{\nu\sigma} - \Gamma^\rho_{\nu\lambda} \Gamma^\lambda_{\mu\sigma}, \tag{0.4}$$

where $\Gamma^\rho_{\nu\sigma}$ denotes the Levi-Civita connection which is given in terms of the metric as:

$$\Gamma^\sigma_{\mu\nu} = \frac{1}{2} g^{\sigma\rho} \left(\partial_\mu g_{\nu\rho} + \partial_\nu g_{\rho\mu} - \partial_\rho g_{\mu\nu} \right). \tag{0.5}$$

The Ricci scalar R is the trace of the of the Riemann tensor and is a scalar describing the curvature of the geometry. Finally, $T_{\mu\nu}$ is the energy-momentum tensor describing the energy and momentum which acts as a source for the gravitational field or curvature through the Einstein equation. The above equations are the building blocks of GR and are posted here merely as a summary to which we can refer in later texts, not as a full theoretical introduction to GR. With these equations at our disposal we are ready to explore the world of GWs.

Chapter 1

Gravitational Waves

We will begin this thesis with an introduction to GWs similar to the way Einstein derived them over a hundred years ago in sections 1.1, 1.2 and 1.3. In section 1.4 a concrete example of a system that can produce GWs is discussed. In section 1.5 an effective energy-momentum tensor for GWs propagating through vacuum is derived. Section 1.6 then uses this result to discuss the energy that can radiate by GWs. A review of the creation of the GW theory by Einstein and his initial problems can be found in [10]. The original article by Einstein is given by [11]. A problem with the formulation of GWs from Einstein was that it heavily depended on the choice of gauge, i.e. which coordinate system one uses. A gauge independent formulation of the theory of GWs was only derived much later in 1980 by James M. Bardeen in [12]. In the following section we will linearise the Einstein equation, which is the approach Einstein followed, but we will do it in the gauge independent way proposed by Bardeen. In [13] a similar approach can be found. In section 1.7 we will show the signal of the first GW observation. We will use the theoretical description set up in the first sections to constrain the parameters of what must have been the source of the first GW observation.

1.1 Linearised Gravity

Although this section will be similar to Einstein's derivation of GWs, it will mostly be based on [9]. We will also follow Appendix B from [14] for the gauge independent formulation of the linearised Einstein equation. GWs are ripples that travel trough spacetime at the speed of light, and they can be generated by sources. Once the waves propagate far away enough from the source, their wavelengths are generally much larger than the radius of curvature of the background spacetime through which they propagate. We will therefore assume that we can write the metric that describes the structure of spacetime as small perturbations around Minkowski spacetime:

$$g_{\mu\nu}(x) = \eta_{\mu\nu} + h_{\mu\nu}(x), \quad |h_{\mu\nu}| \ll 1. \tag{1.1}$$

It will be our goal to solve Einstein's equation using this metric. For this, it will be convenient to decompose the components of the metric perturbation according to their transformation properties under spatial rotations. This is analogous to decomposing the electromagnetic field strength tensor into electric and magnetic fields, which is also where Einstein was inspired by [10]. The full decomposition of the metric perturbation can be found in Appendix A. The important results will be discussed here. To solve the Einstein equation in terms of the metric (1.1) we need to evaluate the Riemann tensor (0.4). The Riemann tensor for the metric (1.1) up to first order in the metric perturbation $h_{\mu\nu}$ is given by:

$$R_{\rho\sigma\mu\nu} = \tfrac{1}{2}(\partial_\mu\partial_\sigma h_{\rho\nu} + \partial_\nu\partial_\rho h_{\mu\sigma} - \partial_\mu\partial_\rho h_{\nu\sigma} - \partial_\nu\partial_\sigma h_{\rho\mu}). \tag{1.2}$$

The Ricci tensor and scalar can be straightforwardly computed from the above expression. The Einstein equation can be expressed in terms of the decomposed quantities outlined in

Appendix A. The only component of the Einstein equation that represents radiating degrees of freedom is:

$$\Box h_{ij}^{\mathrm{TT}} = 0, \tag{1.3}$$

which is the wave equation for GWs. The GW amplitude h_{ij}^{TT} is a gauge invariant quantity which is the transverse traceless part of the metric perturbation. Note that this applies only to linear perturbations. In anything beyond linear theory, h_{ij}^{TT} is not gauge invariant anymore. We can also remark that we started out with a theory with ten degrees of freedom contained in the metric perturbation $h_{\mu\nu}$. Four degrees of freedom are eliminated by fixing the gauge to construct a total of six gauge independent degrees of freedom. The only freely propagating degrees of freedom are from h_{ij}^{TT} and thus h_{ij}^{TT} represents the two physical degrees of freedom of gravity in the absence of matter.

1.2 Gravitational Waves Acting on Matter

We will assume a plane wave propagating in an arbitrary direction as solution to the wave equation (1.3). The plane wave is given by:

$$h_{ij}^{\mathrm{TT}} = A_\sigma \epsilon_{ij}^\sigma \cos(-k_\mu x^\mu) \tag{1.4}$$

where A_σ is a constant, ϵ_{ij}^σ is the polarisation tensor, which specifies the polarisation of the wave and $k^\mu = (\omega, k_1, k_2, k_3)$ is the four-wavevector. Plugging the ansatz back into the wave equation give us the dispersion relation $\omega^2 = k_i k^i$. Considering a wave that travels in the z-direction gives $k^\mu = (\omega, 0, 0, k_3) = (\omega, 0, 0, \omega)$. The polarisation tensor can be specified by considering the transverse condition $\partial^i h_{ij}^{\mathrm{TT}} = 0$ which gives:

$$\partial^i h_{ij}^{\mathrm{TT}} = k^i A_\sigma \epsilon_{ij}^\sigma \sin(-k_\mu x^\mu) = 0, \tag{1.5}$$

such that we must have:

$$k^i A_\sigma \epsilon_{ij}^\sigma = \omega A_\sigma \epsilon_{3j}^\sigma = 0. \tag{1.6}$$

This means that all the ϵ_{3j}^σ components of the polarisation tensor are zero and since it was already only a spatial tensor, the only remaining components of ϵ_{ij}^σ can be:

$$\epsilon_{ij}^\sigma = \begin{pmatrix} \epsilon_{11} & \epsilon_{12} & 0 \\ \epsilon_{12} & -\epsilon_{11} & 0 \\ 0 & 0 & 0 \end{pmatrix}, \tag{1.7}$$

where we can see that the GW is described by two degrees of freedom. We can split the polarisation tensor into two independent polarisations, plus polarised and cross polarised:

$$\epsilon_{ij}^+ = \begin{pmatrix} 1 & 0 & 0 \\ 0 & -1 & 0 \\ 0 & 0 & 0 \end{pmatrix}, \quad \epsilon_{ij}^\times = \begin{pmatrix} 0 & 1 & 0 \\ 1 & 0 & 0 \\ 0 & 0 & 0 \end{pmatrix}, \tag{1.8}$$

where we normalised the individual components. The solution (1.5) with the above given polarisation tensors represents GWs in the absence of matter. GWs are ripples travelling through spacetime and therefore distort spacetime as they pass by. It is insightful to investigate the effect of the GW on a group of test particles. This can be done by considering the geodesic deviation equation, which reads for a separation vector S^μ between two nearby particle trajectories:

$$\frac{D^2}{d\tau^2} S^\mu = R^\mu_{\nu\rho\sigma} \frac{dx^\nu}{d\tau} \frac{dx^\rho}{d\tau} S^\sigma. \tag{1.9}$$

Where $\frac{D}{d\tau}$ is the directional covariant derivative that is given by $\frac{dx^\mu}{d\tau}\nabla_\mu$ and τ is the proper time. If we assume the particles to be slowly moving and expand the r.h.s. up to first order in h_{ij}^{TT} we can write $\frac{dx^\nu}{d\tau} = (1, 0, 0, 0)$ since the Riemann tensor is already first order in h_{ij}^{TT}

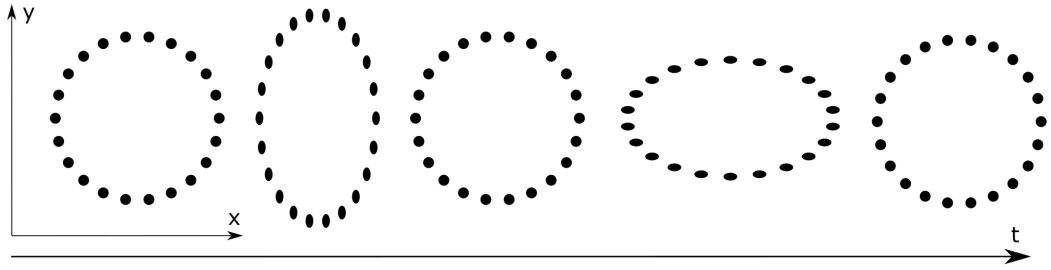

Figure 1.1: The effect of a + polarised GW moving in the plane perpendicular to the page on a ring of free particles floating in space. The dots represent point particles.

and spatial corrections to the particle's trajectory will also be of first order in h_{ij}^{TT}. Using the Riemann tensor in terms of the metric perturbation (1.2) gives us:

$$R^{\mu}_{00\sigma} = \tfrac{1}{2}(\partial_0\partial_0 h^{\mathrm{TT}}_{\mu\sigma} + \partial_\sigma\partial_\mu h^{\mathrm{TT}}_{00} - \tfrac{1}{2}\partial_\sigma\partial_0 h^{\mathrm{TT}}_{\mu 0} - \tfrac{1}{2}\partial_\mu\partial_0 h^{\mathrm{TT}}_{\sigma 0}), \tag{1.10}$$

but since $\epsilon^{\sigma}_{0j} = 0$ and thus $h^{\mathrm{TT}}_{\mu 0} = 0$ this reduces to:

$$R^{\mu}_{00\sigma} = \tfrac{1}{2}\partial_0\partial_0(h^{\mathrm{TT}})^{\mu}_{\sigma}. \tag{1.11}$$

For slowly moving particles to lowest order we have $\tau = t$ such that the geodesic deviation equation becomes:

$$\frac{\partial^2}{\partial t^2}S^{\mu} = \tfrac{1}{2}\partial_0\partial_0(h^{\mathrm{TT}})^{\mu}_{\sigma}S^{\sigma}. \tag{1.12}$$

Since only $(h^{\mathrm{TT}})^{\mu}_1$ and $(h^{\mathrm{TT}})^{\mu}_2$ are non-zero components, only S^1 and S^2 will be affected. This is analogous to electromagnetism where the electric and magnetic fields in a plane wave are perpendicular to the wave vector. Considering only the plus polarised wave tensor yields as only non-zero components:

$$\begin{aligned}\frac{\partial^2}{\partial t^2}S^1 &= -\tfrac{1}{2}\omega^2 A_+\cos(-k_\mu x^\mu)S^1\\ \frac{\partial^2}{\partial t^2}S^2 &= \tfrac{1}{2}\omega^2 A_+\cos(-k_\mu x^\mu)S^2.\end{aligned} \tag{1.13}$$

We can solve the above differential equations up to first order in the amplitude A_+ by saying that S^1 and S^2 must be of zeroth order in A_+, i.e. $S^1 = S^1_{(0)}$ and $S^2 = S^2_{(0)}$. This allows us to integrate to yield the solutions:

$$\begin{aligned}S^1_{(1)} &= \tfrac{1}{2}A_+\cos(-k_\mu x^\mu)S^1_{(0)}\\ S^2_{(1)} &= -\tfrac{1}{2}A_+\cos(-k_\mu x^\mu)S^2_{(0)}.\end{aligned} \tag{1.14}$$

Particles initially separated in the x-direction, will oscillate in the x-direction, while particles initially separated in the y-direction will oscillate in the y-direction. If the x-direction separated particles start oscillating inwards, then the y-direction separated particles will start oscillating outwards. If we were to consider a ring of test particles in the xy-plane, these particles oscillate in the shape of a '+' as the GW passes, see Figure 1.1. Analogously, we have as a solution for the cross polarised wave tensor:

$$\begin{aligned}S^1_{(1)} &= \tfrac{1}{2}A_\times\cos(-k_\mu x^\mu)S^1_{(0)}\\ S^2_{(1)} &= \tfrac{1}{2}A_\times\cos(-k_\mu x^\mu)S^2_{(0)}.\end{aligned} \tag{1.15}$$

Where we can see that a ring of test particles will now be distorted in the shape of an '×', see Figure 1.2.

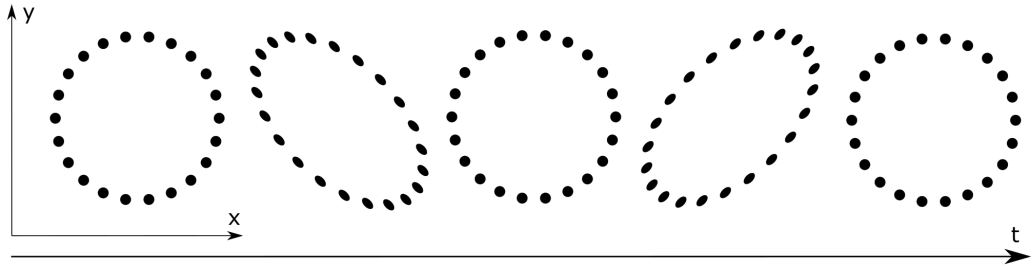

Figure 1.2: The effect of a × polarised GW moving in the plane perpendicular to the page on a ring of free particles floating in space. The dots represent point particles.

1.3 Gravitational Waves from a Source

In the previous discussion we considered GWs far away from sources and therefore assumed $T_{\mu\nu} = 0$, resulting in plane-wave solutions to the linearised vacuum Einstein equation. We will now consider sources that can generate GWs. In the presence of a source we cannot assume anymore that our solution is that of the transverse traceless tensor. The metric perturbation has now been supplemented with non-zero scalar and vector components on top of the strain tensor representing GWs. We will decompose the energy-momentum tensor in a similar manner to that of the decomposition of the metric perturbation. The details of the decomposition can be found in Appendix B. The approach there is similar to [13], but the results are derived independently and worked out with the same decomposition variables used with the metric perturbation. Here we find out that the only component of the Einstein equation representing radiating degrees of freedom is:

$$\Box h_{ij}^{\mathrm{TT}} = -16\pi\sigma_{ij}^{\mathrm{TT}}, \tag{1.16}$$

where $\sigma_{ij}^{\mathrm{TT}}$ represents the transverse traceless part of the energy-momentum tensor. We can conclude that, even with a source, the only freely propagating degrees of freedom are given by the transverse traceless piece of the metric perturbation h_{ij}^{TT}, at sufficiently large distances from the source.

Expressing the Einstein field equations in terms of gauge invariant observables has allowed us to conclude that the only radiating degrees of freedom of the metric perturbation are its transverse traceless degrees of freedom. This holds for vacuum spacetimes as well as spacetimes with a source, evaluated far from the source. Although it is possible to choose a gauge in which other metric perturbation components appear to be radiative, we now know that they will not be. They only appear to be radiative due to the choice of coordinates. Einstein struggled very much himself with the gauge-dependent nature of GWs. It took him several times of getting it wrong before he managed to figure out what the real physical modes were and what the pure gauge modes were [11].

We can therefore say that the above analysis, done in a gauge independent way, is of great value to us. We can freely pick a gauge without having to fear that we will wrongly identify gauge modes for physical radiation. In Box 1 the linearised Einstein equation with a source is solved in the Lorenz gauge, which is a popular gauge in the literature. We will continue, however, with the transverse traceless equation of (1.16). The analysis in Box 1 will be completely analogous to this.

Equation (1.16) is a wave equation with a source, where $\sigma_{ij}^{\mathrm{TT}}$ is the transverse traceless spatial part of the Energy-Momentum tensor. A wave equation with a source is a well-studied problem and can be solved using the Green's function method. The Green's function for the wave

operator $\Box$ is the solution to the wave equation with the delta-function as a source:

$$\Box G\left(t,\mathbf{x};t',\mathbf{x}'\right)=\delta\left(t-t'\right)\delta\left(\mathbf{x}-\mathbf{x}'\right). \tag{1.17}$$

The field that arises from our actual source is given by integrating the Green's function over the source $\sigma_{ij}^{\mathrm{TT}}$:

$$h_{ij}^{\mathrm{TT}}(t,\mathbf{x})=-16\pi\int dt'd^3x'G\left(t,\mathbf{x};t',\mathbf{x}'\right)\sigma_{ij}^{\mathrm{TT}}(t',\mathbf{x}'). \tag{1.18}$$

The Green's function associated with the wave operator is well known, see for example [15]. It has two solutions, namely a 'retarded' and 'advanced' solution, depending on whether it represents waves travelling forward or backwards in time. We are interested in the retarded Green's function since it represents all the effects of signals to the past of the points under consideration. The retarded solution is given by:

$$G\left(t,\mathbf{x};t',\mathbf{x}'\right)=-\frac{\delta\left(t'-\left[t-\left|\mathbf{x}-\mathbf{x}'\right|\right]\right)}{4\pi\left|\mathbf{x}-\mathbf{x}'\right|}\theta(t-t'), \tag{1.19}$$

where $\theta(t-t')$ denotes the theta function which equals 1 for $t>t'$ and is 0 otherwise. The quantity $t-|\mathbf{x}-\mathbf{x}'|\equiv t_r$ is referred to as retarded time and takes into account that information cannot be transmitted instantly from events taking place at position $\mathbf{x}$ to $\mathbf{x}'$. The above solution for $G\left(t,\mathbf{x};t',\mathbf{x}'\right)$ can be plugged into the integral of $h_{ij}(t,\mathbf{x})$, where the t' integral can be done to yield.

$$h_{ij}^{\mathrm{TT}}(t,\mathbf{x})=4\int d^3x'\frac{\sigma_{ij}^{\mathrm{TT}}\left(t_r,\mathbf{x}'\right)}{\left|\mathbf{x}-\mathbf{x}'\right|}. \tag{1.20}$$

We will make the assumption that the source is isolated and far away such that $|\mathbf{x}-\mathbf{x}'|=r$. We then have:

$$h_{ij}^{\mathrm{TT}}(t,\mathbf{x})=\frac{4}{r}\int d^3x'\sigma_{ij}^{\mathrm{TT}}\left(t_r,\mathbf{x}'\right). \tag{1.21}$$

We can rewrite this by making use of the Leibniz rule:

$$\partial_k\left[\sigma_{ki}^{\mathrm{TT}}x^j\right]=\left[\partial_k\sigma_{ki}^{\mathrm{TT}}\right]x^j+\sigma_{ji}^{\mathrm{TT}}, \tag{1.22}$$

and energy-momentum conservation $\partial^\mu T_{\mu\nu}=0$, which implies $\partial_0 T_{0i}=\partial_k T_{ki}$, to yield:

$$\begin{aligned}h_{ij}^{\mathrm{TT}}(t,\mathbf{x})&=\frac{4}{r}\int d^3x'\left(\partial_k\left[\sigma_{ki}^{\mathrm{TT}}x'^j\right]-\left[\partial_k\sigma_{ki}^{\mathrm{TT}}\right]x'^j\right)\\&=\frac{4}{r}\int d^3x'\left(\partial_k\left[\sigma_{ki}^{\mathrm{TT}}x'^j\right]-\left[\partial_0\sigma_{0i}^{\mathrm{TT}}\right]x'^j\right).\end{aligned} \tag{1.23}$$

Using the divergence theorem the first term can be written as a surface integral. Since the source is isolated and far away, the surface can be chosen outside of the source, and the first term vanishes:

$$h_{ij}^{\mathrm{TT}}(t,\mathbf{x})=-\frac{4}{r}\partial_0\int d^3x'x'^j\sigma_{0i}^{\mathrm{TT}}\left(t_r,\mathbf{x}'\right). \tag{1.24}$$

We took the time derivative outside the integral since only T_{0i} depends on time. We can make use of the Leibniz rule again to rewrite $T_{0i}x'^j$:

$$\begin{aligned}\partial_k\left[\sigma_{k0}^{\mathrm{TT}}x^jx^i\right]&=\left[\partial_k\sigma_{k0}^{\mathrm{TT}}\right]x^jx^i+\sigma_{j0}^{\mathrm{TT}}x^i+\sigma_{i0}^{\mathrm{TT}}x^j\\&=\partial_0\left[\sigma_{00}^{\mathrm{TT}}x^jx^i\right]+\sigma_{j0}^{\mathrm{TT}}x^i+\sigma_{i0}^{\mathrm{TT}}x^j,\end{aligned} \tag{1.25}$$

where in going to the second line we made use of energy-momentum conservation. Integrating both sides yields:

$$0=\int d^3x'\partial_0\left[\sigma_{00}^{\mathrm{TT}}x'^jx'^i\right]+2\int d^3x'\sigma_{i0}^{\mathrm{TT}}x'^j, \tag{1.26}$$

where the l.h.s. again vanishes because the source is isolated. We combined the last two terms because we assumed $T_{i0}x^j$ to be symmetric since T_{ij} is also symmetric and thus so is h_{ij}. Using the above identity we have:

$$h_{ij}^{\mathrm{TT}}(t,\mathbf{x}) = \frac{2}{r}\partial_0^2 \int d^3x' x'^i x'^j \sigma_{00}^{\mathrm{TT}}\left(t_r,\mathbf{x}'\right), \tag{1.27}$$

which is called the Einstein quadrupole formula. It is usually written as:

$$h_{ij}^{\mathrm{TT}}(t,\mathbf{x}) = \frac{2}{r}\frac{d^2 I_{kl}\left(t_r\right)}{dt^2}\left(P_{ik}P_{jl} - \tfrac{1}{2}P_{ij}P_{kl}\right), \tag{1.28}$$

where I_{kl} is defined as the quadrupole moment tensor:

$$I_{kl}(t) = \int d^3x' \left(x'^k x'^l - \tfrac{1}{3}\left|\boldsymbol{x'}\right|^2 \delta_{kl}\right) T_{00}\left(t,\mathbf{x}'\right), \tag{1.29}$$

and P_{ij} is defined as a transverse traceless projection operator:

$$P_{ij} = \delta_{ij} - n_i n_j, \tag{1.30}$$

where n^i is a unit vector along the direction of propagation. The metric perturbation h_{ij}^{TT} is now manifestly traceless and transverse, since P_{ij} eliminates the parts that are parallel to the direction of propagation of the GW. This also allows us to write T_{00} instead of $\sigma_{00}^{\mathrm{TT}}$. Remember that we derived the quadrupole formula for an isolated source, that is far away and slowly moving. Also, the above formula assumes the linearised Einstein equation. For systems which are dominated by self-gravity the Einstein quadrupole formula loses its validity. In weakly gravitating systems, however, the gravitational-binding energy will be negligible to the rest-mass energy and it can be shown that the quadrupole formula (1.28) can still be used as an approximation to describe self-gravitating systems such as a binary star system [13].

Box 1: Linearised Einstein Equation in the Lorenz Gauge

Let us introduce the trace-reversed metric perturbation:

$$\bar{h}_{\mu\nu} = h_{\mu\nu} - \tfrac{1}{2}h\eta_{\mu\nu}, \tag{1.31}$$

where the trace of the trace-reversed metric perturbation is given by $\bar{h} = \eta^{\mu\nu}\bar{h}_{\mu\nu} = -h$. Under the gauge transformation (A.9), the trace-reversed metric perturbation transforms as:

$$\bar{h}_{\mu\nu} \to \bar{h}_{\mu\nu} = \bar{h}_{\mu\nu} - 2\partial_{(\mu}\xi_{\nu)} + \eta_{\mu\nu}\partial^\lambda \xi_\lambda. \tag{1.32}$$

By choosing the gauge parameter ξ to satisfy:

$$\Box\xi_\mu = \partial^\lambda \bar{h}_{\lambda\mu}, \tag{1.33}$$

we can set:

$$\partial^\mu \bar{h}_{\mu\nu} = 0, \tag{1.34}$$

which is known as the Lorenz gauge. It is always possible to find ξ such that the Lorenz gauge condition can be met. The Einstein tensor for the metric perturbation can be found from the expressions of the Ricci tensor and scalar that we derived above and is given by:

$$\begin{aligned} G_{\mu\nu} &= R_{\mu\nu} - \frac{1}{2}R\eta_{\mu\nu} \\ &= \frac{1}{2}\left(\partial_\sigma\partial_\nu h^\sigma{}_\mu + \partial_\sigma\partial_\mu h^\sigma_\nu - \partial_\mu\partial_\nu h - \Box h_{\mu\nu} - \eta_{\mu\nu}\partial_\mu\partial_\nu h^{\mu\nu} + \eta_{\mu\nu}\Box h\right). \end{aligned} \tag{1.35}$$

In the Lorenz gauge it reduces to the simple form:

$$G_{\mu\nu} = -\tfrac{1}{2}\Box\bar{h}_{\mu\nu}, \tag{1.36}$$

which is just the wave operator operating on the trace-reversed metric perturbation. The linearised Einstein equation is then given by:

$$\Box\bar{h}_{\mu\nu} = -16\pi T_{\mu\nu}, \tag{1.37}$$

which is a wave equation with a source. We know exactly how to solve this now using the Green's function method. From which we will obtain the result:

$$\bar{h}_{\mu\nu}(t,\mathbf{x}) = 4\int d^3x' \frac{T_{\mu\nu}\left(t_r,\mathbf{x}'\right)}{|\mathbf{x}-\mathbf{x}'|}. \tag{1.38}$$

We know by now that the freely propagating degrees of freedom are contained entirely in the transverse traceless spatial part of the metric. We will therefore consider only the spatial part of the metric. After making the assumption that the source is far away and isolated we then have:

$$\bar{h}_{ij}(t,\mathbf{x}) = \frac{4}{r}\int d^3x' T_{ij}\left(t_r,\mathbf{x}'\right). \tag{1.39}$$

This can be massaged a bit by making repeated use of the Leibniz rule - which can also be thought of as integration by parts in reverse - and by making use of energy-momentum conservation (B.2):

$$\bar{h}_{ij} = \frac{2}{r}\partial_0^2\int d^3x' T_{00} x'^i x'^j. \tag{1.40}$$

This seems to be already the desired result except that the quadrupole moment tensor is not yet transverse and traceless. Removing the trace gives us the expression:

$$\bar{h}_{ij} = \frac{2}{r}\partial_0^2\int d^3x' T_{00}\left(x'^i x'^j - \tfrac{1}{3}|\boldsymbol{x}|^2\delta_{ij}\right). \tag{1.41}$$

To project out the non transverse pieces we can use the transverse traceless projection operator P_{ij} such that the transverse traceless metric perturbation is given by:

$$\bar{h}_{ij}^{\mathrm{TT}} = \frac{2}{r}\partial_0^2\int d^3x' T_{00}\left(x'^k x'^l - \tfrac{1}{3}|\boldsymbol{x'}|^2\delta_{kl}\right)\left(P_{ik}P_{jl} - \tfrac{1}{2}P_{ij}P_{kl}\right), \tag{1.42}$$

which exactly agrees with (1.28). Thus, far away from the source, the trace-reversed metric perturbation in the Lorenz gauge is equal to the original metric perturbation.

Let us think for a moment what the Einstein quadrupole formula actually means. We can see that the GW produced by an isolated source that is slowly moving and evaluated far away is proportional to the second time derivative of the quadrupole moment of the energy density. As a reminder, in electromagnetism the electric potential is given by the multipole expansion of the charge density. If a system has a net total charge the first non-zero term in the multipole expansion will be given by the monopople moment, which is then usually a good approximation for the electric potential. The monopole moment is given by the charge density integrated over the volume of the charge distribution and denotes the net charge of the system. If a system has a net zero charge the first non-zero term in the multipole expansion will be given by the dipole moment, which is then usually a good approximation for the electric potential at distances far away from the charge distribution. The dipole moment denotes the polarity of the charge distribution. In electromagnetism, charge distributions usually consist of a superposition of dipole moments - most atoms have non-zero dipole moments, it is however, possible to find charge distributions for which the net polarity is zero. In this case, the quadrupole moment will be the first non-zero term in the multipole expansion, and it will be a measure of the shape of the charge distribution. A complete description of the system is given by all the terms in the

multipole expansion, but truncating at the first non-zero contribution will usually be a good approximation. Electromagnetic radiation corresponds to the change in the multipole moment. The leading term in electromagnetic radiation is therefore usually given by the change of the dipole moment, since charge is a conserved quantity. A changing dipole moment corresponds to motion of the centre of charge density.

Analogous to electromagnetism, for gravity, we have the multipole expansion of the energy density: the monopole moment is given by the density integrated over the volume of mass distribution, i.e. the mass of the system; the dipole moment is a measure of the mass density distribution around the center of mass of the system and the quadrupole moment is a measure of the shape of the system, i.e the moment of inertia. This leads us to the Einstein quadrupole formula derived above: GWs are proportional to the second derivative of the quadrupole moment of the energy density. This begs the question: why is there no contribution from the dipole moment? We know that mass is a conserved quantity in closed systems such that there is no contribution from the monopole moment to gravitational radiation. A changing dipole moment corresponds to motion of the centre of mass of the system, which violates conservation of momentum in a closed system. The changing quadrupole moment is therefore the first non-zero term generating gravitational radiation, and it corresponds to changes in the shape of the system around the centre of mass. This means that a star on its own and even a rotating star will not emit GWs, i.e. systems with spherical and rotational symmetry do not emit GWs. An example of a system that does emit GWs is a binary system of two bodies orbiting each other, which we will consider more closely in the next section.

1.4 Binary Star System

Let us consider two stars of mass M_A and mass M_B in a circular orbit in the xy-plane separated by a distance r_A and r_B respectively from their center of mass. We assume the masses to be point masses, we will define the path of star A to be given by:

$$x_A^1 = x_A = r_A \cos\omega t, \quad x_A^2 = y_A = r_A \sin\omega t \tag{1.43}$$

and the path of star B to be given by:

$$x_B^1 = x_B = -r_B \cos\omega t, \quad x_B^2 = y_B = -r_B \sin\omega t. \tag{1.44}$$

The 00-component of the energy-momentum tensor is defined as the mass density or energy density of the system, and since the bodies are point masses, it is given by:

$$\begin{aligned} T_{00} = {} & M_A \delta\left(x - r_A\cos(\Omega t)\right)\delta\left(y - r_A \sin(\Omega t)\right)\delta(z) \\ & + M_B \delta\left(x + r_B\cos(\Omega t)\right)\delta\left(y + r_B \sin(\Omega t)\right)\delta(z). \end{aligned} \tag{1.45}$$

We will evaluate the field on the z-axis such that the direction of propagation is in the z-direction. The projection operators serve to remove the zx- and zy-components of the tensor. Plugging T_{00} in (1.29) yields the following non-zero quadrupole moment tensor components:

$$\begin{aligned} I_{xx} &= M_A\left[r_A^2\cos^2(\Omega t) - \frac{1}{3}r_A^2\right] + M_B\left[r_B^2\cos^2(\Omega t) - \frac{1}{3}r_B^2\right], \\ I_{yy} &= M_A\left[r_A^2\sin^2(\Omega t) - \frac{1}{3}r_A^2\right] + M_B\left[r_B^2\sin^2(\Omega t) - \frac{1}{3}r_B^2\right], \\ I_{zz} &= M_A\left[-\frac{1}{3}r_A^2\right] + M_B\left[-\frac{1}{3}r_B^2\right], \\ I_{xy} &= I_{yx} = M_A\left[r_A^2\cos(\Omega t)\sin(\Omega t)\right] + M_B\left[r_B^2\cos(\Omega t)\sin(\Omega t)\right]. \end{aligned} \tag{1.46}$$

In a center of mass frame we have:

$$R = r_A + r_B, \quad M_A r_A - M_B r_B = 0, \tag{1.47}$$

from which immediately follows:

$$r_A = \frac{M_B}{M_A + M_B} R, \quad r_B = \frac{M_A}{M_A + M_B} R, \tag{1.48}$$

such that:

$$M_A r_A^2 + M_B r_B^2 = \mu R^2, \tag{1.49}$$

where we defined the reduced mass as: $\mu = M_A M_B/(M_A + M_B)$. The non-zero quadrupole moment tensor components can therefore be written as:

$$\begin{aligned} I_{xx} &= \frac{\mu R^2}{2}\left[\cos(2\Omega t) + \frac{1}{3}\right], & I_{yy} &= \frac{\mu R^2}{2}\left[-\cos(2\Omega t) + \frac{1}{3}\right], \\ I_{zz} &= \mu R^2\left[-\frac{1}{3}\right], & I_{xy} &= \frac{\mu R^2}{2}[\sin(2\Omega t)], \end{aligned} \tag{1.50}$$

where we also made use of trigonometric identities. The non-vanishing second time derivatives become:

$$\ddot{I_{xx}} = -\ddot{I_{yy}} = -2\mu R^2 \Omega^2 \cos(2\Omega t), \quad \ddot{I_{xy}} = -2\mu R^2 \Omega^2 [\sin(2\Omega t)]. \tag{1.51}$$

The metric perturbation components can now be evaluated and are given by the Einstein quadrupole formula (1.28):

$$h_{ij}^{\mathrm{TT}}(t, \mathbf{x}) = \frac{4\mu}{r}\Omega^2 R^2 \begin{pmatrix} -\cos 2\Omega t_r & -\sin 2\Omega t_r & 0 \\ -\sin 2\Omega t_r & \cos 2\Omega t_r & 0 \\ 0 & 0 & 0 \end{pmatrix}. \tag{1.52}$$

This represents the GWs radiated from a binary system measured at a distance r from the source. These waves have an amplitude of $h = 4\Omega^2 R^2 \mu / r$. Let us now insert plausible numerical values to get a feeling of what signals GW detectors are looking for. For a binary neutron star system of equal masses typical parameter values could look like [13]:

$$h \simeq 10^{-22} \left(\frac{M}{2.8 M_\odot}\right)^{5/3} \left(\frac{0.01 \text{ s}}{P}\right)^{2/3} \left(\frac{100 \text{ Mpc}}{r}\right) \tag{1.53}$$

where $M_\odot$ denotes the number of solar masses, P denotes the orbital period $P = 2\pi/\Omega$ and h is the magnitude of the GW described by $h_{ij}^{\mathrm{TT}}(t, \mathbf{x})$; h is also called the GW strain and is a dimensionless quantity. The strain represents the distortion of an object by GWs. Remember that GWs travelling trough vacuum distorted particles in the 'plus' and 'cross' direction perpendicular to the direction of propagation of the GW. The GWs produced by sources are no different. Here the 'plus' polarised amplitude is given by $h_+ = h_{xx} = -h_{yy}$ and the 'cross' polarised amplitude is given by $h_\times = h_{xy} = h_{yx}$. The information that is encompassed in the strain can be viewed as depicted in Figure 1.3. Particles initially displaced by d will oscillate between a displacement of $d - \Delta d$ and $d + \Delta d$ as a GW passes by. We can derive a relation between the displacement and the GW strain. Consider a GW propagating in the z-direction and two test particles at $z = 0$ separated along the x-axis by a distance d in their coordinate frame. The proper distance between the two particles as a result of a GW passing by is then given by:

$$\begin{aligned} d + \Delta d &= \int_0^d dx \sqrt{g_{xx}} = \int_0^d dx \sqrt{1 + h_{xx}^{\mathrm{TT}}(t, z = 0)} \\ &\simeq \int_0^d dx \left[1 + \frac{1}{2} h_{xx}^{\mathrm{TT}}(t, z = 0)\right] = d\left[1 + \frac{1}{2} h_{xx}^{\mathrm{TT}}(t, z = 0)\right], \end{aligned} \tag{1.54}$$

from which we can see that the strain is given by the total change in displacement relative to the displacement of the particles or $h = \frac{2\Delta d}{d}$. For GWs with an amplitude of $h \simeq 10^{-22}$, we can calculate how much the earth would be distorted. With a radius of $r \simeq 6 \cdot 10^6$ the earth would be distorted by approximately 10^{-16} metres, which is many orders of magnitude smaller than the size of atoms. No wonder it took until 2015 for the first direct detection of GWs to occur. The next section will devote some words to the first detection of GWs and why GW theory is essential to be able to detect these waves.

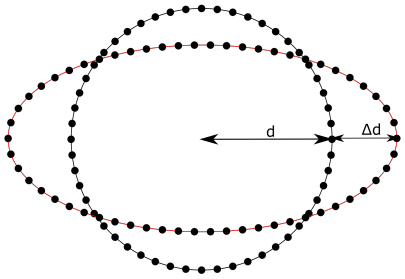

Figure 1.3: Particles displaced by d are displaced by $d + \Delta d$ a quarter period later by a $\times$ polarised GW.

1.5 Effective Energy-Momentum Tensor

We will first investigate the energy flux due to GWs, i.e. the energy loss due to gravitational radiation. The notion of energy in GR, however, is tricky. In Newtonian physics, one must include the gravitational potential energy for energy conservation to hold. In GR, the gravitational potential energy is encompassed in the metric. The notion of energy as a conserved quantity along the trajectory of some point particle does not carry over to GR. The equivalence principle dictates that in a local inertial frame there cannot exist GWs. This also dictates that a local coordinate-invariant definition of the energy is not possible. There is a regime where attempts of considering energy and energy conservation can be done, which is in the weak field limit. Here we think of gravitation as being described by a symmetric tensor propagating on a fixed background metric. The goal is to derive an energy-momentum tensor for the metric perturbation $h_{\mu\nu}$. Although Einstein already was able to produce an expression for the dissipation of energy from GWs, it has been the subject of controversy among physicists over the course of history. In the literature many approaches can be found. An interesting approach is using a Hamiltonian perspective, outlined in [16] which can also be found in Appendix D. The approach followed by [9], which is the standard approach in most textbooks such as originally [17] or more recently in [18], requires the expansion of both the metric and the Ricci tensor up to second order and is the approach followed here.

We have seen that GWs can propagate in vacuum. Our task is to find the energy of these waves. In field theory, the energy can be calculated from the energy-momentum tensor. Although the full energy-momentum tensor can only be found by considering the full theory, it is possible to set up an expression for an effective energy-momentum tensor in linearised gravity. A technical problem arises, however, when considering the linearised Einstein equation. We know that the Einstein equation in vacuum up to linear order in the metric perturbation is given by $G^{(1)}_{\mu\nu}[h^{(1)}] = 0$, where the superscript notation (1) indicates that $G_{\mu\nu}$ is first order in $h^{(1)}$, where $h^{(1)}$ is the first order metric perturbation. We also know that the spatial transverse traceless degrees of freedom are the only radiating degrees of freedom. This means that we can impose the Lorenz gauge such that we have $G^{(1)}_{\mu\nu}[h^{(1)}] = -\frac{1}{2}\Box h^{(1)}_{\mu\nu} = 0$. Unfortunately, it is not possible to identify an effective energy-momentum tensor here. This means that we have to consider one order above linear theory: we have to include second order metric perturbations. The metric can therefore be written as:

$$g_{\mu\nu} = \eta_{\mu\nu} + h^{(1)}_{\mu\nu} + h^{(2)}_{\mu\nu}, \tag{1.55}$$

such that the Einstein equation up to second order in the metric perturbations includes the first order metric perturbation, the second order metric perturbation as well as products of the first order metric perturbation. We already saw that up to first order we have $G^{(1)}_{\mu\nu}[h^{(1)}] = 0$. The Einstein equation in vacuum up to second order in the metric perturbation will look like

$$G^{(2)}_{\mu\nu}[h^{(1)}] + G^{(1)}_{\mu\nu}[h^{(2)}] = 0. \tag{1.56}$$

We know that $G^{(1)}_{\mu\nu}[h^{(2)}]$ must be equal to $-\frac{1}{2}\Box h^{(2)}_{\mu\nu}$, since this involves exactly the same calculation as for $G^{(1)}_{\mu\nu}[h^{(1)}]$. If we define $G^{(2)}_{\mu\nu}[h^{(1)}] = -8\pi t_{\mu\nu}$, where $t_{\mu\nu}$ represents the effective energy-momentum tensor, the Einstein equation up to second order in the metric perturbation can be written as:

$$G^{(1)}_{\mu\nu}[h^{(2)}] = -\tfrac{1}{2}\Box h^{(2)}_{\mu\nu} = 8\pi t_{\mu\nu}. \tag{1.57}$$

The identification of $t_{\mu\nu}$ as an effective energy-momentum tensor seems reasonable. It is a symmetric tensor, quadratic in $h_{\mu\nu}$. In electromagnetism or scalar field theory, the energy-momentum tensor is also quadratic in the relevant fields. The effective energy-momentum tensor $t_{\mu\nu}$ represents how the perturbations affect spacetime just like the usual matter energy-momentum tensor would. It is also conserved in flat background spacetime $\partial_\mu t^{\mu\nu} = 0$ which follows from the Bianchi identity $\partial_\mu G^{\mu\nu} = 0$. Naively, we could just calculate $t_{\mu\nu} = \frac{1}{8\pi}G^{(2)}_{\mu\nu}[h^{(1)}]$. There is still a problem, however, $t_{\mu\nu}$ is not invariant under gauge transformations. This is the problem we touched on before. A local coordinate-invariant definition of the energy is not possible because of the equivalence principle. We can circumvent this problem by averaging $t_{\mu\nu}$ over several wavelengths, an operation that is denoted by angle brackets $\langle ... \rangle$. If we average over enough wavelengths, enough of the physical curvature should be encapsulated in $t_{\mu\nu}$ to make it a gauge-invariant measure. The limit of a large averaging region compared to the wavelength also has the practical advantage that derivatives vanish:

$$\langle \partial_\mu F(x) \rangle = 0, \tag{1.58}$$

which allows us to integrate by parts under the averaging brackets:

$$\langle F(x)\partial_\mu G(x) \rangle = -\langle G(x)\partial_\mu F(x) \rangle, \tag{1.59}$$

since the boundary term can be neglected in the leading order approximation. To calculate the effective energy-momentum tensor $t_{\mu\nu}$, we have to consider the Einstein equation up to second order in the metric perturbation, which requires a lengthy calculation that can be found in Appendix C. This calculation is skipped in the textbooks referenced above, but is by no means trivial. We can therefore consider the result in Appendix C a result of this thesis. The final result is given by:

$$\langle t_{\mu\nu} \rangle = \tfrac{1}{32\pi}\langle \eta^{\alpha\beta}\eta^{\gamma\zeta}\partial_\mu h^{(1)}_{\alpha\gamma}\partial_\nu h^{(1)}_{\beta\zeta} \rangle, \tag{1.60}$$

where it is implied that $h^{(1)}$ is the transverse traceless part of the metric perturbation.

1.6 Energy Flux from Gravitational Waves

We can use the effective energy-momentum tensor to derive the energy flux radiated by GWs. This is again a derivation that is omitted by textbooks such as [9], [17] and [18]. The average energy flux from GWs in some spatial direction i is given by $\langle t_{0i} \rangle$. The total energy radiation from GWs at a distance r far away from the effective source $t_{\mu\nu}$ is then given by the integral:

$$\left\langle \frac{dE}{dt} \right\rangle = \int_0^\pi \int_0^{2\pi} d\theta d\phi r^2 \sin\theta \langle t_{0\mu} \rangle n^\mu, \tag{1.61}$$

where we can choose our integration domain in a way such that $n^i = \hat{r}$. The integral then reduces to:

$$\left\langle \frac{dE}{dt} \right\rangle = 4\pi r^2 \langle t_{0r} \rangle = \frac{r^2}{8}\left\langle \partial_0 h^{(1)\beta\zeta}\partial_r h^{(1)}_{\beta\zeta} \right\rangle. \tag{1.62}$$

The only freely propagating degrees of freedom are the spatial transverse traceless degrees of freedom of the metric, which we already assumed for the metric perturbation in the above expression. We can therefore use the expression for the spatial transverse traceless first order

metric perturbation h_{ij}^{TT} from equation (1.28) to yield:

$$\begin{aligned}\left\langle \frac{dE}{dt} \right\rangle &= \frac{r^2}{8} \left\langle \frac{2}{r} \frac{d^3 I_{ij}\left(t_r\right)}{dt^2} \left(P_{ik}P_{jl} - \tfrac{1}{2}P_{ij}P_{kl}\right) \partial_r \frac{2}{r} \frac{d^2 I_{ij}\left(t_r\right)}{dt^2} \left(P_{ik}P_{jl} - \tfrac{1}{2}P_{ij}P_{kl}\right) \right\rangle \\ &= -\tfrac{1}{2} \left\langle \dddot{I}_{ij}\left(t_r\right) \left(P_{ik}P_{jl} - \tfrac{1}{2}P_{ij}P_{kl}\right) \dddot{I}_{ij}\left(t_r\right) \left(P_{ik}P_{jl} - \tfrac{1}{2}P_{ij}P_{kl}\right) \right\rangle + \mathcal{O}(\tfrac{1}{r}) \\ &\approx -\frac{r^2}{8} \left\langle \dot{h}_{ij}^{\mathrm{TT}} \dot{h}_{ij}^{\mathrm{TT}} \right\rangle,\end{aligned} \tag{1.63}$$

where going from the first to the second line we used that I_{ij} only depends on $t_r = t - r$ such that $\partial_r I_{ij} = -\partial_t I_{ij}$. Also, since the above energy considerations are only valid for large r, we can neglect all higher order terms in $1/r$. Using (1.30) we can expand the projection operators in the definition of h_{ij}^{TT} as:

$$h_{ij}^{\mathrm{TT}} = \frac{1}{r} \left(2\ddot{I}_{ij} - \ddot{I}_{kk}\delta_{ij} + n_k n_l \ddot{I}_{kl}\delta_{ij} + n_i n_j \ddot{I}_{kk} + n_i n_j n_k n_l \ddot{I}_{kl} - 2n_j n_k \ddot{I}_{ik} - 2n_i n_k \ddot{I}_{jk} \right), \tag{1.64}$$

such that the energy dissipation formula is given by:

$$\begin{aligned}\left\langle \frac{dE}{dt} \right\rangle &= -\frac{1}{8} \langle 4\,\dddot{I}_{ij}\,\dddot{I}_{ij} + 4\,\dddot{I}_{ij} n_i n_j\,\dddot{I}_{mn} n_m n_n - 16\,\dddot{I}_{ij}\,\dddot{I}_{im} n_j n_m - 3\,\dddot{I}_{ij} n_i n_j\,\dddot{I}_{mn} n_m n_n \\ &\quad -7\,\dddot{I}_{ij} n_i n_j\,\dddot{I}_{mn} n_m n_n + 8\,\dddot{I}_{ij}\,\dddot{I}_{im} n_j n_m + 8\,\dddot{I}_{ij} n_i n_j\,\dddot{I}_{mn} n_m n_n \rangle \\ &= -\frac{1}{8} \langle 4\,\dddot{I}_{ij}\,\dddot{I}_{ij} + 2\,\dddot{I}_{ij} n_i n_j\,\dddot{I}_{mn} n_m n_n - 8\,\dddot{I}_{ij}\,\dddot{I}_{im} n_j n_m \rangle .\end{aligned} \tag{1.65}$$

Finally, using the relations [19]:

$$\langle n_i n_j \rangle = \frac{1}{3}\delta_{ij}, \quad \langle n_i n_j n_k n_l \rangle = \frac{1}{15} \left(\delta_{ij}\delta_{kl} + \delta_{ik}\delta_{jl} + \delta_{il}\delta_{jk} \right), \tag{1.66}$$

we obtain the energy dissipation formula for GWs far away from a slowly moving source that is not dominated by self-gravity:

$$\langle \dot{E} \rangle = -\frac{1}{5} \langle\, \dddot{I}_{ij}\,\dddot{I}_{ij} \rangle . \tag{1.67}$$

Let us go back to the binary star system example given by (1.43), (1.44) and the energy density (1.45). The only non-zero third time derivatives of the quadrupole moment tensor (1.29) are given by:

$$\dddot{I}_{xx} = -\,\dddot{I}_{yy} = 4\Omega^3 \mu R^2 \sin(2\Omega t), \qquad \dddot{I}_{xy} = -4\Omega^3 \mu R^2 \cos(2\Omega t), \tag{1.68}$$

such that the energy dissipation due to GWs for this binary system is given by:

$$\begin{aligned}\langle \dot{E} \rangle &= -\frac{1}{5} \left\langle 16\Omega^6 \mu^2 R^4 \sin^2(2\Omega t) + 16\Omega^6 \mu^2 R^4 \sin^2(2\Omega t) + 32\Omega^6 \mu^2 R^4 \cos^2(2\Omega t) \right\rangle \\ &= -\frac{32\mu^2 R^4 \Omega^6}{5}.\end{aligned} \tag{1.69}$$

The above energy dissipation relation was one of the first results of GWs that has been tested. In 1974 Hulse and Taylor discovered a binary system with relatively small component masses of which one of the two was a pulsar [20]. The extremely small orbital period of about eight hours and the fact that one of the two stars was a pulsar provided a very accurate clock that made it possible to measure the change in the period of the orbit as the system lost energy due to gravitational dissipation. The energy loss was consistent with the prediction from general relativity derived above. This was the first, although indirect, experimental confirmation of GWs. Hulse and Taylor received the Nobel prize in physics in 1993 for their findings.

1.7 The First Detection of Gravitational Waves*

We have now seen that, at least theoretically, GWs cause distortions of spacetime. A GW passing by will displace particles in a certain direction. One would think that distortions of spacetime could easily be measured. In the previous section, however, we have seen that the distortion of the earth from GWs are in the order of magnitude of 10^{-16} metres for binary neutron star systems and only one or two orders of magnitude more for binary black hole systems. A long history of failed detections preceded the eventual first detection of a GW by the advanced LIGO detectors on September 14, 2015 [1]. The advanced LIGO detectors, which stands for Laser Interferometer Gravitational-Wave Observatory, are GW detectors based on laser interferometry. Two arms of four kilometre length are able to measure distortions of spacetime down to 10^{-20} metres. In [21] the full specifics of the advanced LIGO detector can be found. It goes without saying that the effect of GWs discussed in the previous section is idealised. We do not expect the GWs to perfectly align with our detectors and therefore, we will not observe a perfectly $+$ or $\times$ polarised GW. In general, the detector will be sensitive to some weighted combination of the two polarisations, with the weights depending on the location in the sky of the source and the relative orientation of the source and the detector. The first detection event, referred to in the literature as GW150914, was reason for the Nobel committee to give Kip Thorne, Rainer Weiss, and Barry Barish the 2017 Nobel prize in physics for their contributions to the LIGO detector. Kip Thorne, has been a great contributor to the theoretical understanding of GWs, of which aspects will be more extensively discussed later in this thesis. The direct observation of GWs was also a confirmation of the theory of GR, since Einstein's GR predicted these waves for over a century now. We will now look at the signal that was published by the LIGO collaboration [1] and see which properties can be extracted from the signal with our knowledge from section 1.1.

In Figure 1.4 the GW signal GW150914 detected on September 14, 2015, by the LIGO collaboration, can be seen. The two topmost figures show the observed strain data from the two LIGO detectors. The middle figures show the best overlapping constructed waveform, of which below, the difference with the signal is shown. The lower two figures show the frequency that the detectors observe over time. This Figure was only published in [1] on February 11, 2016, because it took a long time to verify the detection through the data analysis. Numerous checks needed to be done to make sure this really was a GW signal. The data analysis had to reveal the properties of the source, such as for example the mass of the objects - where we allowed ourselves to prematurely assume the source to be a binary system.

With merely simple Newtonian physics and the concepts of general relativity that we discussed in the previous section we will be able to extract properties of the source from the waveform depicted in Figure 1.4. This simplified analysis is qualitatively consistent with a fully general relativistic analysis. The analysis below extracts concepts from [22] where a complete analysis can be found accessible for anyone with a general physics background. Some explicit properties that we can extract from Figure 1.4 are the frequency and amplitude of the gravitational waveform. We will discuss what properties of the source we can extract from these observables. The energy dissipation due to GWs for a binary system is given by equation (1.69). As long as the velocities in the binary system are not too close to the speed of light, the orbital radius increases only adiabatically and has a period that is described by Kepler's third law, we can use concepts of Newtonian physics as a rough approximation to the binary system. The energy that is lost due to GW dissipation is at the expense of orbital energy. In a center of mass frame, the orbital energy in a Newtonian approximation is given by $E_{\text{orb}} = \frac{M\mu}{2R}$, where we have introduced the total mass M, the reduced mass μ and the orbital separation between the bodies R before. The energy that is lost due to gravitational dissipation that is

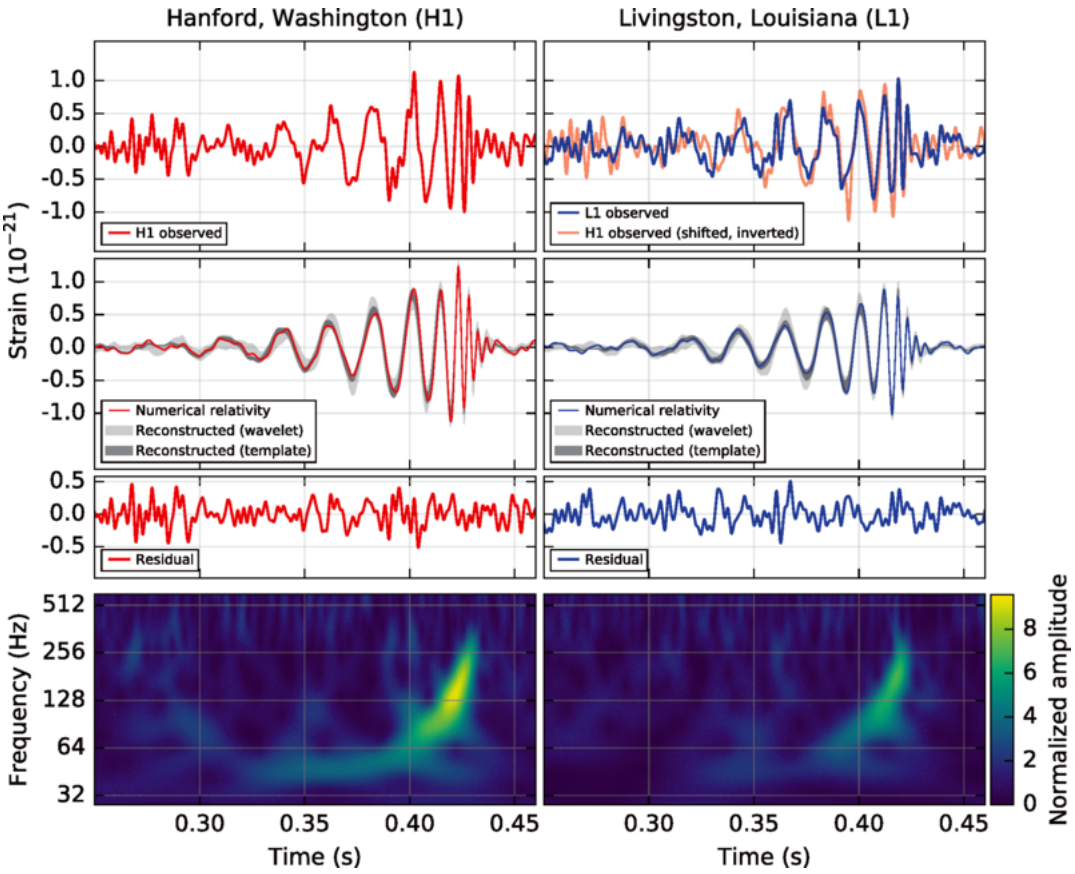

Figure 1.4: The observational data of the LIGO detector from the first GW event GW150914 with from top to bottom: the observed GW strain, the best overlapping constructed waveform, the difference between the observed data and the constructed waveform, the frequency of the observed GW strain as a function of time [1].

at the expense of orbital energy can be given as the following energy conservation balance:

$$\begin{aligned} \frac{dE_{\text{orb}}}{dt} &= -\frac{dE_{\text{GW}}}{dt} \\ \frac{M\mu}{2R^2}\dot{R} &= \frac{32\mu^2 R^4 \Omega^6}{5} \end{aligned} \tag{1.70}$$

which we can rewrite using Kepler's third law $R^3 = \frac{M}{\Omega^2}$ and its time derivative $\dot{R} = -\frac{2R\dot{\Omega}}{\Omega}$:

$$\dot{\Omega}^3 = \left(\frac{96}{5}\right)^3 \Omega^{11}\mu^3 M^2 = \left(\frac{96}{5}\right)^3 \Omega^{11}\mathcal{M}^5, \tag{1.71}$$

where we defined the chirp mass as $\mathcal{M} \equiv (\mu^3 M^2)^{1/5}$. To eliminate the time derivative of the orbital frequency we can rewrite the above equation as:

$$\Omega^{-11/3}\dot{\Omega} = \frac{96\mathcal{M}^{5/3}}{5}, \tag{1.72}$$

which we can integrate from time t and orbital frequency Ω to the time of coalescence t_c where we assume the orbital frequency to diverge, i.e. $\Omega = \infty$:

$$\int_{\Omega}^{\infty} \Omega'^{-11/3} d\Omega' = \int_{t}^{t_c} \frac{96\mathcal{M}^{5/3}}{5} dt', \tag{1.73}$$

which can be easily solved to yield:

$$\Omega = \frac{1}{8}\left[\frac{125}{\mathcal{M}^5(t_c - t)^3}\right]^{1/8} \tag{1.74}$$

or, using the relation between the orbital angular frequency and the GW frequency $\Omega = \pi f_{GW}$:

$$f_{GW} = \frac{1}{8\pi}\left[\frac{125}{\mathcal{M}^5(t_c - t)^3}\right]^{1/8}. \tag{1.75}$$

The above formula can be used to calculate the chirp mass from the time between zero crossings in the strain data of Figure 1.4. First, to obtain a chirp mass in units of kg we have to recover units, because we have worked in units in which $G = c = 1$. The left-hand side has units of 1/s while the right-hand side has units of $\text{kg}^{-5/8}s^{-3/8}$. We can recover the correct units by multiplying with the appropriate factors of G and c, which have units:

$$\begin{aligned} [G] &= \frac{\text{Nm}^2}{\text{kg}^2} = \frac{\text{m}^3}{\text{s}^2\text{kg}} \\ [c] &= \text{m/s}. \end{aligned} \tag{1.76}$$

Multiplying the right hand side with $G^{-5/8}$ yields units of $\text{s}^{7/8}\text{m}^{-15/8}$ after which subsequently multiplying with $c^{15/8}$ gives us the desired units of 1/s. The GW frequency in SI-units is therefore given by:

$$f_{GW} = \frac{1}{8\pi}\left[\frac{125}{(G\mathcal{M}/c^3)^5(t_c - t)^3}\right]^{1/8}. \tag{1.77}$$

In 1.1 the chirp mass is calculated for some very crudely calculated times between zero crossings from Figure 1.4. Note that close to $t = t_c$ the frequency diverges such that the above formula becomes less invalid. Using the real data instead of reading off the figure by eye would increase the accuracy. The LIGO team have estimated the binary system responsible for the GW150914 event to be an equal mass binary system of $35\text{M}_\odot$ component masses [23]. This equals a chirp mass of around $\mathcal{M} = 30\text{M}_\odot$, leaving us to conclude that our crude approximations techniques can indeed be used as an approximation. Note that in order to constrain the

T(s)	t_c(s) - t(s)	$\mathcal{M}(\mathrm{M}_\odot)$
0.01	0.05	35
0.075	0.025	34
0.005	0.005	31

Table 1.1: Period between zero crossings for three periods of the GW from Figure 1.4. The second zero crossing for the three chosen wave parts are at $t = 0.37s$, $t = 0.395$ and $t = 0.415$ respectively and $t_c = 0.42$.

component masses of the binary more in depth analysis is needed that is beyond the scope of this crude estimate.

As a next step in our crude approximation, we want to say something about the properties of the components of the binary system. Let us assume that the components of the binary system have equal masses of $35\mathrm{M}_\odot$. Assuming that the orbit stays Keplerian until the point of peak amplitude gives us the orbital separation of the two bodies during peak amplitude from Kepler's third law:

$$R = \left(\frac{GM}{\Omega^2_{|max}}\right)^{1/3} \approx 350\mathrm{km} \tag{1.78}$$

where we estimated the peak frequency to be $f_{\mathrm{GW}|max} = 150\mathrm{Hz}$ using the zero crossings or the frequency plot from Figure 1.4 such that $\Omega_{|max} = \pi 150\mathrm{Hz}$. The orbital separation indicates that the objects must be extremely compact. Main-sequence stars have radii of order hundreds of thousands of kilometres and would have merged long before reaching an orbital separation of 350km. The most compact stars are neutron stars, which have radii of order ten kilometres. However, the maximum mass that a neutron star can have before collapsing into a black hole is around $3\mathrm{M}_\odot$ [24, 25, 26]. The inevitable conclusion is therefore quickly made that the two compact objects responsible for the GW150914 event must be two black holes.

A final factor to include in our approximation scheme is the fact that GWs are stretched out, or redshifted, as they travel across the expanding universe. Their wavelength increases while their frequency decreases. The GWs measured in the detector frame on earth are therefore redshifted compared to when they were originally emitted. The masses inferred from the GW data above are also scaled because of redshift. We therefore want to know how far away the source is from the GW detector. Using the strain equation (1.52) for our binary star example gives us a strain amplitude of:

$$h = \frac{4G\mu(\pi f_{\mathrm{GW}})^2 R^2}{rc^4}, \tag{1.79}$$

where we recovered the correct SI-units. From Figure 1.4 we know that the peak amplitude is around $h \sim 10^{-21}$. Plugging in the numbers evaluated at the peak amplitude gives us a distance of around 1000Mpc. This corresponds to a redshift of around $z = 0.2$, which means that the masses are scaled by a factor of $1 - z = 0.8$. It turns out that the actual distance calculated by LIGO is around 400Mpc [23]. This corresponds to a smaller redshift of around $z = 0.1$, such that the scaling effect on the masses becomes insignificant in this crude analysis.

We have seen that we are able to calculate the order of magnitudes of the respective quantities and in some cases even quite accurate approximations. It seems that our approximations are a bit too crude to accurately calculate the distance of the source. Problems with the approximation are for instance: equation (1.52) becomes less accurate for systems with large self-gravity compared to the rest-mass energy of the system; Kepler's third law only holds for the beginning of the inspiral where the orbital motion has an adiabatically changing radius and the binary is at nearly infinite separation so that relativistic corrections are negligible. In chapter 2 we will go into a much more detailed analysis: this is where the crude approximations will not do

anymore.

1.8 Detection of Gravitational Waves from a Neutron Star-Black Hole Binary System

We have seen that the chirp mass is a relatively easy property of a binary system to constrain from GW data. We have also seen that to constrain the individual component masses from signals with measurable inspirals, a more detailed analysis is needed. One would construct a waveform numerically [27], phenomenologically [7] or as a combination of the two [8] and choose the free parameters such that the overlap integral from the constructed waveform with the observed gravitational waveform is minimised. This is the resulted waveform that can be seen in the second row of Figure 1.4. It is difficult to employ the simple analysis from above to conclude that observed gravitational waveform data is from an NSBH binary system. It is however, possible to conclude that a waveform must be from an NSBH binary source using the more advanced techniques. The waveforms that are constructed in this way do not make assumptions like the adiabatic assumption and also allow for relativistic effects. In chapter 2 these effects will be discussed.

We will however, first touch on the importance of studying NSBH mergers as opposed to BBH mergers. The GW signal of a BBH merger only depends on the masses, spins and possibly the charges of the progenitor black holes, a property that is known as the *no hair theorem*. For binary mergers, which have at least one component that is not a black hole, more parameters enter the system. NSBH and binary neutron star (BNS) systems, emit GWs that have a dependency on not only the mass, spin and possibly charge of the two objects, but also on the EOS of the neutron star. Studying GWs from these systems can therefore give us information about the EOS of neutron stars. The interior of a neutron star is, apart from black holes, the place where one can find the highest energies in the universe. Furthermore, BBHs are systems of only pure gravity, while NSBHs involve strong gravity with extreme states of matter. NSBHs are therefore excellent candidates to use as an experimental ground to find out more about these extreme states of matter. We do not yet accurately know the exact composition of the interior of neutron stars. Uncovering these secrets is therefore of great interest to us and might lead to new physics being discovered.

The advantage of mergers that have at least one component mass which is not a black hole is that they can emit electromagnetic counterparts. Since both GWs and electromagnetic radiation move with the speed of light, the two signals will be observed simultaneously on earth. Short gamma-ray bursts are an example of an electromagnetic counterpart which can be emitted shortly after the merger of a relevant binary system. Two different signals from the same event can help to increase the accuracy of the measurements of properties of the system. This technique of combining different signals is called multi-messenger and is a promising extra tool that can be used to increase the parameter extraction accuracy for NSBH and BNS merger events. NSBH binaries generally emit stronger signals than BNS binaries since the total mass of NSBH binaries can reach higher values. NBSH binaries are therefore a good candidate to study since they have all the multi-messenger advantages while maintaining a relatively strong signal compared to BNS mergers. It is still uncertain whether NSBH systems are expected to generally have strong electromagnetic counterparts or not [28], but the potential is there. It is however, certain that the new generation of GW detectors: LISA [29] and the Einstein telescope [30], will have a positive impact on the detection rate of multi-messenger events. There has been at least one observed multi-messenger event, namely GW170817 [2], which was a BNS merger. The multi-messenger nature of the event has opened up all kinds of interesting analyses, such as for example an alternative way to accurately measure the Hubble constant to relieve the Hubbel tension [31] among other interesting applications. The first NSBH mergers were observed after the first BNS merger. On January 5 and January 15, 2020, the GW events

GW200105 and GW200115 occurred [3]. It can be concluded that these events were from NSBH binary sources. The reason that only a handful of NSBH binaries have been observed while many more BBH binaries are observed is both because the systems are simply rarer in the universe and because it generates a much weaker signal than BBH systems. BBH systems are also much wider studied because of this. We now know however, that studying NSBH binary waveforms can give us information about the EOS of the neutron star. A waveform model for an NSBH system, fast-to-generate yet accurate over a wide parameter space region, is therefore crucial to extract source parameters from NSBH GW signals. Similar to section 1.7, but now applying the full state-of-the-art physics knowledge, we can construct the ingredients for a sophisticated waveform model. A key input parameter, namely the merger frequency of the NSBH, will be discussed in full detail in the next chapters. This discussion aims to further advance the waveform modelling for the data analysis of GW. We will start with giving the reader more motivation as to why we study these systems along with giving the reader some intuition. Subsequently, the unique dynamics of NSBH systems will be discussed together with the imprints they have on their gravitational waveforms.

Chapter 2

A Binary System of Compact Objects

Now that we have seen that a changing quadrupole moment of a system can generate GWs, we will consider a binary system of two compact objects more closely, a system of which one of the two objects is an extended object. This could be an NSBH binary system for example. It is useful to construct this chapter by explicitly considering the NSBH binary system as the specification of the system at hand. The theory is however, applicable to other binary systems. To deeply understand the GWs such a system can generate, we need to deeply understand the dynamics of the system. We will begin the chapter with some observations in section 2.1 that should give the reader motivation as to why an NSBH binary is interesting to study. After which we will get into the physical phenomenon that makes the dynamics of an NSBH binary unique compared to binary systems without an extended object, namely tidal effects. Section 2.2 will consider tidal effects from a classical Newtonian perspective, which makes it a legible section for the less experienced physicists. In the remaining sections the action of a compact object binary system will be carefully set up in which section 2.3 sets up an action still without any spin couplings. This action is evaluated in the adiabatic regime in section 2.4, and the dynamic regime in 2.5. Finally, section 2.6 discusses the action with spin coupling terms up to first order in the spin.

2.1 Observations from Numerical Studies

In the not too distant past, a physicist used observations to gain intuition on where to start looking, i.e. to find out which properties or dynamics play the most important role in understanding the system at hand. We all know the story of Newton's observation of an apple falling straight to the ground that led him to develop his universal law of gravitation. The apple told Newton where to look, namely that there must exist some law that dictates that every body in the universe is attracted to every other body. In the same way, we want to start our research with an observation that can give us a hint on where to start looking. These days however, a physicist is not limited to only observations anymore. We have the luxury of computers that can simulate reality. These computers give us the ability to 'observe' quantities of systems that would be out of the field of view of our telescopes or GW detectors. This brings us to the SXS Gravitational Waveform Database [4]. Here we can find waveforms of GWs emitted by Black Hole-Black Hole binary systems (BBH) as well as NSBH binary systems for a wide range of parameters that describe these systems. A gravitational waveform is the representation of the GW strain h plotted over time. These waveforms are generated by code that simulates matter subject to Einstein's equations, i.e. NR simulations. An exact description of their methods can be found in [27]. For now, we will use the results from these simulations and treat them as real observations that will give us direction on where to start looking.

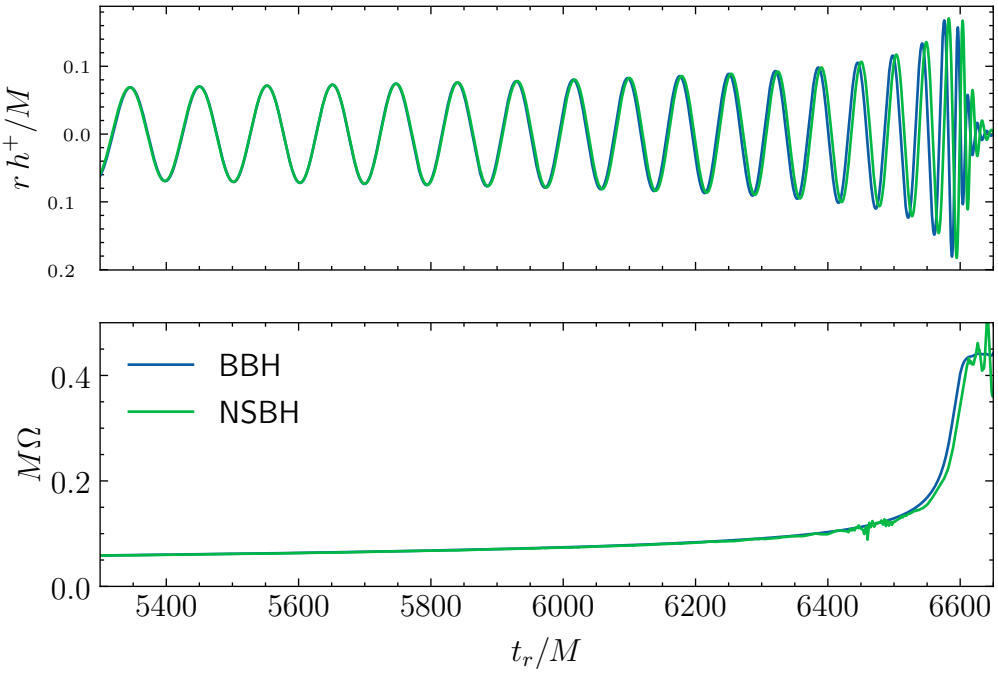

Figure 2.1: GW strain and the angular frequency as a function of retarded time as dimensionless quantities in geometric units from the plus polarised gravitational waveform emitted by a BBH and an NSBH binary for mass ratio $Q = 6$. Data is from numerical relativity simulations [4].

An NSBH binary system is characterised by parameters such as the mass ratio Q between the black hole and the neutron star, the angular momentum of both the black hole and the neutron star, the equation-of-state of the neutron star and many more. We want to use these 'observations' to gain intuition on how the system responds to changes in these parameters. Intuitively, the parameter that must have a significant, if not the most significant, influence on the system is the mass ratio. Since we know that the larger scales can be described by the theory of GR, which is a theory about the interaction of masses. Therefore we started investigating how different mass ratios affect the dynamics of the binary system and thus also the gravitational waveform of the binary system.

In the top panel of Figure 2.1 we can see the waveform of a BBH laid over the waveform of an NSBH binary system for mass ratio $Q = 6$ - this means that the black hole is six times as massive as the neutron star. Here we can see that the waveforms of the two systems almost completely overlap. Before we move on to further observations, it is important to familiarise ourselves with some terminology that is used to describe different stages of a binary system and to connect the different stages of a binary system to different parts of the waveform. The first part, when the two bodies are in orbit around each other, is called the inspiral phase. The second part, when the two bodies merge, is called the merger phase. The final part, when all that is left is a remnant black hole, is called the ringdown phase. According to Kepler's third law, we have $\Omega^2 \sim R^{-3}$ such that the quadrupole formula of chapter 1 equation (1.52) tells us that the amplitude of the GWs coming from a binary system grows inversely proportional to the distance between the two bodies. We can therefore conclude that the first part of the waveform of Figure 2.1 corresponds to the inspiraling phase of the binary system, since the amplitude is slowly increasing. The same quadrupole formula tells us that GWs are emitted because of a change in the quadrupole moment of the system, and thus, because of changes in the shape of the system. We can therefore conclude that the maximum amplitude in the grav-

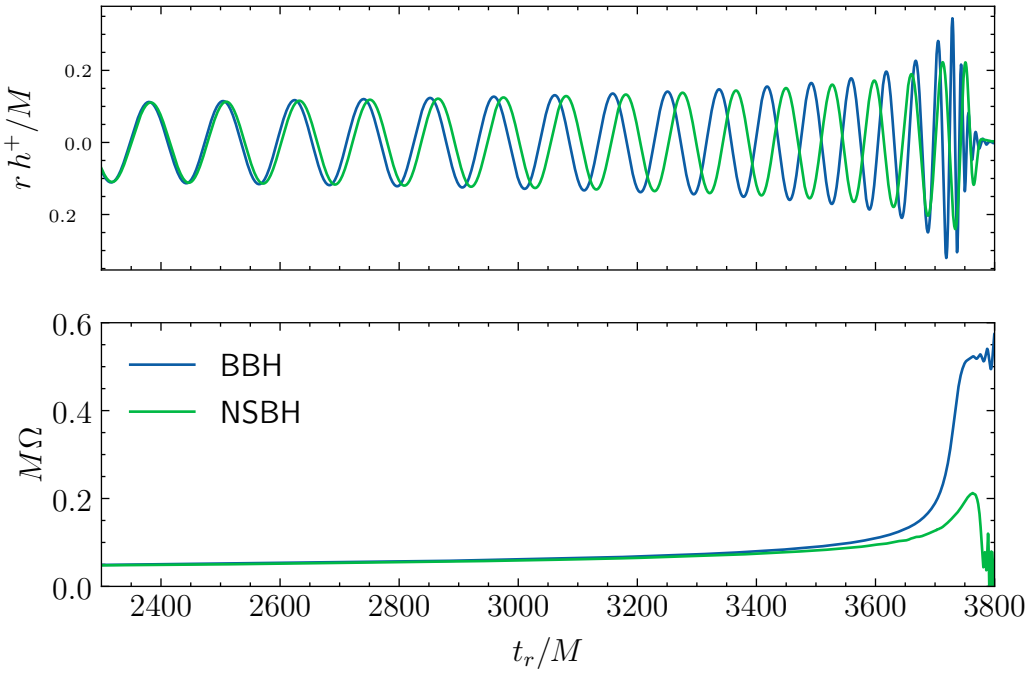

Figure 2.2: GW strain and the angular frequency as a function of retarded time as dimensionless quantities in geometric units from the plus polarised gravitational waveform emitted by a BBH and an NSBH binary for mass ratio $Q = 2$. Data is from numerical relativity simulations [4].

itational waveform is reached during the merger phase, when the system changes from being a binary system to being just a single body. Finally, after the binary system has become a single body, it stops radiating GWs. This is the ringdown phase, for which we can now conclude that it must correspond to the final part of the waveform. A summary of the different phases corresponding to the different parts of the waveform can be seen in Figure 2.3.

We can now look at the angular frequency of the binary system, which can be seen in the bottom panel of Figure 2.1. We can see that the angular frequency is increasing the most rapidly, at the point of maximum amplitude in the gravitational waveform, i.e. at the point of merger. We can also see that the angular frequency behaviour of the two systems again closely matches - apart from some numeric instability at the end of the angular frequency of the NSBH binary.

From the above observations we can conclude that the dynamics of an NSBH with mass ratio $Q = 6$ must not differ greatly from the dynamics of a BBH. What about binary systems with smaller mass ratios?

In the top panel of Figure 2.2 we can see the waveform of a BBH laid over the waveform of an NSBH binary system for mass ratio $Q = 2$. Here we can see that the waveforms of the two systems do not overlap anymore. The waveforms quickly start getting out of phase and the merger amplitude also differs. In the bottom panel of Figure 2.2 we can observe that the angular frequencies of a BBH and NSBH binary now completely differ.

The intuition we gain from these observations is that NSBH binaries with great mass ratios seem to behave just like a BBH while NSBH binaries with mass ratios closer to 1 seem to behave differently - this claim is also supported by more NR data investigation and not just

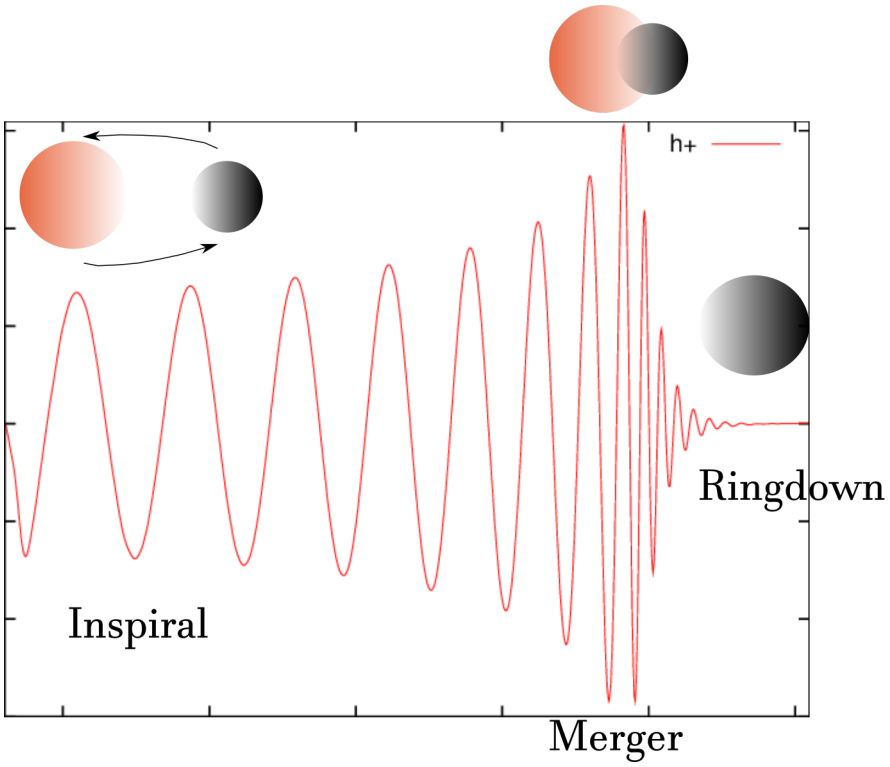

Figure 2.3: The three different phases of a binary merger: the two bodies start out in mutual orbit, due to gravitational radiation orbital energy is lost and the two bodies start oscillating at a higher orbital frequency at a smaller orbital separation until eventually merging into a remnant black hole. The horizontal axis represents time evolution.

by the two discussed cases. In section 1.7 we stated that BBH systems are well studied. It is therefore not interesting for us to focus on the large mass ratio regime. However, the theory of NSBH binaries is much lesser-known. The regime of mass ratios close to $Q = 1$ is therefore a very interesting regime for us to study.

Let us first qualitatively hypothesise why NSBH binaries of equal mass ratios behave so differently than NSBH binaries or much larger mass ratios. Let us do a thought experiment about the different limits we can have. Consider an NSBH binary with an infinite mass ratio. It is not hard to see that such a system corresponds to a black hole with a neutron star companion that can be seen as a point mass. The backreaction of the point mass on the larger object of infinite mass is negligible and the background metric is fixed. The dynamics of the system will be completely described by the trajectory of the point mass around the black hole. We know from GR that a point mass will follow the geodesics induced by the metric of the black hole. The geodesic of the neutron star will be of decreasing radius since energy is lost due to gravitational radiation, such that eventually the point mass will merge with the black hole. If we assume that the point mass is a black hole instead of a neutron star, all the dynamics stay exactly the same since a point mass has no equation-of-state type characteristics. Now consider a NSBH with mass ratio $Q = 1$. Since black holes are the most compact objects in the universe, we can assume that the radius of the neutron star will be at least not smaller than that of the black hole. The size of the neutron star has implications, namely that the gravitational force from the black hole at one point at the surface of the neutron star can be vastly different from this force on another point at the surface of the neutron star. This difference in gravitational force is called the differential tidal force or just tidal force. The difference in gravitational force on the surface is negligible when the distance between the neutron star

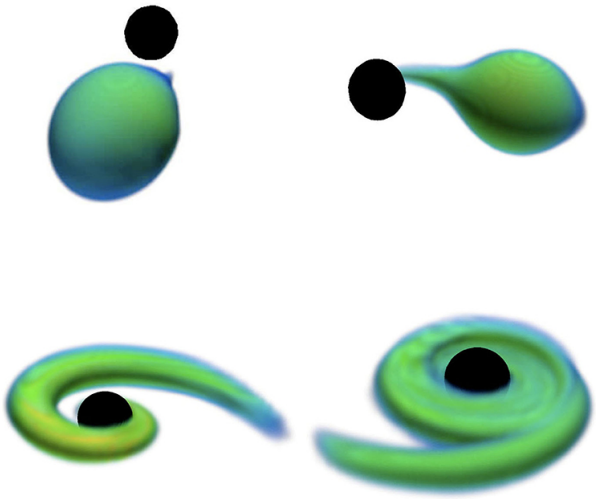

Figure 2.4: Time evolution of a disrupting NSBH binary [32].

and the black hole is large enough, but when the orbital distance between the black hole and the neutron star becomes smaller, the differential tidal force can be so big that the neutron star can be ripped apart. The evolution of such a merger where the neutron star is ripped apart can be seen in Figure 2.4. Since these effects come into play because of the neutron star not being a point mass anymore, i.e. because of the neutron star not having an infinitely small size, they are called finite size effects. Intuitively it comes as no surprise that the way an object is ripped apart depends highly on the type of object we are considering, i.e. on the equation-of-state of the object. It should therefore now come as no surprise that for mass ratios Q closer to 1, the dynamics of a binary system highly depend on the type of objects at hand.

We had already established that NSBH binaries with mass ratios close to $Q = 1$ were interesting to study, but we have now also qualitatively established that tidal effects are responsible for this interesting behaviour. The reader should therefore be motivated enough to accept that to understand an NSBH binary, we must study tidal effects, which will be the topic of the remainder of this section.

2.2 Tidal Effects in Classical Newtonian Mechanics*

In this section we will study the tidal effects that are the cause of the interesting dynamics of an NSBH binary. First, we will study these tidal effects in a classical Newtonian mechanics formalism. In the next section we will study the tidal effects in a classical Lagrangian mechanics formalism which can be easily carried over to a general relativistic description of the system.

In section 2.1 we have seen observational evidence that at a certain point during the inspiral of an NSBH binary, the masses of the stellar objects can not be estimated as point masses anymore and that one of the main processes that becomes of great significance during the final phase of the inspiral is tidal disruption. All bodies that are not point masses are subject to tidal forces. The difference between the gravitational force of the black hole on a point mass in the centre of the neutron star and a point mass at the surface of the neutron star is what is known as the differential tidal force $\Delta\vec{F}$ or just tidal force. This is the force relative to the centre of the neutron star, which we can derive using Newtonian theory.

We will derive the tidal force field in two spatial dimensions, which can be straightforwardly extended to three spatial dimensions. Consider a neutron star in the form of a spherical body with radius R_{NS}, subject to the gravitational field of a black hole with mass M_{BH}. The orbital

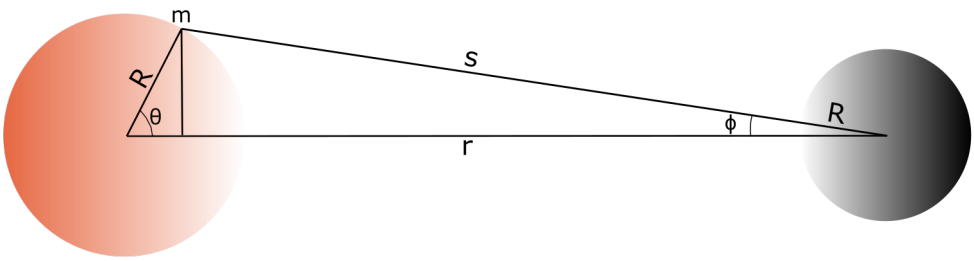

Figure 2.5: Geometry for calculating the differential tidal force. The left object is considered to be the neutron star that will be subject to tidal effects from the black hole.

separation of the two objects is given by r, which will be assumed to be much greater than R_{NS} ($r \gg R_{NS}$). A test-mass m in the centre of the neutron star is subject to the gravitational force of the black hole by:

$$\vec{F_C} = \frac{M_{\mathrm{BH}} m}{r^2} \hat{\boldsymbol{e}}_x, \tag{2.1}$$

where G is Newtons gravitational constant and $\hat{\boldsymbol{e}}_x$ is the unit vector in the x-direction. Similarly, a test-mass m on the surface of the neutron star is subject to the gravitational force of the black hole. We will use θ as the angle between the neutron star-black hole line and the radial line to m from the neutron star, ϕ as the same angle but with the radial line to m from the black hole and finally s as the radial line to m from the black hole, see Figure 2.5. We then have:

$$\vec{F_S} = \frac{M_{\mathrm{BH}} m}{s^2} (\cos(\phi)\hat{\boldsymbol{e}}_x - \sin(\phi)\hat{\boldsymbol{e}}_y). \tag{2.2}$$

The difference between the gravitational force from the black hole on the test-mass on the surface of the neutron star and in the centre of the neutron star is then given by:

$$\Delta\vec{F} = M_{\mathrm{BH}} m \left(\left(\frac{\cos(\phi)}{s^2} - \frac{1}{r^2} \right) \hat{\boldsymbol{e}}_x - \frac{\sin(\phi)}{s^2} \hat{\boldsymbol{e}}_y \right). \tag{2.3}$$

Since we have $r \gg R_{NS}$, we can approximate $\cos(\phi) \approx 1$. From trigonometry we also have:

$$\sin(\phi) = \frac{R_{\mathrm{BH}} \sin(\theta)}{s} \approx \frac{R_{\mathrm{NS}} \sin(\theta)}{r}, \tag{2.4}$$

as well as:

$$\begin{aligned} s^2 &= (r - R_{\mathrm{NS}} \cos(\theta))^2 + (R_{\mathrm{NS}} \sin(\theta))^2 = r^2 \left(1 - \frac{2R_{\mathrm{NS}} \cos(\theta)}{r} + \frac{R_{\mathrm{NS}}^2}{r^2} \right) \\ \frac{1}{s^2} &= \frac{1}{r^2} \left(1 - \frac{2R_{\mathrm{NS}} \cos(\theta)}{r} \right)^{-1} \approx \frac{1}{r^2} \left(1 + \frac{2R_{\mathrm{NS}} \cos(\theta)}{r} \right), \end{aligned} \tag{2.5}$$

where we neglected the R_{NS}^2/r^2 term and Taylor expanded the third term because $r \gg R_{NS}$. We can write equation (2.3) as:

$$\Delta\vec{F} = \frac{M_{\mathrm{BH}} m R_{\mathrm{NS}}}{r^3} \left(2\cos(\theta)\hat{\boldsymbol{e}}_x - \sin(\theta)\hat{\boldsymbol{e}}_y \right). \tag{2.6}$$

Here we can see that for $\theta = 0$ the tidal force is directed at the black hole, while for $\theta = \pi$, counter-intuitively, the tidal force is directed away from the black hole. The net force is still

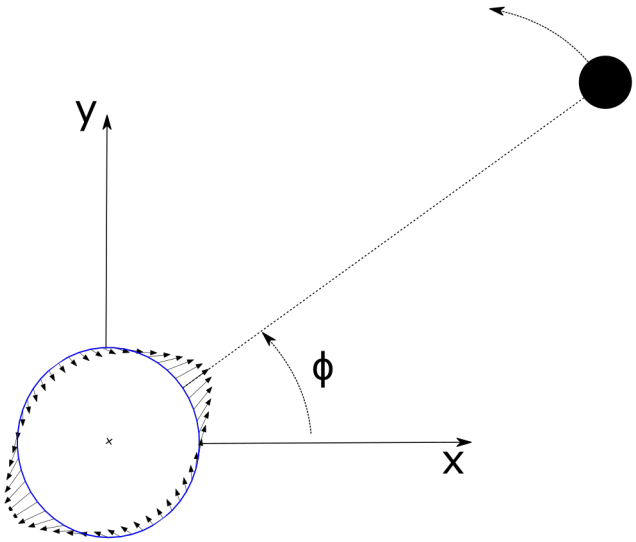

Figure 2.6: Tidal tidal displacement field of a neutron star from the presence of a companion black hole in the body frame of the neutron star. Note that ϕ is now the angle denoting the phase of the orbit of the black hole around the neutron star in anticipation of next sections.

directed in the direction of the black hole, but the tidal force denotes the force on the surface of the neutron star relative to the force on the centre of the neutron star because of the gravitational pull of the black hole. We can see that the tidal force wants to pull the neutron star into an ellipsoidal form. See Figure 2.6 for a visualisation of the tidal displacement field. As long as the self-gravitational force of the neutron star can counteract the tidal force, the neutron star will remain in compact form, but when the tidal force starts to become much greater than the self-gravitational force from the neutron star, the star starts to become tidally disrupted and will no longer be close to a spherical object in space.

We can note that the tidal force is maximal for $\theta = 0$. Before any tidal disruption, the neutron star will still be spherical of form, and therefore the self-gravitational force will be constant along the surface of the neutron star. We will therefore compare the self-gravitational force of the neutron star with the tidal force along the neutron star-black hole line. When the magnitude of the tidal force at $\theta = 0$ exceeds the magnitude of the self-gravitational force, the tidal disruption process will start taking place, beginning along the $\theta = 0$ line before slowly expanding to the rest of the neutron star. This also confirms the time evolution of the tidal disruption prematurely depicted in the previous section in Figure 2.4.

The force balance of the self-gravitational force with the tidal force at the the surface of the neutron star along the common axis of the neutron star and the black hole is given by:

$$\frac{2M_{\mathrm{BH}}mR_{\mathrm{NS}}}{r^3} = \frac{M_{\mathrm{NS}}m}{R_{\mathrm{NS}}^2}. \tag{2.7}$$

We can therefore estimate that tidal disruption starts taking place for orbital radii r_{tidal} that are approximately larger than:

$$r_{\mathrm{tidal}} = R_{\mathrm{NS}}\left(\frac{2M_{\mathrm{BH}}}{M_{\mathrm{NS}}}\right)^{1/3}. \tag{2.8}$$

We should keep in mind that we made the assumption that $r \gg R_{NS}$, which might not hold during the final phase of the inspiral. Also, we know that Newtonian theory does not apply

to compact objects and to relativistic motion. Ref. [33] proposes a correction based on a comparison of the estimated tidal deformation radius with NR results. This correction ensures that compact objects are more strongly bound:

$$\tilde{r}_{\rm tidal} = r_{tidal}(1 - 2M_{\rm NS}/R_{\rm NS}). \tag{2.9}$$

A much better way to incorporate effects from the compactness $M_{\rm NS}/R_{\rm NS}$ of the objects as well relativistic effects is to derive the mechanisms that are responsible for these effects ourselves. This can be done more easily using another formalism, namely that of an action principle which will be discussed in the next section. This formalism has the advantage that it easily carries over to a general relativistic formulation of the problem. Another advantage of this approach is that we will be able to derive the energy of the system, which we can use to estimate a more accurate tidal disruption radius. The radius we have estimated now is calculated from a force balance evaluated at one certain point at the surface of the neutron star, while an energy balance can be used to take the entire system into account.

2.3 Tidal Effects in Classical Lagrangian Mechanics

In the previous section we have discussed tidal forces using Newtonian mechanics. We showed that we can set up a force balance between the self-gravitational force and the tidal force. This force balance gave us an estimate for the radius at which tidal disruption starts having an influence on the behaviour of the binary system. We will now discuss tidal interactions in a different light, namely that of an action principle. Note that the analysis below is still Newtonian.

The analysis below can be considered to be general for any extended compact object denoted by the subscript A and a point mass denoted by the subscript B. The spherical symmetry of the system allows us to express the different potentials as a multipole expansion, which in turn can be written in terms of spherical harmonics. The discussion is based on [34].

In Newtonian gravity the gravitational potential U_A generated by a mass distribution with density ρ_A at a field point in space $\boldsymbol{x}$ is given by the Poisson equation:

$$\nabla^2 U_A = -4\pi\rho_A, \tag{2.10}$$

which can be solved using the Green's function method to yield:

$$U_A(t, \boldsymbol{x}) = \int d^3x' \rho_A\left(t, \boldsymbol{x'}\right) \frac{1}{|\boldsymbol{x} - \boldsymbol{x'}|}, \tag{2.11}$$

for points $\boldsymbol{x} > \boldsymbol{x'}$ outside the body's mass distribution. The inverse distance term can be Taylor expanded around a moving reference point $z_A(t)$ as:

$$\begin{aligned}
\frac{1}{|\boldsymbol{x} - \boldsymbol{x'}|} = {} & \frac{1}{|\boldsymbol{x} - \boldsymbol{z_A}|} - (x_1' - z_A)\left(\frac{\partial}{\partial x_1'}\frac{1}{|\boldsymbol{x} - \boldsymbol{x'}|}\right)\Big|_{\boldsymbol{x'}=\boldsymbol{z}_A} \\
& - (x_2' - z_A)\left(\frac{\partial}{\partial x_2'}\frac{1}{|\boldsymbol{x} - \boldsymbol{x'}|}\right)\Big|_{\boldsymbol{x'}=\boldsymbol{z}_A} - (x_3' - z_A)\left(\frac{\partial}{\partial x_3'}\frac{1}{|\boldsymbol{x} - \boldsymbol{x'}|}\right)\Big|_{\boldsymbol{x'}=\boldsymbol{z}_A} \\
& + \tfrac{1}{2}(x_1' - z_A)^2\left(\frac{\partial^2}{\partial^2 x_1'}\frac{1}{|\boldsymbol{x} - \boldsymbol{x'}|}\right)\Big|_{\boldsymbol{x'}=\boldsymbol{z}_A} + \tfrac{1}{2}(x_2' - z_A)^2\left(\frac{\partial^2}{\partial^2 x_2'}\frac{1}{|\boldsymbol{x} - \boldsymbol{x'}|}\right)\Big|_{\boldsymbol{x'}=\boldsymbol{z}_A} \\
& + \tfrac{1}{2}(x_3' - z_A)^2\left(\frac{\partial^2}{\partial^2 x_3'}\frac{1}{|\boldsymbol{x} - \boldsymbol{x'}|}\right)\Big|_{\boldsymbol{x'}=\boldsymbol{z}_A} + (x_1' - z_A)(x_2' - z_A)\left(\frac{\partial^2}{\partial x_1' \partial x_2'}\frac{1}{|\boldsymbol{x} - \boldsymbol{x'}|}\right)\Big|_{\boldsymbol{x'}=\boldsymbol{z}_A} \\
& + (x_1' - z_A)(x_3' - z_A)\left(\frac{\partial^2}{\partial x_1' \partial x_3'}\frac{1}{|\boldsymbol{x} - \boldsymbol{x'}|}\right)\Big|_{\boldsymbol{x'}=\boldsymbol{z}_A} \\
& + (x_2' - z_A)(x_3' - z_A)\left(\frac{\partial^2}{\partial x_2' \partial x_3'}\frac{1}{|\boldsymbol{x} - \boldsymbol{x'}|}\right)\Big|_{\boldsymbol{x'}=\boldsymbol{z}_A} + O(x'^3).
\end{aligned} \tag{2.12}$$

We will write this compactly as:

$$\begin{aligned} U_A &= \int d^3x' \rho_A(t, \boldsymbol{x}') \sum_{\ell=0}^{\infty} \frac{1}{\ell!} (x' - z_A)^L \left(\frac{\partial}{\partial x'^L} \frac{1}{|\boldsymbol{x} - \boldsymbol{x}'|} \right) \Bigg|_{\boldsymbol{x}'=\boldsymbol{z}_A} \\ &= \int d^3x' \rho_A(t, \boldsymbol{x}') \sum_{\ell=0}^{\infty} \frac{(-1)^\ell}{\ell!} (x' - z_A)^L \partial_L \frac{1}{|\boldsymbol{x} - \boldsymbol{z}_A|}, \end{aligned} \tag{2.13}$$

where we introduced the notation L which denotes a string of indices $L = a_1 a_2 ... a_\ell$ and $\partial / \partial x'^L = \partial_L$. The full expression of the expanded potential (2.12) is given to make the map to the compact notation from above (2.13) explicit. It can be shown that $\partial_L |\boldsymbol{x} - \boldsymbol{z}_A|^{-1}$ is a symmetric trace-free (STF) tensor. The symmetric part can be seen immediately since partial derivatives commute. The trace-free part can be shown by calculating the trace. Let us choose the origin of the coordinate system such that we have $z_A = 0$, $\partial_L |\boldsymbol{x} - \boldsymbol{z}_A|^{-1}$ is then given by:

$$\frac{\partial^l}{\partial_{a1} \partial_{a2} ... \partial_{al}} \frac{1}{|\boldsymbol{x} - \boldsymbol{z}_A|} = \frac{\partial^l}{\partial_{a1} \partial_{a2} ... \partial_{al}} \frac{1}{|\boldsymbol{r}|} \tag{2.14}$$

in spherical coordinates. Taking the trace yields:

$$\frac{\partial^l}{\partial_{a1} \partial_{a1} ... \partial_{al}} \frac{1}{|\boldsymbol{r}|} = \frac{\partial^l}{\partial_{a3} \partial_{a4} ... \partial_{al}} \nabla^2 \frac{1}{|\boldsymbol{r}|}. \tag{2.15}$$

Note that taking the trace is done by setting any two indices equal. The Laplacian in spherical coordinates is given by:

$$\nabla^2 \frac{1}{|\boldsymbol{r}|} = \frac{1}{r^2} \frac{\partial}{\partial r} \left(r^2 \frac{\partial}{\partial r} \frac{1}{|\boldsymbol{r}|} \right) + \frac{1}{r^2} \nabla_\theta^2 \frac{1}{|\boldsymbol{r}|} = 0, \tag{2.16}$$

where $|\boldsymbol{r}| = r$. This holds for all points outside the body A. We can therefore conclude that $\partial_L |\boldsymbol{x} - \boldsymbol{z}_A|^{-1}$ is trace-free. Note that this result holds true for any choice of origin of the coordinate system. The derivatives project out only the trace-free part of the potential. We can therefore define the Newtonian mass multipole moments as:

$$M_A = \int_A d^3x \rho_A(t, \boldsymbol{x}), \quad Q_A^L = \int_A d^3x \rho_A(t, \boldsymbol{x}) (x - z_A)^{<L>}, \tag{2.17}$$

where the $< L >$ notation denotes the symmetric trace-free projection of the tensor, and write the potential in terms of these multipole moments:

$$U_A(t, \boldsymbol{x}) = \frac{M_A}{|\boldsymbol{x} - \boldsymbol{z}_A|} + \sum_{\ell=2}^{\infty} \frac{(-1)^\ell}{\ell!} Q_A^L \partial_L \frac{1}{|\boldsymbol{x} - \boldsymbol{z}_A|}. \tag{2.18}$$

Note that the mass dipole $\ell = 1$ term has been omitted from the expansion. The spherical symmetry of the system enforces that this term can always be made to vanish by choosing the reference point z_A to be the center of mass of the system. The derivatives can be further evaluated. We will do this by evaluating the first three terms and using the generated pattern to set up a general expression. We will denote $|\boldsymbol{x} - \boldsymbol{z}_A|^{-1}$ as $|\boldsymbol{r}|^{-1}$ for convenience and we will use the notation $\boldsymbol{r} = |\boldsymbol{r}| \hat{\boldsymbol{n}} = r \hat{\boldsymbol{n}}$. The derivatives of r and $\hat{\boldsymbol{n}}$ are given by:

$$\begin{aligned} \partial_i r &= \partial_i (x_j x_j)^{1/2} = \frac{1}{2} (x_k x_k)^{-1/2} \partial_i (x_j x_j) = \frac{1}{2r} 2 x_j \delta_{ij} = \frac{x_i}{r} = \hat{n}_i \\ \partial_i \hat{n}_j &= \partial_i \left(\frac{x_j}{r} \right) = \frac{\delta_{ij}}{r} - \frac{1}{r^2} x_j \partial_i r = \frac{1}{r} (\delta_{ij} - \hat{n}_i \hat{n}_j). \end{aligned} \tag{2.19}$$

The first three derivative terms of the expansion are then given by:

$$\begin{aligned}
\partial_i\left(\frac{1}{r}\right) &= -\frac{1}{r^2}\hat{n}_i \\
\partial_i\partial_j\left(\frac{1}{r}\right) &= \frac{3}{r^3}\hat{n}_i\hat{n}_j - \frac{\delta_{ij}}{r^3} \\
\partial_i\partial_j\partial_k\left(\frac{1}{r}\right) &= -\frac{15}{r^4}\hat{n}_i\hat{n}_j\hat{n}_k + \frac{3}{r^4}\Big(\hat{n}_i\delta_{jk} + \hat{n}_j\delta_{ik} + \hat{n}_k\delta_{ij}\Big).
\end{aligned} \tag{2.20}$$

Note that the tracelessness is manifest in these expressions. The general formula, which can be proven by induction, is given by:

$$\frac{\partial^\ell}{\partial_{a1}\partial_{a2}...\partial_{a\ell}}\frac{1}{|\boldsymbol{x}-\boldsymbol{z}_A|} = \frac{(-1)^\ell(2\ell-1)!!}{|\boldsymbol{x}-\boldsymbol{z}_A|^{\ell+1}}\hat{n}^{<L>}. \tag{2.21}$$

The potential can be written as:

$$U_A(t,\boldsymbol{x}) = \frac{M_A}{|\boldsymbol{x}-\boldsymbol{z}_A|} + \sum_{\ell=2}^{\infty}\frac{(2\ell-1)!!}{\ell!\,|\boldsymbol{x}-\boldsymbol{z}_A|^{\ell+1}}Q_A^L\hat{n}^{<L>}. \tag{2.22}$$

Note that the double factorial is defined as $n!! = n\cdot(n-2)\cdot(n-4)\cdot...\cdot 3\cdot 1$ for odd n. We have seen earlier that Q_A^L is an STF-tensor, which is invariant under rotations. Therefore there exists a one-to-one mapping to spherical harmonics of order ℓ. More technically stated: The set of all symmetric trace-free tensors of rank ℓ generates an irreducible representation of the rotation group of weight ℓ, hence there exists a one-to-one mapping between them and the spherical harmonics of order ℓ [35]. We want to make this mapping explicit, for which we will follow the discussion of [35] and [19]. We can define the spherical-harmonic multipole moments in terms of the Cartesian multipole moments as:

$$Q_{\ell m}^A = \frac{4\pi}{2\ell+1}y_L^{\ell m*}Q_A^L, \tag{2.23}$$

where $y_L^{\ell m}$ are complex STF-tensors with constant complex coefficients discussed in more detail below, and the *-operator is the complex conjugation operator. The inverse can be found by projecting with $y_L^{'}$ and summing over m':

$$Q_A^L = \frac{\ell!}{(2\ell-1)!!}\sum_{m=-\ell}^{\ell}Q_{\ell m}^A y_L^{\ell m}. \tag{2.24}$$

Where we can see that the conversion between unit vectors $\hat{\boldsymbol{n}}$ and spherical harmonics gives rise to the conversion factor $y_L^{\ell m}$. The conversion is given by:

$$Y_{\ell m} = y_L^{\ell m}\hat{n}^{<L>}, \tag{2.25}$$

which can be inverted as:

$$\hat{n}^{<L>} = \frac{4\pi\ell!}{(2\ell+1)!!}\sum_{m=-\ell}^{\ell}y_L^{\ell m}Y_{\ell m}^*. \tag{2.26}$$

The explicit form of the conversion factor will be omitted here but can be found in [35] and [19]. Finally, plugging the spherical-harmonic expansion of Q_A^L into the potential U_A yields:

$$\begin{aligned}
U_A(t,\boldsymbol{x}) &= \frac{M_A}{|\boldsymbol{x}-\boldsymbol{z}_A|} + \sum_{\ell=2}^{\infty}\sum_{m=-\ell}^{\ell}\frac{(2\ell-1)!!}{\ell!\,|\boldsymbol{x}-\boldsymbol{z}_A|^{\ell+1}}\frac{\ell!}{(2\ell-1)!!}Q_{\ell m}^A y_L^{\ell m}\hat{n}^{<L>} \\
&= \frac{M_A}{|\boldsymbol{x}-\boldsymbol{z}_A|} + \sum_{\ell=2}^{\infty}\sum_{m=-\ell}^{\ell}\frac{Q_{\ell m}^A}{|\boldsymbol{x}-\boldsymbol{z}_A|^{\ell+1}}Y_{\ell m}.
\end{aligned} \tag{2.27}$$

Here the spherical harmonics $Y_{lm}(\theta, \phi)$ are generally given as a function of spherical coordinates $(x - z_A)^i / |\boldsymbol{x} - \boldsymbol{z}_A| = (\sin\theta\cos\phi, \sin\theta\sin\phi, \cos\theta)$.

Consider now a binary system of bodies A and B in orbit around each other. The potential because of external sources that is felt by body A is given by U_A^{ext} and can be written as a Taylor expansion:

$$U_A^{ext}(t, \boldsymbol{x}) = \sum_{\ell=0}^{\infty} \frac{1}{\ell!}(x - z_A)^L \left(\frac{\partial}{\partial x^L} U_A^{ext}(t, \boldsymbol{x}) \right) \Big|_{\boldsymbol{x}=\boldsymbol{z_A}}. \tag{2.28}$$

In a binary system, the source of the potential is the potential of body B given by U_B. The tidal moments of body A can be defined in terms of the external potential and thus in terms of the potential of body B:

$$\mathcal{E}_A^L = -\left(\frac{\partial}{\partial x^L} U_B(t, \boldsymbol{x}) \right) \Big|_{\boldsymbol{x}=\boldsymbol{z_A}}. \tag{2.29}$$

The external potential can therefore be written as:

$$U_A^{ext}(t, \boldsymbol{x}) = -\sum_{\ell=0}^{\infty} \frac{1}{\ell!}(x - z_A)^L \mathcal{E}_A^L. \tag{2.30}$$

Now that we have derived an expression for the self-gravitational potential of an isolated body A as a spherical harmonic expansion and have shown that we can state the potential from the presence of an external body as an expansion of the tidal moments, we are ready to summarise the dynamics by an action principle, which was ultimately the goal of this section. In classical mechanics the Lagrangian is given by $\mathcal{L} = T - V$, where T is the total kinetic energy of the system and V the total potential energy of the system. The kinetic energy of body A will be given by:

$$T_A = \frac{1}{2} \int_A d^3x \rho_A(t, \boldsymbol{x}) \dot{z_A}^2 + T_A^{int}, \tag{2.31}$$

where T_A^{int} is the internal contribution of the body that comes from the body not being a point mass [36]. The potential energy of body A is given by:

$$V_A = -\frac{1}{2} \int_A d^3x \rho_A(t, \boldsymbol{x}) U_B(t, \boldsymbol{x}) + V_A^{int}, \tag{2.32}$$

where we can again see an internal contribution. We will now assume body A to be an extended body and body B to be a point mass. The total kinetic energy can easily be calculated since z_A only depends on time:

$$T = T_A + T_B = \frac{1}{2} M_A \dot{z_A}^2 + T_A^{int} + \frac{1}{2} M_B \dot{z_B}^2. \tag{2.33}$$

It is useful to transform this expression to a barycentric frame, i.e. a frame where the center of mass coincides with the origin. In a barycentric frame we have:

$$\boldsymbol{r} = \boldsymbol{z}_A - \boldsymbol{z}_B, \quad M_A \boldsymbol{z}_A + M_B \boldsymbol{z}_B = 0, \tag{2.34}$$

from which immediately follows:

$$\boldsymbol{z}_A = \frac{M_B}{M_A + M_B} \boldsymbol{r}, \quad \boldsymbol{z}_B = -\frac{M_A}{M_A + M_B} \boldsymbol{r}. \tag{2.35}$$

The total kinetic energy is then given by:

$$\begin{aligned} T &= \frac{1}{2} \frac{M_A M_B^2}{(M_A + M_B)^2} \dot{r}^2 + \frac{1}{2} \frac{M_B M_A^2}{(M_A + M_B)^2} \dot{r}^2 + T_A^{int} \\ &= \frac{1}{2} \frac{M_A M_B (M_A + M_B)}{(M_A + M_B)^2} \dot{r}^2. \end{aligned} \tag{2.36}$$

We will now introduce the reduced mass as $\mu = M_A M_B/(M_A + M_B)$, the total mass as $M = M_A + M_B$ and the velocity as $v^2 = \dot{r}^2$, such that the total kinetic energy in the barycentric frame is given by:

$$T = \frac{1}{2}\mu v^2 + T_A^{int}. \tag{2.37}$$

We can see that in the barycentric frame the kinetic energy of a binary system reduces to the kinetic energy of a one-body system with mass μ. For the total potential energy, we have to be a bit more careful since only body A is an extended body. The total potential energy is therefore given by:

$$V = V_A + V_B = -\frac{1}{2}\int_A d^3x \rho_A(t,\boldsymbol{x}) U_B(t,\boldsymbol{x}) + V_A^{int} - \frac{1}{2}\int_B d^3x \rho_B(t,\boldsymbol{x}) U_A(t,\boldsymbol{x}) \delta(\boldsymbol{x} - \boldsymbol{z}_B). \tag{2.38}$$

For the V_A integral we can use the expression for $U_B = U_A^{ext}$ we derived earlier such that we have:

$$\begin{aligned} V_A &= -\frac{1}{2}\int_A d^3x \rho_A(t,\boldsymbol{x}) U_B(t,\boldsymbol{z}_A) + \frac{1}{2}\int_A d^3x \rho_A(t,\boldsymbol{x}) \sum_{\ell=2}^{\infty} \frac{1}{\ell!}(x - z_A)^L \mathcal{E}_A^L + V_A^{int} \\ &= -\frac{1}{2}\frac{M_A M_B}{|\boldsymbol{z}_A - \boldsymbol{z}_B|} + \frac{1}{2}\sum_{\ell=0}^{\infty}\frac{1}{\ell!} Q_A^L \mathcal{E}_A^L + V_A^{int}. \end{aligned} \tag{2.39}$$

Here the mass dipole moment again vanishes. For the V_B integral we can use the STF form of the self-gravitational potential, such that we have:

$$V_B = -\frac{1}{2}\frac{M_B M_A}{|\boldsymbol{z}_B - \boldsymbol{z}_A|} - \frac{1}{2} M_B \sum_{\ell=2}^{\infty} \frac{(2\ell-1)!!}{\ell!\,|\boldsymbol{z}_B - \boldsymbol{z}_A|^{\ell+1}} Q_A^L \hat{n}^{<L>}. \tag{2.40}$$

For systems where the separation between the bodies is large compared to the characteristic size of the bodies the tidal moments are given by:

$$\begin{aligned} \mathcal{E}_A^L &= -\left(\frac{\partial}{\partial x^L} U_B(t,\boldsymbol{x})\right)\Big|_{\boldsymbol{x}=\boldsymbol{z}_A} \\ &= -\left(\frac{\partial}{\partial x^L}\frac{M_B}{|\boldsymbol{x} - \boldsymbol{z}_B|}\right)\Big|_{\boldsymbol{x}=\boldsymbol{z}_A} \\ &= -(-1)^\ell (2\ell-1)!! \frac{\hat{n}^{<L>}}{|\boldsymbol{z}_A - \boldsymbol{z}_B|^{\ell+1}} M_B. \end{aligned} \tag{2.41}$$

Naively one could now write the potential energy V_B in terms of the tidal moments and one would think that the tidal moments of V_A cancel against the tidal moments of V_B. We have to be careful though, in the expression of V_B the unit vector $\hat{n}^{<L>} = \hat{n}_{i1}...\hat{n}_{i\ell}$ has its components given by:

$$\hat{n}^i = \frac{z_B^i - z_A^i}{r}, \tag{2.42}$$

while in the expression of $\mathcal{E}_A^L$ the components are given by:

$$\hat{n}^i = \frac{z_A^i - z_B^i}{r}, \tag{2.43}$$

such that $\hat{n}_{AB}^{<L>} = \hat{n}_{BA}^{<L>}$ when ℓ is even and $\hat{n}_{AB}^{<L>} = -\hat{n}_{BA}^{<L>}$ when ℓ is odd. The meaning of the subscript notation is the obvious. The potential energy of body A then becomes:

$$V_B = -\frac{1}{2}\frac{M_B M_A}{|\boldsymbol{z}_B - \boldsymbol{z}_A|} + \frac{1}{2}\sum_{\ell=2}^{\infty}\frac{1}{\ell!} Q_A^L \mathcal{E}_A^L, \tag{2.44}$$

such that the total potential energy in the barycentric frame is given by:

$$V = -\frac{\mu M}{r} + \sum_{\ell=2}^{\infty} \frac{1}{\ell!} Q_A^L \mathcal{E}_A^L + V_A^{int}. \tag{2.45}$$

The first term represents the potential energy of the binary system as if the bodies were point masses. We can see that in the barycentric frame, the potential energy of a binary system reduces to that of the potential energy of a binary system of bodies with masses μ and M. The second term gives the tidal corrections because of body A being an extended body. The Lagrangian can be split up into a part that describes the orbital motion of point masses, a part that describes the tidal corrections and a part that describes the internal dynamics of the multipole moments that we will leave unspecified for now. The total action is now given by:

$$\begin{aligned} S = \int dt \mathcal{L} &= \int dt \left[\frac{1}{2}\mu v^2 + \frac{\mu M}{r} - \sum_{\ell=2}^{\infty} \frac{1}{\ell!} Q_A^L \mathcal{E}_A^L + \mathcal{L}^{int} \right] \\ &= S_{orbit} + \int dt \left[- \sum_{\ell=2}^{\infty} \frac{1}{\ell!} Q_A^L \mathcal{E}_A^L + \mathcal{L}^{\text{int}} \right]. \end{aligned} \tag{2.46}$$

We have the dynamics of the binary system encapsulated in a single scalar function. While an advantage on its own, the main advantage of all this preparation is that the formalism carries easily over to a general relativistic description of the system, which will be explored later.

We will now let go of the specifics of a system with two bodies but will instead focus on the case of a spherically symmetric body in isolation whose multipole moments result from the response to the companion's tidal field. The internal Lagrangian depends on the type of body considered. The body of our interest is a neutron star. For now, we will not work through the derivation of the internal Lagrangian of a neutron star but merely post the result:

$$\mathcal{L}^{\text{int}} = \sum_{\ell=2}^{\infty} \frac{1}{2\ell! \lambda_\ell \omega_{0\ell}^2} \left[\dot{Q}_L \dot{Q}^L - \omega_{0\ell}^2 Q_L Q^L \right]. \tag{2.47}$$

Here $\omega_{0\ell}$ denote the fundamental-mode (f-mode) frequencies. The parameters λ_ℓ are the tidal deformability coefficients. An explicit derivation can be found in [37]. We can however, reason where this Lagrangian comes from and why it should be there. Just like a bridge has an f-mode frequency, which can be excited by a large group of people all walking in the same frequency on it; just like a kid on a swing has an f-mode frequency which can be excited by its parent pushing in just the right frequency; just like the tidal waves in the ocean have an f-mode frequency, which can be excited by a bay or an inlet having just the right length such that the tidal wave's resonance frequency is excited; á compact object like a neutron star has an f-mode frequency, which can be excited by an external object orbiting it at just the right frequency. To be a bit more precise: the f-mode frequency, in this case, is the f-mode frequency of the multipole moments of the neutron star. This means that the mass distribution of the neutron star has a preferred frequency in which it wants to oscillate. An orbiting object like a companion black hole lets the mass distribution of the neutron star oscillate. It would therefore also be possible for the black hole to orbit at exactly the right frequency such that the f-modes are excited. At this point, resonance would occur and the tidal disruption process would be enhanced. This resonance process is what is encapsulated in the internal Lagrangian and $\omega_{0\ell}$ is exactly this preferred frequency in which the mass distribution wants to oscillate. It should therefore come as no surprise that the given internal Lagrangian has the form of a Lagrangian that describes a harmonic oscillator. This is illustrated in Box 2.

Box 2: Neutron Star as a Harmonic Oscillator

The internal Lagrangian of a neutron star

$$\mathcal{L}^{\rm int} = \sum_{\ell=2}^{\infty} \frac{1}{2\ell!\lambda_\ell \omega_{0\ell}^2}\left[\dot{Q}_L\dot{Q}^L - \omega_{0\ell}^2 Q_L Q^L\right] \tag{2.48}$$

is analogous to a simple harmonic oscillator with

$$\mathcal{L} = T - V = \frac{1}{2}m\dot{x}^2 - \frac{1}{2}kx^2 = \frac{1}{2\lambda\omega^2}\left(\dot{x}^2 - \omega^2 x^2\right) \tag{2.49}$$

with $k/m = \omega^2$ and $k = 1/(\ell!\lambda_\ell)$, where the factor $\ell!$ comes from the definition of the tidal deformability.

In a simple harmonic oscillator x represents the deviation from equilibrium. A force that brings the system out of equilibrium will induce an oscillating x. The amplitude of the oscillation will be magnified close to its f-mode frequency. Completely analogous, the neutron star's multipole moments describe the deformation from spherical symmetry, in this case, induced by mass density perturbations from the presence of a companion. Mass density perturbations that bring the neutron star away from spherical symmetry will therefore induce an oscillating Q_L. Oscillations close to the f-mode frequency will be magnified because of resonance. Therefore in this example $x^2 \to \sum_\ell Q_L Q^L$ [38].

2.4 Adiabatic Tides

We have set up the total action of the system - we will talk about spin interactions later - and now want to find a solution for the multipole moments of the neutron star. We will later also derive an expression of the energy of the system. This section is not based on any literature and can therefore be seen as a result of this thesis. From this point, we will also specialise to an NSBH system again, and the A and B subscripts will be NS and BH subscripts.

We can define λ_ℓ by considering Q^L as our dynamical field and varying the action w.r.t. Q^L. We will start by considering the adiabatic limit, the limit where the body's internal dynamics have enough time to equilibrate to the tidal field, i.e. where the internal timescales $\tau^{int} \sim \sqrt{R_{\rm NS}^3/M_{\rm NS}}$ are fast compared to the time scale of variations in the tidal field $\tau_{orb} \sim \sqrt{r^3/M}$. The adiabatic limit is the simplest way of considering the tidal effects of an NSBH binary and therefore works as a didactic tool to familiarise ourselves with the system at hand and the different calculations involved. Once we have set up a description of adiabatic tides, we will move on to dynamic tides where we let go of the adiabatic limit. The calculations involving dynamic tides are also of instructive nature and will therefore be presented in full glory before we move on to add more effects to our description of the system. A full description will consist of extra couplings of the different angular momenta of the bodies to the tidal bulge of the neutron star. The calculations for a full description again require a different approach which will be presented at the end of this chapter.

The action with the internal Lagrangian included is given by:

$$S = S_{orbit} + \int dt \sum_{\ell=2}^{\infty}\left[-\frac{1}{\ell!}Q_L\mathcal{E}^L + \frac{1}{2\ell!\lambda_\ell\omega_{0\ell}^2}\left[\dot{Q}_L\dot{Q}^L - \omega_{0\ell}^2 Q_L Q^L\right]\right]. \tag{2.50}$$

We derived this action for the Newtonian case. In this form however, it can be straightforwardly generalised to a relativistic action. The equivalence principle states that locally the

relativistic and the Newtonian action should match. The coefficients in the action that contain the strong field parameters characterising the details of how the neutron star responds to the tidal perturbation, e.g. the tidal deformability parameter λ_ℓ and the f-mode frequencies $\omega_{0\ell}$, come from the full GR description and therefore do not represent Newtonian versions of these quantities.

In the adiabatic limit $\dot{Q}_L = 0$. The variation of the action (2.50) is given by.

$$\frac{\delta S}{\delta Q^L} = -\frac{1}{\ell!}\mathcal{E}_L - \frac{1}{\ell!\lambda_\ell}Q_L = 0. \tag{2.51}$$

The tidal deformability coefficients characterise the equation-of-state dependent ratio between the induced multipole moments and the tidal field as a linear response relation:

$$Q_L^{\text{adiab}} = -\lambda_\ell \mathcal{E}_L, \tag{2.52}$$

which is the solution for the multipole moments of the neutron star in the adiabatic case.

We mentioned before that in the action (2.50) the quantities λ_ℓ and $\omega_{0\ell}$ are computed from the full GR description. Quantities at the orbital scale however, like the explicit expressions for the tidal moments given below, can at large orbital separations be approximated by their Newtonian result to leading order.

The expression for the tidal moments is given by (2.41) and can be evaluated up to quadrupole order as:

$$\begin{aligned}\mathcal{E}_{ij} &= -\left(\partial_i\partial_j\frac{1}{r}\right)M_{\text{BH}} \\ &= -\left(\frac{3}{r^3}\hat{n}_i\hat{n}_j - \frac{\delta_{ij}}{r^3}\right)M_{\text{BH}}.\end{aligned} \tag{2.53}$$

Using the unit vector $\hat{\boldsymbol{n}}$ in spherical coordinates:

$$\hat{\boldsymbol{n}} = \sin\theta\cos\phi\hat{\boldsymbol{e}}_x + \sin\theta\sin\phi\hat{\boldsymbol{e}}_y + \cos\theta\hat{\boldsymbol{e}}_z, \tag{2.54}$$

we can explicitly write down the tidal moment matrix in the equatorial plane as:

$$\mathcal{E}_{ij} = -\begin{pmatrix} \frac{1}{2r^3} + \frac{3\cos 2\phi}{2r^3} & \frac{3\sin 2\phi}{2r^3} & 0 \\ \frac{3\sin 2\phi}{2r^3} & \frac{1}{2r^3} - \frac{3\cos 2\phi}{2r^3} & 0 \\ 0 & 0 & -\frac{1}{r^3} \end{pmatrix} M_{\text{BH}}. \tag{2.55}$$

Note that this matrix is manifestly symmetric and trace-free, as expected. With the linear response relation between the quadrupole moment of the neutron star and the tidal moment, we have an explicit expression for the quadrupole moment of the neutron star.

Now that we have found the first meaningful solution to the NSBH binary system, it is a good moment to reflect on what we have done and what this solution actually means. We have seen that the gravitational potential generated by some mass distribution can be expressed as a multipole expansion. We have given the expansion as a Cartesian multipole expansion, which is a series of STF-tensors, and as a spherical harmonics expansion. Furthermore, we have seen that the potential induced by external sources that is felt by a neutron star can be written as a Taylor expansion where the tidal moments tensor is given by the derivatives of the potential in the expansion. Up to quadrupole order, the tidal moments tensor can be evaluated, as is done above. This allows us to evaluate the quadrupole moment tensor using the linear response relation between the tidal quadrupole moment tensor and the quadrupole moment tensor, which yields:

$$Q_{ij} = \lambda_2\begin{pmatrix} \frac{1}{2r^3} + \frac{3\cos 2\phi}{2r^3} & \frac{3\sin 2\phi}{2r^3} & 0 \\ \frac{3\sin 2\phi}{2r^3} & \frac{1}{2r^3} - \frac{3\cos 2\phi}{2r^3} & 0 \\ 0 & 0 & -\frac{1}{r^3} \end{pmatrix} M_{\text{BH}}. \tag{2.56}$$

For our approximation of adiabatic tidal effects, the only generators of a non-zero quadrupole moment, are the tidal effects from the presence of a companion black hole, illustrated by the simple linear response relation. The quadrupole moment tensor gives the mass deformation away from spherical symmetry of the neutron star. In this case, this mass deformation is only because of tidal effects and comes from the tidal deformation field of the black hole. This is exactly the same tidal displacement field that we derived in section 2.2 where we named it the differential tidal force given by (2.3). This shows us that truncating up to quadrupole order is analogous to the truncation scheme used in section 2.2. The quadrupole tensor given above is evaluated in the body frame of the neutron star. The ϕ-coordinate gives the angle of the black hole with the x-axis. For example for $\phi = 0$ we can see that the deformation of the neutron star on the x-axis is given by $\frac{2\lambda_2 M_{\rm BH}}{r^3}\hat{\boldsymbol{e}}_x$, which can be found by multiplying the first row or column with $(\hat{\boldsymbol{e}}_x, \hat{\boldsymbol{e}}_y, \hat{\boldsymbol{e}}_z)$. Note that by the deformation on the x-axis we mean the deformation of the neutron star where the x-axis intersects the surface of the neutron star. The deformation of the neutron star on the y-axis is given by $-\frac{\lambda_2 M_{\rm BH}}{r^3}\hat{\boldsymbol{e}}_y$. Note that this is equal to (2.3) with $\theta = 0$, up to the difference of the tidal deformability parameter that has not been taken into account in section 2.2. Through the tidal deformability parameter, the radius of the neutron star comes into the equation. In Figure 2.6 the tidal displacement field is visualised, which can be done by letting the black hole orbit the neutron star and extrapolating the displacements back to the frame of the neutron star.

We can use the action to derive an expression for the energy of the system. The linear response relation (2.52) allows us to write the action for adiabatic motion as:

$$\begin{aligned} S_{\rm adiab} &= S_{orbit} + \int dt \sum_{\ell=2}^{\infty} \left[-\frac{1}{\ell!} Q_L^{\rm adiab} \mathcal{E}^L - \frac{1}{2\ell!\lambda_\ell} Q_L^{\rm adiab} Q_L^{\rm adiab} \right] \\ &= S_{orbit} + \int dt \sum_{\ell=2}^{\infty} \left[\frac{\lambda_\ell}{2\ell!} \mathcal{E}_L \mathcal{E}^L \right]. \end{aligned} \tag{2.57}$$

Note that we do not yet have to work up to only quadrupole order since the linear response relation (2.52) for adiabatic motion allows us to write the mass multipole moments in terms of the tidal moments. Using the explicit expression of the tidal moments $\mathcal{E}^L$ (2.41) we can write the action as:

$$S_{\rm adiab} = S_{orbit} + \int dt \sum_{\ell=2}^{\infty} \left[\frac{\lambda_\ell}{2\ell!} \left[(2\ell-1)!!\right]^2 \frac{\hat{n}^{<L>}\hat{n}_{<L>}}{r^{2(\ell+1)}} M_{\rm BH}^2 \right], \tag{2.58}$$

where the contraction of two STF-tensors is given by:

$$\hat{n}_{<L>}\hat{n}^{<L>} = \frac{\ell!}{(2\ell-1)!!}, \tag{2.59}$$

such that we have:

$$S_{\rm adiab} = S_{orbit} + \int dt \sum_{\ell=2}^{\infty} \left[\frac{(2\ell-1)!!\lambda_\ell}{2r^{2(\ell+1)}} M_{\rm BH}^2 \right]. \tag{2.60}$$

For motion in the equatorial plane, in which $v^2 = \dot{r}^2 + r^2\dot{\phi}^2$ in spherical coordinates, the action is given by:

$$S_{\rm adiab} = \int dt \left[\frac{1}{2}\mu\dot{r}^2 + \frac{1}{2}\mu r^2\dot{\phi}^2 + \frac{\mu M}{r} + \sum_{\ell=2}^{\infty} \frac{(2\ell-1)!!\lambda_\ell}{2r^{2(\ell+1)}} M_{\rm BH}^2 \right]. \tag{2.61}$$

The Euler-Lagrange equation for ϕ is given by:

$$\frac{d}{dt}\frac{\partial \mathcal{L}}{\partial \dot{\phi}} - \frac{\partial \mathcal{L}}{\partial \phi} = \frac{d}{dt}\left[\mu r^2\dot{\phi}\right] = 2\mu r\dot{r}\dot{\phi} + \mu r^2\ddot{\phi} = 0, \tag{2.62}$$

and for r:

$$\frac{d}{dt}\frac{\partial \mathcal{L}}{\partial \dot{r}} - \frac{\partial \mathcal{L}}{\partial r} = \mu\ddot{r} - \mu r\dot{\phi}^2 + \frac{\mu M}{r^2} + \sum_{\ell=2}^{\infty} \frac{(\ell+1)(2\ell-1)!!\lambda_\ell}{r^{2\ell+3}} M_B^2 = 0. \tag{2.63}$$

For stable circular orbits, i.e. when $\dot{r} = \ddot{r} = 0$ we can immediately conclude from the ϕ Euler-Lagrange equation that $\dot{\phi} =$ constant. We will therefore define the orbital frequency as $\dot{\phi} = \Omega$. For stable circular orbits the r Euler-Lagrange equation becomes:

$$-\mu r\Omega^2 + \frac{\mu M}{r^2} + \sum_{\ell=2}^{\infty} \frac{(\ell+1)(2\ell-1)!!\lambda_\ell}{r^{2\ell+3}} M_{\rm BH}^2 = 0. \tag{2.64}$$

The final term represents the tidal correction to the circular motion. We want to solve this equation for r. We can see that the tidal correction scales with at least r^{-7} for widely separated bodies. We will therefore work to linear order in the tidal effects: $r = r_0(1+\delta_r)$, where the δ_r represents the tidal correction. For no tidal corrections, the final term just vanishes, and the above equation reduces to Kepler's third law, which allows us to solve for r_0:

$$r_0 = \frac{M^{1/3}}{\Omega^{2/3}}. \tag{2.65}$$

Dividing the r equation of motion by μr and expanding to linear order in the tidal effects yields the following equation for the linear tidal corrections:

$$-3\delta_r \frac{M}{r_0^3} + \sum_{\ell=2}^{\infty} \frac{(\ell+1)(2\ell-1)!!\lambda_\ell}{\mu r_0^{2\ell+4}} M_{\rm BH}^2 = 0. \tag{2.66}$$

Note that the tidal correction term was already linear in the tidal effects, and we could therefore just replace r with r_0. Also, note that the Ω^2 term has no tidal contribution such that at linear order in the tidal contributions this term vanishes. Substituting Kepler's third law for r_0 and solving for δ_r gives for the linear order tidal corrections:

$$\delta_r = \sum_{\ell=2}^{\infty} \frac{(\ell+1)(2\ell-1)!!\lambda_\ell}{3M\mu\left(M^{1/3}\Omega^{-2/3}\right)^{2\ell+1}} M_{\rm BH}^2. \tag{2.67}$$

The stable circular orbit radius as a function of the orbital frequency is given by:

$$r(\Omega) = \frac{M^{1/3}}{\Omega^{2/3}} + \sum_{\ell=2}^{\infty} \frac{(\ell+1)(2\ell-1)!!\lambda_\ell}{3M\mu\left(M^{1/3}\Omega^{-2/3}\right)^{2\ell}} M_{\rm BH}^2. \tag{2.68}$$

Here we can see that the tidal effects come in as a correction to Kepler's third law. Now that we have the radius as a function of the orbital frequency, we also want to find an expression for the energy of the system as a function of Ω. The energy of the system for motion in the equatorial plane for stable circular orbits can be immediately read of the action, i.e. switch the sign of all non-kinetic terms and is given by:

$$E = \frac{1}{2}\mu r^2\Omega^2 - \frac{\mu M}{r} - \sum_{\ell=2}^{\infty} \frac{(2l-1)!!\lambda_\ell}{2r^{2(\ell+1)}} M_{\rm BH}^2. \tag{2.69}$$

We will again assume the tidal corrections to be small and expand to linear order in the tidal corrections:

$$E = \frac{1}{2}\mu r_0^2\Omega^2(1+2\delta_r) - \frac{\mu M}{r_0}(1-\delta_r) - \sum_{\ell=2}^{\infty} \frac{(2\ell-1)!!\lambda_\ell}{2r_0^{2(\ell+1)}} M_{\rm BH}^2, \tag{2.70}$$

where we can now substitute the known results for r_0 and δ_r to yield the final expression for the energy of the system for adiabatic motion in the equatorial plane as a coordinate invariant

expression:

$$E(\Omega) = \frac{1}{2}\mu(M^{1/3}\Omega^{-2/3})^2\Omega^2 + \sum_{\ell=2}^{\infty} \frac{\Omega^2(\ell+1)(2\ell-1)!!\lambda_\ell}{3M\big(M^{1/3}\Omega^{-2/3}\big)^{2\ell-1}} M_{\rm BH}^2 - \frac{\mu M}{M^{1/3}\Omega^{-2/3}}$$
$$+ \sum_{\ell=2}^{\infty} \frac{(\ell+1)(2\ell-1)!!\lambda_\ell}{3\big(M^{1/3}\Omega^{-2/3}\big)^{2\ell+2}} M_{\rm BH}^2 - \sum_{\ell=2}^{\infty} \frac{(2\ell-1)!!\lambda_\ell}{2(M^{1/3}\Omega^{-2/3})^{2(\ell+1)}} M_{\rm BH}^2$$
$$= -\frac{1}{2}\mu\big(M\Omega\big)^{2/3} + \sum_{\ell=2}^{\infty} \frac{\lambda_\ell M_{\rm BH}^2}{(M^{1/3}\Omega^{-2/3})^{2(\ell+1)}} \left[\frac{2}{3}(\ell+1)(2\ell-1)!! - \frac{1}{2}(2\ell-1)!!\right]. \quad (2.71)$$

Here we can again see that the finite size effects come in as a correction to the energy of a system given by point masses. For now, we have derived expressions for all the quantities that we need to describe the system, namely the energy of the system and the quadrupole moment. These expressions can be found up to quadrupole order in the literature, higher order quadrupole moments are usually negelected in the literature and this result can therefore be used as reference. In the next section we will let go of the adiabatic approximation and we will therefore also have to let go of keeping higher quadrupole moment terms.

2.5 Dynamic Tides

For the early inspiral, we have seen that the internal structure of the neutron star depends only on the tidal deformability parameters λ_ℓ. For the final phase of the inspiral, we have to let go of the adiabatic approximation, since when the orbital motion approaches the resonance frequency it no longer holds, i.e. we can no longer set $\dot{Q}_L = 0$. Note that this is true for the f-modes, higher modes can be excited early in the inspiral. The f-mode has the greatest influence on the dynamics of the system however, and therefore the effect of the higher modes is neglected. Before we move to a complete description of the system, we will analyse the dynamic case, which is given by the same Lagrangian as the adiabatic case but this time without $\dot{Q}_L = 0$. We will start with this Lagrangian without the addition of any other effects because it is instructive to see the calculations involved. The addition of the extra terms requires another approach to solve the system. It will be valuable to the reader to have seen all the different methods available. The approach in this section is similar to the approach discussed in [39]. The results for the circular orbit radius and the energy are independently derived results of this thesis that agree with existing literature [40]. We can make use of the total action (2.50) to find the equation of motion for the dynamical field Q^L. The Euler-Lagrange equation gives us:

$$\frac{d}{dt}\frac{\partial \mathcal{L}}{\partial \dot{Q}_L} - \frac{\partial \mathcal{L}}{\partial Q_L} = \frac{\ddot{Q}_L}{\omega_{0\ell}^2} + Q_L = -\lambda_\ell \mathcal{E}_L. \quad (2.72)$$

We no longer have the simple linear response relation between the multipole moments and the tidal moments of the neutron star, but instead, we have a tensorial differential equation. Until this point, we could include the higher multipole moments without extra work, but from this point onward, the equations will simplify greatly when we only consider the quadrupole moment. We will therefore start by considering the above differential equation for the quadrupole moment Q_{ij} and tidal quadrupole moment $\mathcal{E}_{ij}$. In a differential equation with matrices, all the components should also separately obey the differential equation. We know that Q_{ij} and $\mathcal{E}_{ij}$ are symmetric and trace-free, and we also know the components of $\mathcal{E}_{ij}$ explicitly. We can use this information to constrain the components of Q_{ij}. We will parametrise Q_{ij} to be of the same form as the tidal quadrupole moment, namely in the form:

$$Q_{ij} = \begin{pmatrix} a+b & c & 0 \\ c & a-b & 0 \\ 0 & 0 & -2a \end{pmatrix}. \quad (2.73)$$

The equation of motion for the field Q_{ij} can therefore be written as:

$$\frac{1}{\omega_{02}^2}\begin{pmatrix} \ddot{a}+\ddot{b} & \ddot{c} & 0 \\ \ddot{c} & \ddot{a}-\ddot{b} & 0 \\ 0 & 0 & -2\ddot{a} \end{pmatrix}+\begin{pmatrix} a+b & c & 0 \\ c & a-b & 0 \\ 0 & 0 & -2a \end{pmatrix}=\lambda_2\begin{pmatrix} \frac{1}{2r^3}+\frac{3\cos 2\phi}{2r^3} & \frac{3\sin 2\phi}{2r^3} & 0 \\ \frac{3\sin 2\phi}{2r^3} & \frac{1}{2r^3}-\frac{3\cos 2\phi}{2r^3} & 0 \\ 0 & 0 & \frac{1}{r^3} \end{pmatrix} M_{\rm BH}. \tag{2.74}$$

Evaluating the different components of the the above differential equation gives us three equations for a, b and c:

$$\begin{Bmatrix} \ddot{a} \\ \ddot{b} \\ \ddot{c} \end{Bmatrix}+\omega_{02}^2\begin{Bmatrix} a \\ b \\ c \end{Bmatrix}=\omega_{02}^2\mathcal{A}\begin{Bmatrix} 1/3 \\ \cos(2\phi) \\ \sin(2\phi) \end{Bmatrix}. \tag{2.75}$$

Here we have defined the tidal force amplitude as:

$$\mathcal{A}=\frac{3\lambda_2 M_{\rm BH}}{2r^3}. \tag{2.76}$$

Note that the a-equation is obtained by adding the (11)-component of the equation of motion to the (22)-component, the b-equation is obtained by subtracting the (22)-component from the (11)-component and the c-equation is obtained by evaluating the (12)-component. It is also important to note that the radial coordinate r is not constant in time. The binary system inspirals because of gravitational damping. The linear system above can be solved using the method variation of parameters and with trigonometric identities [39].

$$\begin{aligned} \frac{2}{\omega_{02}}\begin{Bmatrix} b \\ c \end{Bmatrix} &= \cos(\omega_{02}t)\int dt\mathcal{A}\begin{Bmatrix} -\sin(2\phi+\omega_{02}t) \\ \cos(2\phi+\omega_{02}t) \end{Bmatrix} \\ &+\sin(\omega_{02}t)\int dt\mathcal{A}\begin{Bmatrix} \cos(2\phi+\omega_{02}t) \\ \sin(2\phi+\omega_{02}t) \end{Bmatrix} \\ &+\cos(\omega_{02}t)\int dt\mathcal{A}\begin{Bmatrix} \sin(2\phi-\omega_{02}t) \\ -\cos(2\phi-\omega_{02}t) \end{Bmatrix} \\ &+\sin(\omega_{02}t)\int dt\mathcal{A}\begin{Bmatrix} \cos(2\phi-\omega_{02}t) \\ \sin(2\phi-\omega_{02}t) \end{Bmatrix} \\ &+\begin{Bmatrix} c_1^b \\ c_1^c \end{Bmatrix}\cos(\omega_{02}t)+\begin{Bmatrix} c_2^b \\ c_2^c \end{Bmatrix}\sin(\omega_{02}t), \end{aligned} \tag{2.77}$$

with unspecified integration constants in the homogeneous solution (last two terms). Note that the phase coordinate ϕ is dependent on time through $\phi=\Omega t$. For $\Omega\sim\omega_{02}/2$ resonance will occur, for which we should be careful. For the moment we will consider the regime away from resonance. We will therefore also assume the boundary condition that the initial mode oscillations are zero, i.e. the integration constants are set to zero. Also, locally in time the gravitational damping can be neglected and $\mathcal{A}$ is constant in time. In this limit a is a static component and is given by $a=\mathcal{A}/3$. The integrals above can be evaluated to:

$$\begin{aligned} \frac{2}{\omega_{02}}\begin{Bmatrix} b \\ c \end{Bmatrix} &= \cos(\omega_{02}t)\frac{\mathcal{A}}{2\Omega+\omega_{02}}\begin{Bmatrix} \cos(2\phi+\omega_{02}t) \\ \sin(2\phi+\omega_{02}t) \end{Bmatrix} \\ &+\sin(\omega_{02}t)\frac{\mathcal{A}}{2\Omega+\omega_{02}}\begin{Bmatrix} \sin(2\phi+\omega_{02}t) \\ -\cos(2\phi+\omega_{02}t) \end{Bmatrix} \\ &+\cos(\omega_{02}t)\frac{\mathcal{A}}{2\Omega-\omega_{02}}\begin{Bmatrix} -\cos(2\phi-\omega_{02}t) \\ -\sin(2\phi-\omega_{02}t) \end{Bmatrix} \\ &+\sin(\omega_{02}t)\frac{\mathcal{A}}{2\Omega-\omega_{02}}\begin{Bmatrix} \sin(2\phi-\omega_{02}t) \\ -\cos(2\phi-\omega_{02}t) \end{Bmatrix}. \end{aligned} \tag{2.78}$$

Making use of trigonometric identities this can be written as:

$$\begin{Bmatrix} b \\ c \end{Bmatrix}=\frac{\mathcal{A}}{1-\frac{4\Omega^2}{\omega_{02}^2}}\begin{Bmatrix} \cos(2\phi) \\ \sin(2\phi) \end{Bmatrix}. \tag{2.79}$$

We can see that close to resonance this will diverge. Far away from resonance we now have solved the equation of motion for Q_{ij}. Q_{ij} is given by:

$$Q_{ij} = \mathcal{A} \begin{pmatrix} \frac{1}{3} + \frac{\cos(2\phi)}{1-\frac{4\Omega^2}{\omega_{02}^2}} & \frac{\sin(2\phi)}{1-\frac{4\Omega^2}{\omega_{02}^2}} & 0 \\ \frac{\sin(2\phi)}{1-\frac{4\Omega^2}{\omega_{02}^2}} & \frac{1}{3} - \frac{\cos(2\phi)}{1-\frac{4\Omega^2}{\omega_{02}^2}} & 0 \\ 0 & 0 & \frac{-2}{3} \end{pmatrix}. \tag{2.80}$$

We can see that the above expression is the same as for the adiabatic case except for the included resonance factor. For angular frequencies of $\Omega \sim \omega_0/2$ resonance will occur. To see why this is the resonance frequency one can look back at Figure 2.6. Let us say that ω_{02} is the preferred frequency of the neutron star in which it wants to oscillate. Oscillation of the quadrupole moment can be thought of as the equatorial tidal bulge oscillating outwards and inwards while the polar tidal bulge is oscillating inwards and outwards. When the black hole has orbited halfway around the neutron star, the tidal displacement field has undergone a full cycle, i.e. the tidal displacement field is precisely equal to the displacement field at the begin of the orbit. Half an orbit of the black hole, therefore corresponds to a full period of oscillations for the tidal bulges. For the angular frequency to be fully in phase with the f-mode frequency it needs to be $\Omega \sim \omega_0/2$.

Now that we have found explicit relations for Q_{ij} and $\mathcal{E}_{ij}$ we can follow the same approach as for the adiabatic case to find a coordinate independent expression of the energy of the system. The total action can be found by substituting the found quadrupole moments and tidal moments into the total action:

$$S = S_{orbit} + \int dt \left[\frac{3\lambda_2 M_{\rm BH}^2 \left(1 - \frac{\Omega^2}{\omega_{02}^2}\right)}{2r^6 \left(1 - \frac{4\Omega^2}{\omega_{02}^2}\right)} \right]. \tag{2.81}$$

We can see that in the adiabatic limit, $\Omega \ll \omega_0$, the action precisely reduces to the adiabatic action up to quadrupole moment that we derived above. For motion in the equatorial plane, the action becomes:

$$S = \int dt \left[\frac{1}{2}\mu \dot{r}^2 + \frac{1}{2}\mu r^2 \dot{\phi}^2 + \frac{\mu M}{r} + \frac{3\lambda_2 M_{\rm BH}^2 \left(1 - \frac{\Omega^2}{\omega_{02}^2}\right)}{2r^6 \left(1 - \frac{4\Omega^2}{\omega_{02}^2}\right)} \right]. \tag{2.82}$$

For stable circular orbits the Euler-Lagrange equation for r then becomes:

$$\frac{d}{dt}\frac{\partial \mathcal{L}}{\partial \dot{r}} - \frac{\partial \mathcal{L}}{\partial r} = -\mu r \Omega^2 + \frac{\mu M}{r^2} + \frac{9\lambda_2 M_{\rm BH}^2 \left(1 - \frac{\Omega^2}{\omega_{02}^2}\right)}{r^7 \left(1 - \frac{4\Omega^2}{\omega_{02}^2}\right)} = 0. \tag{2.83}$$

Where for stable circular orbits we have $\dot{r} = \ddot{r} = 0$ and $\dot{\phi} = \Omega$. Analogous to the adiabatic case we can divide the r equation of motion by μr and expand to linear order in the tidal effects to yield for the linear tidal corrections:

$$-3\delta_r \frac{M}{r_0^3} + \frac{9\lambda_2 M_B^2 \left(1 - \frac{\Omega^2}{\omega_{02}^2}\right)}{\mu r_0^8 \left(1 - \frac{4\Omega^2}{\omega_{02}^2}\right)} = 0. \tag{2.84}$$

Substituting Kepler's third law, $r_0 = M^{1/3}\Omega^{-2/3}$, and solving for δ_r yields:

$$\delta_r = \frac{3\lambda_2 M_{\rm BH}^2 \left(1 - \frac{\Omega^2}{\omega_{02}^2}\right)}{\mu M^{8/3} \Omega^{-10/3} \left(1 - \frac{4\Omega^2}{\omega_{02}^2}\right)}, \tag{2.85}$$

such that the stable circular orbit radius is given by:

$$r(\Omega) = \frac{M^{1/3}}{\Omega^{2/3}} + \frac{3\lambda_2 M_{\rm BH}^2 \left(1 - \frac{\Omega^2}{\omega_{02}^2}\right)}{\mu M^{7/3} \Omega^{-8/3} \left(1 - \frac{4\Omega^2}{\omega_{02}^2}\right)}. \tag{2.86}$$

The energy can again be read of the action by reversing the sign of all the potential terms:

$$\begin{aligned} E(\Omega) &= \frac{1}{2}\mu r^2\Omega^2 - \frac{\mu M}{r} + \frac{1}{2}Q_{ij}\mathcal{E}^{ij} + \frac{1}{2\lambda\omega_0^2}\left[\dot{Q}_{ij}\dot{Q}^{ij} + \omega_{02}^2 Q_{ij}Q^{ij}\right] \\ E(\Omega) &= \frac{1}{2}\mu r^2\Omega^2 - \frac{\mu M}{r} - \frac{3\lambda_2 M_{\rm BH}^2\left(1 - \frac{11\Omega^2}{\omega_{02}^2} + \frac{4\Omega^4}{\omega_{02}^4}\right)}{2r^6\left(1 - \frac{4\Omega^2}{\omega_{02}^2}\right)^2}. \end{aligned} \tag{2.87}$$

Expanding to linear order in the tidal effects gives:

$$E(\Omega) = \frac{1}{2}\mu r_0^2\Omega^2(1+2\delta_r) - \frac{\mu M}{r_0}(1-\delta_r) - \frac{3\lambda_2 M_{\rm BH}^2\left(1 - \frac{11\Omega^2}{\omega_{02}^2} + \frac{4\Omega^4}{\omega_{02}^4}\right)}{2r_0^6\left(1 - \frac{4\Omega^2}{\omega_{02}^2}\right)^2}, \tag{2.88}$$

where we can now again substitute the known results for r_0 and δ_r:

$$\begin{aligned} E(\Omega) &= \frac{1}{2}\mu(M^{1/3}\Omega^{-2/3})^2\Omega^2 + \frac{3\lambda_2 M_{\rm BH}^2\left(1 - \frac{\Omega^2}{\omega_{02}^2}\right)}{M^{6/3}\Omega^{-12/3}\left(1 - \frac{4\Omega^2}{\omega_{02}^2}\right)} \\ &\quad - \frac{\mu M}{(M^{1/3}\Omega^{-2/3})} + \frac{3\lambda_2 M_{\rm BH}^2\left(1 - \frac{\Omega^2}{\omega_{02}^2}\right)}{M^2\Omega^{-12/3}\left(1 - \frac{4\Omega^2}{\omega_{02}^2}\right)} - \frac{3\lambda_2 M_{\rm BH}^2\left(1 - \frac{11\Omega^2}{\omega_{02}^2} + \frac{4\Omega^4}{\omega_{02}^4}\right)}{2(M^{1/3}\Omega^{-2/3})^6\left(1 - \frac{4\Omega^2}{\omega_{02}^2}\right)^2} \\ &= -\frac{1}{2}\mu(M\Omega)^{2/3} + \frac{9\lambda_2\Omega^4 M_{\rm BH}^2\left(1 - \frac{3\Omega^2}{\omega_{02}^2} + \frac{4\Omega^4}{\omega_{02}^4}\right)}{2M^2\left(1 - \frac{4\Omega^2}{\omega_{02}^2}\right)^2}. \end{aligned} \tag{2.89}$$

The expressions $r(\Omega)$ and $E(\Omega)$ coincide with the literature [40]. Note that in the limit $\Omega \ll \omega_{02}$ we retrieve back the energy for the adiabatic case (2.71). For angular frequencies of $\Omega \sim \omega_{02}/2$ resonance will occur.

2.6 Spin interactions

Finally, we also want to consider the interactions that the different angular momenta of the system can have. In Newtonian gravity, a spinning object does not affect the gravitational potential around itself. Fictitious forces can arise however, due to the rotation of the reference frame. Furthermore, in GR, a spinning object distorts the spacetime around it. Therefore spinning objects do alter the gravitational potential around themselves. These spin interactions come in as spin-couplings in the Lagrangian. The present angular momenta of the system are the angular momenta of the neutron star, the black hole and the orbital angular momentum. Additionally, we have seen that the neutron star gets deformed due to tidal effects. This deformation away from spherical symmetry, which we call the tidal bulge of the neutron star, can also be considered as a spin which can interact with the other spins. The spin-spin and spin-orbit interaction terms in the Lagrangian can be derived in an effective field theory formalism which is outside the scope of this thesis. We will use the first post-Newtonian order results from [41]. The post-Newtonian (PN) expansion is the expansion of the Einstein equation in orders of v^2/c^2, which amounts to orders of deviation away from Newtonian gravity. The first order PN spin-spin interaction Lagrangian is given by:

$$\mathcal{L}^{SS} = -\frac{1}{r^3}\left[3\hat{n}_i S_A^i \hat{n}_j S_B^j - S_{Ai}S_B^i\right], \tag{2.90}$$

where S_A^i represents an angular momentum vector and $\hat{n}_i$ the unit normal vector through the common axis of the two objects. For aligned spin systems the first term vanishes. The first order PN spin-orbit interaction Lagrangian is given by:

$$\mathcal{L}^{SO} = -\frac{1}{r^3}S_A^i L_i\left[2 + \frac{3}{2}\frac{M_B}{M_A}\right] - \frac{1}{r^3}S_B^i L_i\left[2 + \frac{3}{2}\frac{M_A}{M_B}\right], \tag{2.91}$$

where L_i represents the orbital angular momentum vector.

It is now possible to construct the couplings between the neutron star's spin $S^i_{\rm NS}$, the black hole's spin $S^i_{\rm BH}$, the tidal spin S^i_Q and the orbital angular momentum L_i. The tidal spin is the spin associated with the quadrupole moment of the neutron star and can be expressed as:

$$S^i_Q = \frac{1}{2\lambda_2\omega^2_{02}}\epsilon^i_{jk}Q^j_l\dot{Q}^{kl}, \tag{2.92}$$

where ϵ_{ijk} is the Levi-Civita tensor. One can check that this has the properties of an angular momentum vector, with units of $\mathrm{kg^2m^2s^{-1}}$. In section 2.6.1 the coupling between the tidal spin S^i_Q and the neutron star's spin $S^i_{\rm NS}$ will be discussed. In Appendix E the coupling between S^i_Q and both $S^i_{\rm BH}$ and L_i are discussed, which have negligible effects on the energy of the system. In section 2.6.2 the coupling between $S^i_{\rm BH}$ and L_i is discussed. The couplings between $S^i_{\rm NS}$ and both $S^i_{\rm BH}$ and L_i are neglected because the neutron star spin is not expected to reach extremal values. Realistically, a dimensionless spin $\chi_{\rm NS}$ of at most 0.7 can be acquired [42].

2.6.1 Angular Momentum of the Neutron Star

We will first discuss the interaction of the neutron star's angular momentum with the tidal spin. We discussed above that the interaction terms with the other spins, S^i_B and L^i, can be neglected. With this new term included in the action, a new approach to solving the system is required. The approach of the previous section does not work anymore, i.e. the tensorial differential equation cannot be solved anymore. Therefore we will present a final approach in this section where we will try to solve for the degrees of freedom of the quadrupole moment tensor independently. The results in this and the following subsections are not present in the literature and are therefore a contributing result of this thesis.

The effects that we want to capture in this new term are effects attributable to the angular momentum or spin of the neutron star. Intuitively, the spin of the neutron star should alter the frequency at which resonance occurs. Spin in the same direction of the orbital velocity should increase the orbital velocity that is needed for resonance to occur and spin in the opposite direction as the orbital velocity should lower the orbital velocity needed for resonance to occur. According to the spin-spin interaction term (2.90) we can write down the contributing term in the Lagrangian:

$$\mathcal{L}^{SS} = \frac{1}{2\lambda_2\omega^2_{02}}C_{\rm NS}\epsilon_{ijk}S^k_N Q^i_k\dot{Q}^{jk}, \tag{2.93}$$

where the coefficient $C_{\rm NS}$ replaces the $1/r^3$ factor in (2.90) following a matching procedure coming from the effective field theory formalism. The coefficient $C_{\rm NS}$ is a yet to be determined coefficient which depends on the neutron star's equation-of-state which must have dimension $[C_{\rm NS}] = \mathrm{m}^{-3}$, which is included following [43]. Although this term arises directly from plugging S^i_Q and $S^i_{\rm NS}$ in (2.90) and thus from the effective field theory approach, it can also be considered as a description of the Coriolis effect, a fictitious force that arises in a rotating frame of reference. In our case, a spinning neutron star, i.e. the rotating neutron star's body frame, generates a Coriolis-like term in the Lagrangian. The total action is given by:

$$S = S_{orbit} + \int dt\Big[-\frac{1}{2}Q_{ij}\mathcal{E}^{ij} + \frac{1}{4\lambda_2\omega^2_{02}}\Big[\dot{Q}_{ij}\dot{Q}^{ij} - \omega^2_{02}Q_{ij}Q^{ij}\Big] + \frac{1}{2\lambda_2\omega^2_{02}}C_{\rm NS}\epsilon_{ijk}S^k_{\rm NS}Q^i_k\dot{Q}^{jk}\Big]. \tag{2.94}$$

Box 3: From the Neutron Star's Body Frame to a Corotating Frame

If the quadrupole moment tensor in the neutron star's body frame is given by:

$$Q_{ij} = R^{-1}(\phi) Q_{ij} R(\phi) = \begin{pmatrix} a+b & c & 0 \\ c & a-b & 0 \\ 0 & 0 & -2a \end{pmatrix}, \tag{2.95}$$

we can easily transform this to a corotating frame by making use of the rotation matrix around the z-axis with an angle ϕ, which is given by:

$$R(\phi) = \begin{pmatrix} \cos\phi & -\sin\phi & 0 \\ \sin\phi & \cos\phi & 0 \\ 0 & 0 & 1 \end{pmatrix}. \tag{2.96}$$

The quadrupole moment tensor in the corotating frame is then given by:

$$\tilde{Q}_{ij} = R^{-1}(\phi) Q_{ij} R(\phi) = \begin{pmatrix} a + b\cos 2\phi + c\sin 2\phi & c\cos 2\phi - b\sin 2\phi & 0 \\ c\cos 2\phi - b\sin 2\phi & a - b\cos 2\phi - c\sin 2\phi & 0 \\ 0 & 0 & -2a \end{pmatrix}. \tag{2.97}$$

We can parametrise the quadrupole tensor in the corotating frame in terms of new corotating frame variables α, β and γ as:

$$\tilde{Q}_{ij} = \begin{pmatrix} \alpha+\beta & \gamma & 0 \\ \gamma & \alpha-\beta & 0 \\ 0 & 0 & -2\alpha \end{pmatrix}, \tag{2.98}$$

such that the relation between the variables in the two frames is given by:

$$\alpha = a, \quad \beta = b\cos 2\phi + c\sin 2\phi, \quad \gamma = c\cos 2\phi - b\sin 2\phi. \tag{2.99}$$

Using the above transformation laws, it is also possible to express Q_{ij} in the body frame in terms of the corotating frame variables:

$$Q_{ij} = \begin{pmatrix} \alpha + \beta\cos 2\phi - \gamma\sin 2\phi & \gamma\cos 2\phi + \beta\sin 2\phi & 0 \\ \gamma\cos 2\phi + \beta\sin 2\phi & \alpha - \beta\cos 2\phi + \gamma\sin 2\phi & 0 \\ 0 & 0 & -2\alpha \end{pmatrix}. \tag{2.100}$$

In Figure 2.7 the transformation of the neutron star body frame to the corotating frame is visualised, which is done by rotating the body frame by an angle ϕ.

We will consider the aligned spin case in which we have $S^i_{\rm NS} = (0, 0, S^z_N)$. In the previous section we were able to solve the differential equations that arose from the Euler-Lagrange equation that the independent components of the quadrupole moment tensor obeyed, this is however not possible anymore. There is another way though, we can express the quadrupole moment tensor in terms of corotating frame variables, see (2.100) in Box 3. This transformation of the neutron star's body frame to the corotating frame is also depicted in Figure 2.7. Using the parametrisation of (2.100) we can explicitly perform the contractions such that we have 3 new Euler-Lagrange equations for the 3 new dynamical variables $\alpha(t)$, $\beta(t)$ and $\gamma(t)$. For

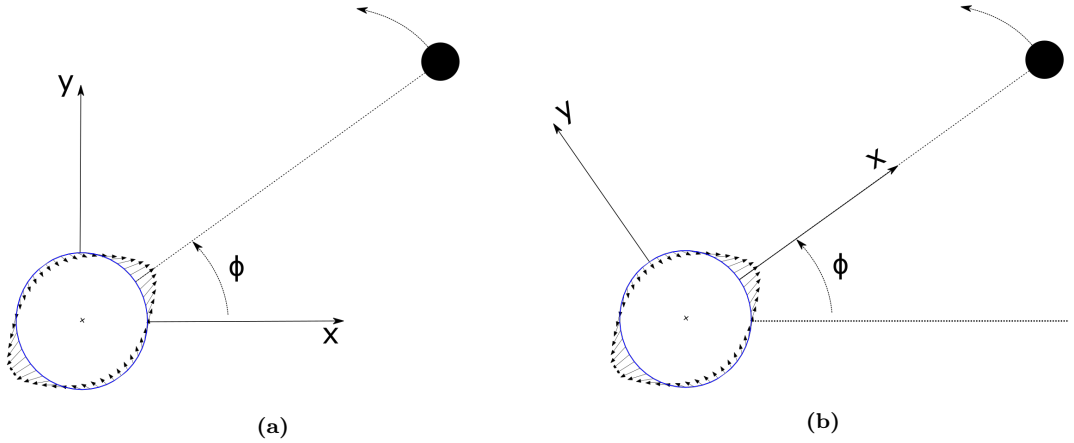

Figure 2.7: NSBH binary from the perspective of a: (a) body reference frame in which the quadrupole moment tensor components induced by the companion black hole are dynamic (b) corotating reference frame in which the quadrupole moment tensor components induced by the companion black hole are static.

stable circular orbits, in which $\dot{\phi} = \Omega$, we then have:

$$\begin{aligned}
&\frac{d}{dt}\frac{\partial \mathcal{L}}{\partial \dot{\alpha}} - \frac{\partial \mathcal{L}}{\partial \alpha} = -\frac{3M_{\rm BH}}{2r^3} + \frac{3\alpha}{\lambda_2} = 0, \\
&\frac{d}{dt}\frac{\partial \mathcal{L}}{\partial \dot{\beta}} - \frac{\partial \mathcal{L}}{\partial \beta} = -\frac{3M_{\rm BH}}{2r^3} + \frac{4\omega_{02}^2\beta - 16\Omega^2 - 16\Omega C_{\rm NS}S^z_{\rm NS}\beta}{4\lambda_2\omega_{02}^2} = 0, \\
&\frac{d}{dt}\frac{\partial \mathcal{L}}{\partial \dot{\gamma}} - \frac{\partial \mathcal{L}}{\partial \gamma} = -8\Omega C_{\rm NS}S^z_{\rm NS}\gamma + \frac{4\omega_{02}^2\gamma - 16\Omega^2\gamma - 16\Omega C_{\rm NS}S^z_{\rm NS}\gamma}{4\lambda_2\omega_{02}^2} = 0.
\end{aligned} \tag{2.101}$$

The key reason that we use corotating frame variables is that they should all be static in the non-spinning neutron star case. This can also be seen in Figure 2.7, where we can see that in the corotating frame, the induced quadrupole moment rotates along with the reference frame. For $S^z_{\rm NS} = 0$ the above relations should therefore reduce to the non-spinning case. From which we can conclude that all the derivatives of $\alpha(t)$, $\beta(t)$ and $\gamma(t)$ should vanish and therefore have been set to zero to obtain the above expressions. We can now easily solve the Euler-Lagrange equations to find an expression for the quadrupole moment tensor:

$$Q_{ij} = \mathcal{A}\begin{pmatrix} \frac{1}{3} + \frac{\omega_{02}^2\cos 2\phi}{\left(\omega_{02}^2 - 4\Omega^2 - 4\Omega C_{\rm NS}S^z_{\rm NS}\right)} & \frac{\omega_{02}^2\sin 2\phi}{\left(\omega_{02}^2 - 4\Omega^2 - 4\Omega C_{\rm NS}S^z_{\rm NS}\right)} & 0 \\ \frac{\omega_{02}^2\sin 2\phi}{\left(\omega_{02}^2 - 4\Omega^2 - 4\Omega C_{\rm NS}S^z_{\rm NS}\right)} & \frac{1}{3} - \frac{\omega_{02}^2\cos 2\phi}{\left(\omega_{02}^2 - 4\Omega^2 - 4\Omega C_{\rm NS}S^z_{\rm NS}\right)} & 0 \\ 0 & 0 & -\frac{2}{3} \end{pmatrix}. \tag{2.102}$$

Where again $\mathcal{A} = \frac{3\lambda_2 M_{\rm BH}}{2r^3}$. Note that this expression is similar to the quadrupole moment tensor derived in the previous section up to the resonance frequency, which was what we expected. The resonance frequency is now altered by the spin of the neutron star. We can perform the same analysis as we have done twice before, namely substituting the above-found quadrupole moment tensor as well as the tidal moment tensor into the action and performing all the contractions, after which we can use the r Euler-Lagrange equation to find an expression for $r(\Omega)$, which in turn can give us an expression for $E(\Omega)$. We will post merely the final results here. For the individual steps in the derivation, the reader is referred back to the previous sections. The stable circular orbit radius is given by:

$$r(\Omega) = \frac{M^{1/3}}{\Omega^{2/3}} + \frac{3\lambda_2\Omega^{8/3}M_{\rm BH}^2\left(\omega_{02}^2 - \Omega^2 - \Omega C_{\rm NS}S^z_{\rm NS}\right)}{M^{7/3}\mu\left(\omega_{02}^2 - 4\Omega^2 - 4\Omega C_{\rm NS}S^z_{\rm NS}\right)}, \tag{2.103}$$

and the energy is given by:

$$E(\Omega) = -\frac{1}{2}\mathrm{M}^{2/3}\mu\Omega^{2/3} + \frac{9\lambda_2\Omega^4\mathrm{M}_{\mathrm{BH}}^2\left(\omega_{02}^4 - 3\omega_{02}^2\Omega^2 + 4\Omega^4 - \Omega\left(5\omega_{02}^2 - 8\Omega^2\right)\mathrm{C}_{\mathrm{NS}}S_{\mathrm{NS}}^z\right)}{2\mathrm{M}^2\left(\omega_{02}^2 - 4\Omega^2 - 4\Omega C_{\mathrm{NS}}S_{\mathrm{NS}}^z\right)^2}. \tag{2.104}$$

Apart from expanding to linear order in the tidal effects, we also kept only terms up to linear order in the neutron star's spin. Note that in the limit of a non-spinning neutron star the above expressions reduce exactly to the expressions from section 2.5. We can see that the resonance frequency is now altered by the neutron star's spin. Instead of resonance at $\Omega \sim \omega_{02}/2$, we have resonance at $\Omega \sim \frac{1}{2}\left(\left(\omega_{02}^2 + C_{\mathrm{NS}}^2{S_{\mathrm{NS}}^z}^2\right)^{1/2} - C_{\mathrm{NS}}S_{\mathrm{NS}}^z\right)$.

2.6.2 Angular Momentum of the Black Hole

We also want to allow for the black hole to have a non-zero angular momentum in our system. In the same way that the neutron star's angular momentum can couple to the tidal spin, which we have discussed in the previous section, the black hole's angular momentum and the orbital angular momentum can couple to the tidal spin. These effects are called frame dragging effects. The spin of the companion black hole, as well as the orbital spin of the system cause spacetime to distort and lead to precession of the orbit of the neutron star and thus the neutron star's body frame. These effects are small however, and will be discussed in Appendix E. The biggest effect of the black hole's angular momentum comes from the coupling to the orbital angular momentum. According to the spin-orbit interaction term (2.91) we can write down the contributing term in the Lagrangian:

$$\mathcal{L}^{SO} = -\frac{1}{r^3}S_{\mathrm{BH}}^i L_i\left[2 + \frac{3}{2}\frac{M_{\mathrm{BH}}}{M_{\mathrm{NS}}}\right]. \tag{2.105}$$

For stable circular orbits and aligned spins in the xy-plane, expressed in the barycentric frame, we have $S_{\mathrm{NS}}^i = (0, 0, S_{\mathrm{NS}}^z)$ and $L^z = \mu r^2\Omega$. The total action including all effects is given by:

$$\begin{aligned} S = \int dt\Bigg[&\frac{1}{2}\mu\dot{r}^2 + \frac{1}{2}\mu r^2\dot{\phi}^2 + \frac{\mu M}{r} - \frac{1}{2}Q_{ij}\mathcal{E}^{ij} + \frac{1}{4\lambda_2\omega_{02}^2}\left[\dot{Q}_{ij}\dot{Q}^{ij} - \omega_{02}^2 Q_{ij}Q^{ij}\right] \\ &+ \frac{1}{2\lambda_2\omega_{02}^2}C_{\mathrm{NS}}\epsilon_{ijk}S_{\mathrm{NS}}^k Q_k^i\dot{Q}^{jk} - \frac{1}{r^3}S_{\mathrm{BH}}^i L_i\left[2 + \frac{3}{2}\frac{M_{\mathrm{BH}}}{M_{\mathrm{NS}}}\right]\Bigg]. \end{aligned} \tag{2.106}$$

We can use the techniques discussed in the previous sections to calculate all the desired quantities. The spin-spin and spin-orbit interaction terms are given up to linear order in the separate spins, we will therefore also work up to linear order in the black hole and neutron star angular momenta. The spin-orbit term does not alter the quadrupole moment of the neutron star, which is therefore given by (2.102). The stable circular orbit radius as a function of the orbital frequency is given by:

$$\begin{aligned} r(\Omega) = &\frac{2M - \Omega\left(\frac{3M_{\mathrm{BH}}}{M_{\mathrm{NS}}} + 4\right)S_B^z}{2M^{2/3}\Omega^{2/3}} \\ &- \frac{3\lambda\Omega^{8/3}M_{\mathrm{BH}}^2\left(7\Omega\left(4M_{\mathrm{NS}} + 3M_{\mathrm{BH}}\right)S_{\mathrm{BH}}^z + 2MM_A\right)\left(\Omega C_{\mathrm{NS}}S_{\mathrm{NS}}^z - \omega^2 + \Omega^2\right)}{2\mu M^{10/3}M_{\mathrm{NS}}\left(-4\Omega C_{\mathrm{NS}}S_{\mathrm{NS}}^z + \omega^2 - 4\Omega^2\right)}. \end{aligned} \tag{2.107}$$

We can see that the first term is altered by the black hole's spin, i.e. a modified Kepler's third law. Positive (aligned) black hole spin decreases the stable circular orbit radius, while negative (anti-aligned) black hole spin increases the stable circular orbit radius. The tidal correction term is altered in the same way: positive (aligned) black hole spin decreases the tidal correction radius, while negative (anti-aligned) black hole spin increases the tidal correction radius.

The energy as a function of the orbital frequency is given by:

$$\begin{aligned}E(\Omega) = &-\frac{1}{2}\mathrm{M}^{2/3}\mu\Omega^{2/3} - S^z_{\mathrm{BH}}\frac{\mu\Omega^{5/3}\left(4M_{\mathrm{NS}}+3M_{\mathrm{BH}}\right)}{2M^{1/3}M_{\mathrm{NS}}}\\ &+\frac{9\lambda_2\Omega^4\mathrm{M}^2_{\mathrm{BH}}\left(\omega_{02}^4-3\omega_{02}^2\Omega^2+4\Omega^4-\Omega\left(5\omega_{02}^2-8\Omega^2\right)\mathrm{C}_{\mathrm{NS}}S^z_{\mathrm{NS}}\right)}{2\mathrm{M}^2\left(\omega_{02}^2-4\Omega^2-4\Omega C_{\mathrm{NS}}S^z_{\mathrm{NS}}\right)^2}\\ &+S^z_{\mathrm{BH}}\frac{3\lambda_2\Omega^5M^2_{\mathrm{BH}}\left(4M_{\mathrm{NS}}+3M_{\mathrm{BH}}\right)\left(11\Omega C_{\mathrm{NS}}\left(8\Omega^2-5\omega_{02}^2\right)S^z_{\mathrm{NS}}+11\omega_{02}^4-37\omega_{02}^2\Omega^2+44\Omega^4\right)}{2M^3M_{\mathrm{NS}}\left(\omega_{02}^2-4\Omega^2-4\Omega C_{\mathrm{NS}}S^z_{\mathrm{NS}}\right)^2}.\end{aligned} \tag{2.108}$$

The above energy can be used to calculate a tidal disruption frequency that can in turn be used to calculate a tidal disruption radius. Instead of the approach from section 2.2 where we compared the self-gravitational force of the neutron star to the tidal force because of the companion black hole, we are now able to compare the self-gravitational energy to the tidal energy. The advantage of comparing energies is that we can make statements about the system as a whole. With the force balance approach we had to choose a point at the surface of the neutron star to compare the forces. The fact that tidal disruption starts taking place at a certain point does not mean that tidal disruption has a significant impact on the whole system and therefore on the GW it produces. With an energy consideration it is possible to more generally derive a point at which the system starts to become tidally disrupted as a whole. Also, the energy calculated above has a very complex resonance dependence that is not included in the force balance from section 2.2. To explicitly compute energies from the waveforms of explicit binary systems we need expressions in physical units. From [43] we deduce that $C_N = -3/4I$, where I is the moment of inertia of the Neutron star. Recovering units by dimensional analysis allows us to express the distance $r(\Omega)$ and the energy $E(\Omega)$ in dimensionless variables:

$$\begin{aligned}\tilde{r}(x) = &\left(\frac{2X_{\mathrm{NS}}-3x^{3/2}\chi_{\mathrm{BH}}X^2_{\mathrm{BH}}\left(4X_{\mathrm{NS}}+3X_{\mathrm{BH}}\right)}{2x^3X_{\mathrm{NS}}}\right)^{1/3}\\ &+\frac{12\sqrt[3]{2}\Lambda_2x^4X_{\mathrm{NS}}^{22/3}X^2_{\mathrm{BH}}\left(x^{3/2}\tilde{\mathrm{I}}\chi_{\mathrm{NS}}+X_{\mathrm{NS}}x^3-y^3\right)}{\nu\left(2X_{\mathrm{NS}}-3x^{3/2}\chi_{\mathrm{BH}}X^2_{\mathrm{BH}}\left(4X_{\mathrm{NS}}+3X_{\mathrm{BH}}\right)\right)^{7/3}\left(4x^{3/2}\tilde{\mathrm{I}}\chi_{\mathrm{NS}}+4X_{\mathrm{NS}}x^3-y^3\right)},\end{aligned} \tag{2.109}$$

and

$$\begin{aligned}\tilde{E}(x) = &-\frac{\nu x}{2}-\chi_{\mathrm{BH}}\frac{\nu x^{5/2}X^2_{\mathrm{BH}}\left(4X_{\mathrm{NS}}+3X_{\mathrm{BH}}\right)}{2X_{\mathrm{NS}}}\\ &+\frac{9\Lambda_2x^6X^5_{\mathrm{NS}}X^2_{\mathrm{BH}}\left(x^{3/2}\tilde{\mathrm{I}}X_{\mathrm{NS}}\chi_{\mathrm{NS}}\left(8x^3X^2_{\mathrm{NS}}-5y^3\right)+4x^6X^4_{\mathrm{NS}}-3x^3y^3X^2_{\mathrm{NS}}+y^6\right)}{2\left(y^3-4x^3X^2_{\mathrm{NS}}-4x^{3/2}\tilde{\mathrm{I}}X_{\mathrm{NS}}\chi_{\mathrm{NS}}\right)^2}\\ &+\chi_{\mathrm{BH}}\frac{3\Lambda_2x^{15/2}X^4_{\mathrm{NS}}X^4_{\mathrm{BH}}\left(4X_{\mathrm{NS}}+3X_{\mathrm{BH}}\right)\left(11x^{3/2}\tilde{\mathrm{I}}X_{\mathrm{NS}}\chi_{\mathrm{NS}}\left(8x^3X^2_{\mathrm{NS}}-5y^3\right)+44x^6X^4_{\mathrm{NS}}-37x^3y^3X^2_{\mathrm{NS}}+11y^6\right)}{2\left(y^3-4x^3X^2_{\mathrm{NS}}-4x^{3/2}\tilde{\mathrm{I}}X_{\mathrm{NS}}\chi_{\mathrm{NS}}\right)^2}\end{aligned} \tag{2.110}$$

where we defined dimensionless quantities, partly analogous to [43]:

$$\begin{aligned}&x=\left(\frac{GM\Omega}{c^3}\right)^{2/3},\quad y=\left(\frac{GM_{\mathrm{NS}}\omega_{02}}{c^3}\right)^{2/3},\quad X_{\mathrm{NS}}=\frac{M_{\mathrm{NS}}}{M},\quad X_{\mathrm{BH}}=\frac{M_{\mathrm{BH}}}{M},\quad \tilde{\mathrm{I}}=-\frac{3}{4I}\frac{G^2M^3_{\mathrm{NS}}}{c^4}\\ &\chi_{\mathrm{NS}}=\frac{cS^z_{\mathrm{NS}}}{GM^2_{\mathrm{NS}}},\quad \chi_{\mathrm{BH}}=\frac{cS^z_{\mathrm{BH}}}{GM^2_{\mathrm{BH}}},\quad \Lambda_2=G\lambda_2\left(\frac{c^2}{GM_{\mathrm{NS}}}\right)^5,\quad \nu=\frac{\mu}{M},\quad \tilde{r}=\frac{rc^2}{GM},\quad \tilde{E}=\frac{E}{Mc^2}.\end{aligned} \tag{2.111}$$

Chapter 3

Tidal Disruption Frequency

We can use the energy for an NSBH binary system derived in the previous chapter to calculate a tidal disruption frequency Ω_{tidal}. This will be outlined in section 3.1. In section 3.2 the dependence of the tidal disruption frequency as a function of the different parameters is shown: Λ_2 in section 3.2.1, Q in section 3.2.2, χ_{NS} in section 3.2.3 and χ_{BH} in section 3.2.4. We will compare the tidal disruption frequency to NR simulations to verify the model. It is not possible to derive an explicit analytic expression for the tidal disruption frequency, in section 3.3 a fitting procedure is outlined to generate an explicit functional form of the tidal disruption frequency as a function of the four model parameters Λ_2, Q, χ_{NS} and χ_{BH}. Note that fitting a function of four variables, in this case $\Omega(\Lambda_2, Q, \chi_{\text{NS}}, \chi_{\text{BH}})$, to the tidal disruption frequency data, can be a research project on its own. We therefore by no means claim that the fit produced in section 3.3 is an end product to be used for the generation of gravitational waveforms. The purpose of this section is to show a simple way to generate an explicit functional form of the model. Once the validity of the model is confirmed, more advanced fitting techniques should be applied.

3.1 Calculating the Tidal Disruption Frequency from the Energy Balance

Equating the tidal energy of the NSBH binary system to the self-gravitational energy of the neutron star and solving for the orbital frequency will yield the tidal disruption frequency. The tidal energy is given by the terms proportional to Λ_2 in (2.110). The self-gravitational energy can be obtained from the difference between the gravitational mass and the baryonic mass or rest mass M_{bar} of the neutron star. The gravitational mass is what we usually denote as just the mass of the neutron star and is given by M_A. The baryonic mass is the mass obtained by integrating the density over the matter distribution using the appropriate metric factor $\sqrt{g_{rr}}$ for the radial integration. In [44] an empirical formula relating the baryonic mass to the compactness $M_{\text{NS}}/R_{\text{NS}}$ of the neutron star is given:

$$\frac{M_{\text{bar}}}{M_{\text{NS}}} = 1 + 0.8858 \left(\frac{M_{\text{NS}}}{R_{\text{NS}}}\right)^{1.2082} . \tag{3.1}$$

The baryonic mass in the self-gravitational energy, and both the f-mode frequency and the moment of inertia in the tidal energy are EOS-dependent. There exist however, universal relations between $M_{\text{NS}}/R_{\text{NS}}$, ω_{02}, I and Λ_2. These relations are of the form:

$$x = \sum_{k=0}^{2} a_k \left(\ln \Lambda_2\right)^k . \tag{3.2}$$

The self-gravitational energy:

$$E_{\text{SG}} = (M_{\text{bar}} - M_{\text{NS}}), \tag{3.3}$$

x	$k=0$	$k=1$	$k=2$	$k=3$	$k=4$
$\ln M_{\rm NS}^{-3} I$	1.47	8.17×10^{-2}	1.49×10^{-2}	2.87×10^{-4}	-3.64×10^{-5}
$M_{\rm NS}\omega_{02}$	1.820×10^{-1}	-6.836×10^{-3}	-4.196×10^{-3}	5.215×10^{-4}	-1.857×10^{-5}
$M_{\rm NS}R_{\rm NS}^{-1}$	3.60×10^{-1}	-3.55×10^{-1}	7.05×10^{-4}	0	0

Table 3.1: Estimated numerical coefficients for the fitting formulas relating $M_{\rm NS}R_{\rm NS}^{-1}$-$\Lambda_2$ [45], ω_{02}-Λ_2 [46] and I-Λ_2 [47].

therefore only depends on Λ_2, and Q after using the relation 3.2 with coefficients given in Table 3.1. Furthermore, the tidal energy (2.110) only depends on $\bar{\Omega}$, Λ_2, Q, $\chi_{\rm NS}$ and $\chi_{\rm BH}$ after using the relations:

$$x=\bar{\Omega}^{2/3},\quad X_{\rm NS}=\frac{1}{1+Q},\quad X_{\rm BH}=\frac{Q}{1+Q},\quad \nu=\frac{Q}{(1+Q)^2}, \tag{3.4}$$

and 3.2 with coefficients given in Table 3.1. It is more convenient to have a dimensional parameter directly proportional to Ω instead of x being proportional to $\Omega^{2/3}$. We therefore redefined x such that $\bar{\Omega}$ is proportional to Ω.

In theory, it is possible to solve the energy balance $E_{\rm tidal}(\bar{\Omega},\Lambda_2,Q,\chi_{\rm NS},\chi_{\rm BH})=E_{\rm SG}(\Lambda_2,Q)$ for $\bar{\Omega}$. Since this is an important result of this thesis, the energy balance will be explicitly stated here for clarity, using (2.108) and (3.3):

$$\begin{aligned}
E_{\rm SG}(\Lambda_2,Q)/M &= E_{\rm tidal}(\bar{\Omega},\Lambda_2,Q,\chi_{\rm NS},\chi_{\rm BH})/M\\
\frac{M_{\rm bar}}{M}(\Lambda_2,Q)-\frac{1}{1+Q} &= -\chi_{\rm BH}\frac{Q\bar{\Omega}^{2/3}}{2(Q+1)^2}-\frac{Q^3(3Q+4)\bar{\Omega}^{5/3}}{2(Q+1)^4}\\
&\quad+\frac{9\Lambda Q^2\bar{\Omega}^4\left(-(Q+1)\bar{\Omega}\tilde{\rm I}\chi_{\rm NS}\left(5(Q+1)^2y^3-8\bar{\Omega}^2\right)+(Q+1)^4y^6-3(Q+1)^2y^3\bar{\Omega}^2+4\bar{\Omega}^4\right)}{2(Q+1)^7\left(-4(Q+1)\bar{\Omega}\tilde{\rm I}\chi_{\rm NS}+(Q+1)^2y^3-4\bar{\Omega}^2\right)^2}\\
&\quad+\chi_{\rm BH}\frac{3\Lambda_2Q^4(3Q+4)\bar{\Omega}^5\left(11(Q+1)^4y^6-37(Q+1)^2y^3\bar{\Omega}^2+44\bar{\Omega}^4\right)}{2(Q+1)^9\left(-4(Q+1)\bar{\Omega}\tilde{\rm I}\chi_{\rm NS}+(Q+1)^2y^3-4\bar{\Omega}^2\right)^2}\\
&\quad-\chi_{\rm BH}\chi_{\rm NS}\frac{33\Lambda_2Q^4(3Q+4)\bar{\Omega}^6\tilde{\rm I}\left(5(Q+1)^2y^3-8\bar{\Omega}^2\right)}{2(Q+1)^8\left(-4(Q+1)\bar{\Omega}\tilde{\rm I}\chi_{\rm NS}+(Q+1)^2y^3-4\bar{\Omega}^2\right)^2}
\end{aligned} \tag{3.5}$$

where y and $\tilde{\rm I}$ now explicitly depend on Λ_2 and Q. The complex dependence of the tidal energy on the orbital frequency makes it difficult to solve the equation analytically. We will therefore generate a fitting formula for the tidal disruption frequency in section 3.3. Once the system is specified however, i.e. when Λ_2, Q, $\chi_{\rm NS}$ and $\chi_{\rm BH}$ are known, the tidal disruption frequency can be computed. It is possible to write functions in computer programming languages that give you a tidal disruption frequency once Λ_2, Q, $\chi_{\rm NS}$ and $\chi_{\rm BH}$ are specified. Such a function can be used in any kind of model, e.g. a model which generates NSBH binary system waveforms. To test the behaviour of the tidal disruption frequency, we will plot $E_{\rm SG}$ together with $E_{\rm tidal}$ with different variables being held constant.

3.1.1 Energy as a Function of the Tidal Deformability Parameter Λ_2

In Figure 3.1 the tidal energy and the self-gravitational energy as a function of the orbital frequency are shown for different Λ_2. The mass ratio Q is fixed at $Q=2$ and both the spins are set to zero. The tidal disruption frequency is the frequency at which the two energy curves intersect for the first time. We observe that indeed the tidal disruption occurs close to the point of resonance, i.e. the point where the tidal energy diverges. This will also be the case when considering the dependence on the other variables. From Figure 3.1 it can be observed

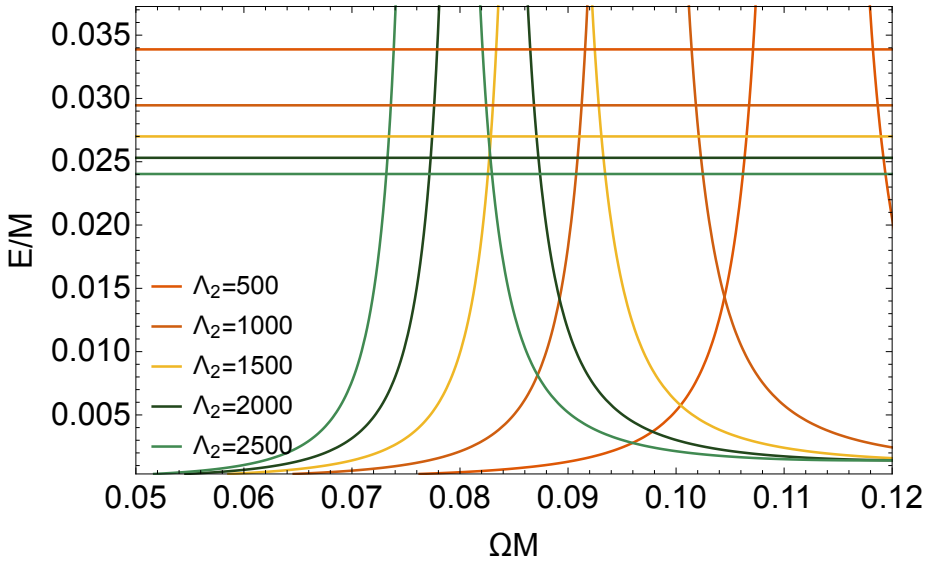

Figure 3.1: The tidal energy and and the constant self-gravitational energy plotted as a function of the orbital frequency for different Λ_2. For an NSBH system with $Q = 2$, $\chi_{\rm NS} = 0$ and $\chi_{\rm BH} = 0$.

that the higher the tidal deformability parameter Λ_2 of the neutron star, the earlier in the inspiral the neutron star gets tidally disrupted - indeed, the tidal deformability parameter is a measure for how easily the star gets tidally deformed. Furthermore, we observe that the spacings between $\Omega_{\rm tidal}$ increase with constant reductions of Λ_2. This behaviour is general for most parameter settings, i.e. for different Q, $\chi_{\rm NS}$ and $\chi_{\rm BH}$. The exact behaviour of the tidal disruption frequency will be more explicitly visible when plotting $\Omega_{\rm tidal}$ against Λ_2 in section 3.2.1.

3.1.2 Energy as a Function of the Mass Ratio Q

In Figure 3.2 $E_{\rm SG}$ and $E_{\rm tidal}$ as a function of Ω are shown for different Q. The tidal deformability is fixed at $\Lambda_2 = 1110$ and both the compact objects are spinless. We observe that the higher the mass ratio Q, the higher the tidal disruption frequency. This confirms our intuition built up in section 2.1: the higher the mass ratio, the more the NS can be seen as a point mass-like object relative to the black hole, the more the system behaves like a BBH, the later in the inspiral finite size effects come in. We observe that the spacings between $\Omega_{\rm tidal}$ are close to constant, even though the spacings between $E_{\rm SG}$ for different Q are not. This translates to a linear $\Omega_{\rm tidal}$-Q relation in section 3.2.2.

3.1.3 Energy as a Function of the Neutron Star's Angular Momentum $\chi_{\rm NS}$

In Figure 3.3 $E_{\rm SG}$ and $E_{\rm tidal}$ as a function of Ω are shown for different $\chi_{\rm NS}$. The tidal deformability is fixed at $\Lambda_2 = 1110$, the mass ratio at $Q = 2$ and $\chi_{\rm BH} = 0$. We observe that the lower $\chi_{\rm NS}$, the earlier in the inspiral tidal disruption takes place. This is expected following our discussion in 2.6.1. The spacings between $\Omega_{\rm tidal}$ seem to increase slightly for increasing NS spins, but the exact $\Omega_{\rm tidal}$-$\chi_{\rm NS}$ behaviour will be shown in 3.2.3. One thing to point out is that the variation of Λ_2, Q and $\chi_{\rm NS}$ all lead to both a shift and a widening/narrowing in the resonance peak.

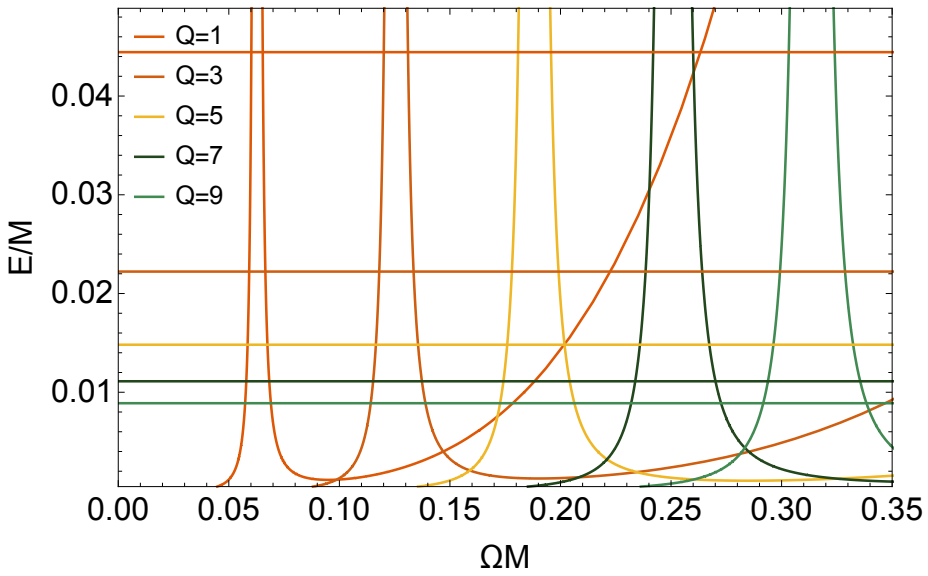

Figure 3.2: The tidal energy and the constant self-gravitational energy plotted as a function of the orbital frequency for different Q. For an NSBH system with $\Lambda_2 = 1110$, $\chi_{\rm NS} = 0$ and $\chi_{\rm BH} = 0$.

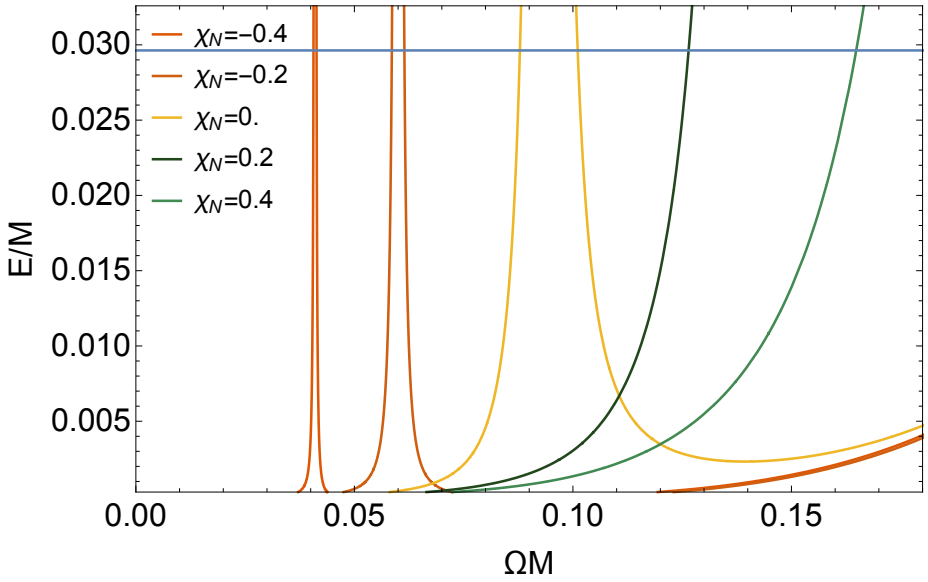

Figure 3.3: The tidal energy and the constant self-gravitational energy plotted as a function of the orbital frequency for different $\chi_{\rm NS}$. For an NSBH system with $\Lambda_2 = 1110$, $Q = 2$ and $\chi_{\rm BH} = 0$.

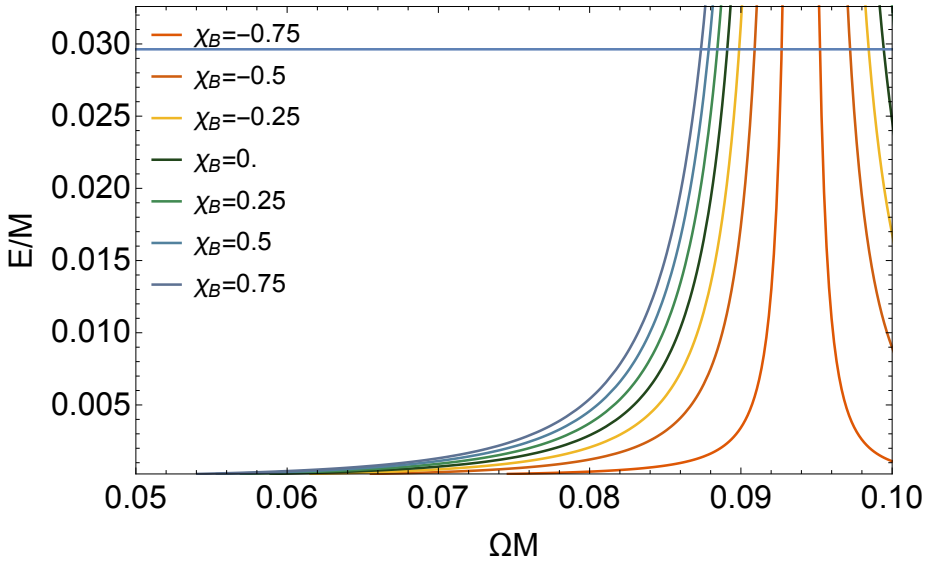

Figure 3.4: The tidal energy and and the constant self-gravitational energy plotted as a function of the orbital frequency for different $\chi_{\rm BH}$. For an NSBH system with $\Lambda_2 = 1110$, $Q = 2$ and $\chi_{\rm NS} = 0$.

3.1.4 Energy as a Function of the Black Hole's Angular Momentum $\chi_{\rm BH}$

In Figure 3.4 $E_{\rm SG}$ and $E_{\rm tidal}$ as a function of Ω are shown for different $\chi_{\rm BH}$. The tidal deformability is fixed at $\Lambda_2 = 1110$, the mass ratio at $Q = 2$ and $\chi_{\rm NS} = 0$. We observer that the higher $\chi_{\rm BH}$, the earlier in the inspiral tidal disruption takes place. The spacings between $\Omega_{\rm tidal}$ seem to increase slightly for decreasing BH spins, but the exact $\Omega_{\rm tidal}$-$\chi_{\rm NS}$ behaviour will be shown in 3.2.3. While the variation of Λ_2, Q and $\chi_{\rm NS}$ all lead to both a shift and a widening/narrowing in the resonance peak, the variation of $\chi_{\rm BH}$ leads to only a widening/narrowing of the resonance peak. This is directly attributable to the term in the Lagrangian where the black hole spin enters (2.105) not being coupled to the tidal parameter λ_2.

3.2 The Tidal Disruption Frequency Model Results

In the previous section 3.1 we have shown how to find the tidal disruption frequency $\Omega_{\rm tidal}$ from the energy balance $E_{\rm tidal}(\bar{\Omega}, \Lambda_2, Q, \chi_{\rm NS}, \chi_{\rm BH}) = E_{\rm SG}(\Lambda_2, Q)$. To verify our model, we compare our results to NR results. In section 2.1 we discussed that these simulations simulate matter subject to the Einstein field equation 0.3. As of today, we have no reason to doubt that GR describes the universe on the scales relevant in this study. We can therefore treat these numerical simulations as observed data with which our model should agree. The problem with these NR simulations is that they are very limited in their coverage of the parameter space. This is a consequence of the computation power that is needed for these simulations. One simulation can take up to months, already using large computer clusters. This once again emphasises the need of computational light methods to generate gravitational waveforms, since we simply cannot cover the entire parameter space with waveforms generated from NR simulations.

We will hypothesise that the tidal disruption frequency coincides with the frequency at which the GW amplitude is at a maximum. This can be qualitatively argued as follows: the disruption of the matter of the neutron star is subject to the energy balance between the tidal energy and the self-gravitational energy. Once the tidal energy has overcome the energy barrier of the

self-gravitational energy, the matter of the neutron star is not gravitationally bound anymore to a common centre of mass; the matter is gravitationally bound to the black hole's centre of mass. At exactly the point where this energy barrier is overcome, the biggest evolution of mass density in the system happens, which according to Einstein's quadrupole formula (1.28) corresponds to a maximum in the GWs. This is also what the NR simulations tell us: the maximum GW amplitude coincides with a rapid decrease in the central density of the neutron star, taking retarded time into account. A small systematic offset of the tidal disruption frequency compared the NR data however, might still be attributable to this hypothesis not being completely valid.

Following the preceding argument, we can say that the tidal disruption mechanism has the effect that all the matter in the binary system will have a common centre of mass at an earlier time in the inspiral compared to a BBH system with equal other parameters, i.e. tidal disruption expedites the merger process. The frequency at which the merger happens of an NSBH system can therefore never exceed the frequency at which a BBH system with equal parameters would merge. Given the frequency Ω_{BBH} at which a BBH with the same parameters as the corresponding NSBH has its maximum amplitude, the final model predicting the merger frequency is given by:

$$\Omega = \min(\Omega_{\mathrm{tidal}}, \Omega_{\mathrm{BBH}}). \tag{3.6}$$

A fitting formula for the BBH merger frequency is given by [48] and reads:

$$\begin{aligned}\Omega_{\mathrm{BBH}} = 0.28134 + &\frac{\left(0.0008715Q^2\chi_{\mathrm{BH}} + 0.0008715\chi_{\mathrm{NS}} - 0.043531Q^2 - 0.043531\right)}{Q^2+1} \\ &\times \ln\left(\frac{Q^2(Q(21.1199\ -25.8198Q)-25.8198)\chi_{\mathrm{BH}} + (Q(21.1199\ -25.8198Q)-25.8198)\chi_{\mathrm{NS}}}{(Q+1)^2\,(Q^2+1)}\right. \\ &\left. + \frac{25.8504\left(Q^2+1\right)\left(Q(Q-0.412082)+1\right)}{(Q+1)^2\,(Q^2+1)}\right).\end{aligned} \tag{3.7}$$

The tidal disruption frequency calculated from (3.5) can be compared with the merger frequency at which the NR waveforms reach their maximum amplitude. We obtained NR data from the SXS waveform database [4] and from the SACRA waveform database [6, 5]. The merger frequencies and their associated parameter settings form the NR simulations can be found in Tables F.1 and F.2 from Appendix F. We will also compute the maximum amplitude frequency from waveforms of the existing waveform model PhenomNSBH [7]. This model uses the Newtonian force balance discussed in 2.2. These waveforms can be generated by the LALsuite from the LIGO scientific collaboration [49].

In the next sections we will present one single plot for every parameter that Ω from (3.6) is dependent on to visualise the general behaviour of the model compared to the NR data. The parameter space spans however, a vastly bigger region than just four one-dimensional plots. We will therefore also compute the average relative error of the model compared to the NR data and compare this to the average relative error of the PhenomNSBH model.

3.2.1 Tidal Deformability Parameter Λ_2

In Figure 3.5 the NSBH merger frequency calculated from (3.6) as a function of the tidal deformability parameter Λ_2 is shown for fixed $Q = 2$ and spinless NS and BH. We observe that our model agrees with the general trend from the NR simulations, although slight deviations can be seen. A part of the explanation could be that we worked to linear order in the tidal effects. We also only included the quadrupole moment in the multipole expansion of the neutron star and the octopole moment could bring additional dependences on Λ_2. The model will therefore not fully capture the dependence on Λ_2. We can also observe that the model outperforms the PhenomNSBH model.

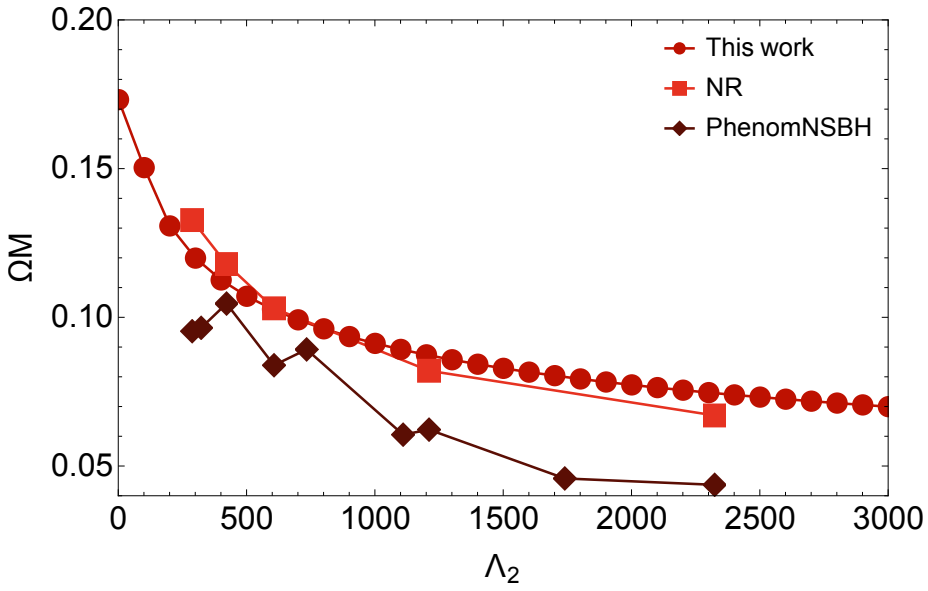

Figure 3.5: NSBH merger frequency (3.6) as a function of Λ_2 for fixed $Q = 2$ and spinless neutron star and black hole compared to NR simulations and the PhenomNSBH model [7].

3.2.2 Mass Ratio Q

In Figure 3.5 the NSBH merger frequency calculated from (3.6) as a function of the mass ration Q is shown for fixed $\Lambda_2 = 1211$ and spinless NS and BH. We observe that the model agrees very well with the trend of the NR data. The deviation at $Q = 5$ can be explained by the fact that we do not have any transition between the Ω_{tidal} and Ω_{BBH}. We just simply take the minimum of the two frequencies. In practice, we expect the frequency to smoothly transition from the disruptive regime where Ω_{tidal} describes the merger frequency, to the non-disruptive regime where Ω_{BBH} describes the merger frequency. This is also the behaviour that is seen in the NR data.

3.2.3 Angular Momentum of the Neutron Star χ_{NS}

In Figure 3.5 the NSBH merger frequency calculated from (3.6) as a function of the neutron star spin χ_{NS} is shown for fixed $\Lambda_2 = 1211$, $Q = 2$ and a spinless BH. Figure 3.5 shows that there are limited NR simulations done for non-zero χ_{NS}. It is therefore not possible to make any observation regarding the trend of the NSBH merger frequency as a function of the neutron star spin. The validation of the model in the neutron star spin regime requires more NR simulations to be done.

3.2.4 Angular Momentum of the Black Hole χ_{BH}

In Figure 3.8 the NSBH merger frequency calculated from (3.6) as a function of the black hole spin parameter χ_{BH} is shown for fixed $\Lambda_2 = 2324$ $Q = 5$ and spinless NS and BH. We observe that our model agrees with the general trend from the NR simulations, although slight deviations can be seen for higher black hole spin. For $\chi_{\text{BH}} > 0.5$, the NR data really starts to diverge. This can be explained by the fact that we work to linear order in the black hole spin. The model will therefore not fully capture the dependence on χ_{BH}. We can also observe that the model greatly outperforms the PhenomNSBH model.

In general, it is remarkable how the model of the merger frequency of an NSBH presented in this thesis captures the dependence on the parameters well. It outperforms the PhenomNSBH

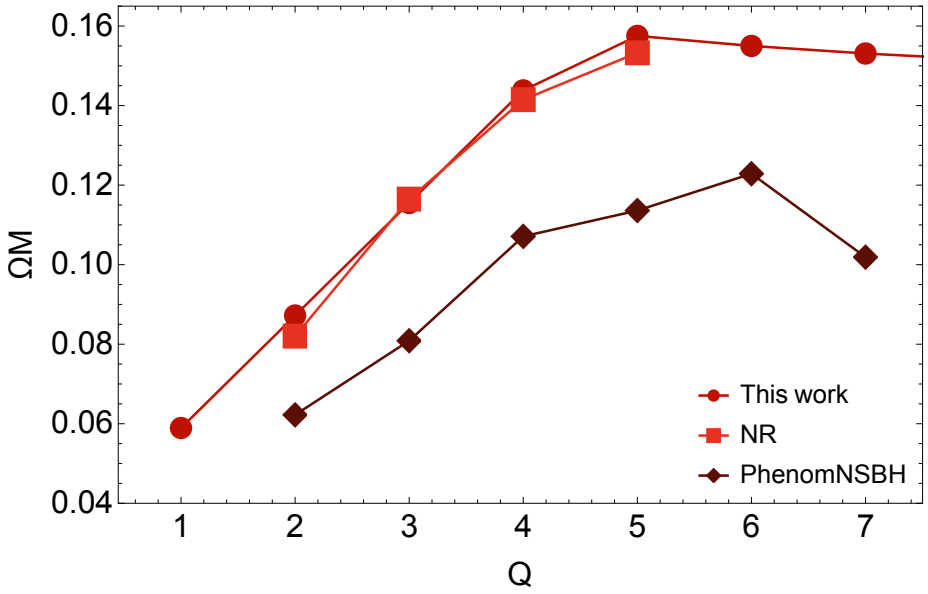

Figure 3.6: NSBH merger frequency (3.6) as a function of Q for fixed $\Lambda_2 = 1211$ and spinless neutron star and black hole compared to NR simulations and the PhenomNSBH model [7].

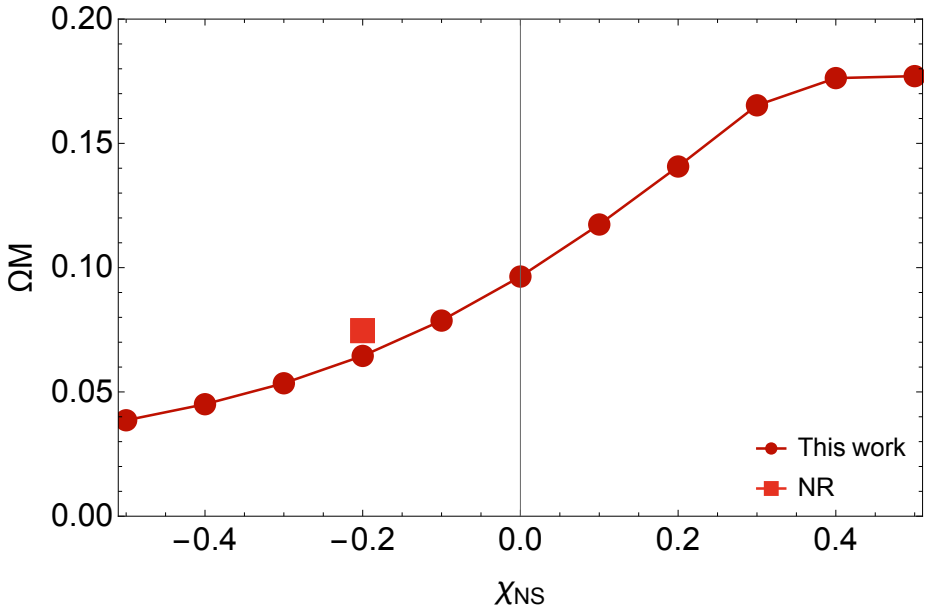

Figure 3.7: NSBH merger frequency (3.6) as a function of $\chi_{\rm NS}$ for fixed $\Lambda_2 = 1211$, $Q = 2$ and a spinless black hole compared to NR simulations and the PhenomNSBH model [7].

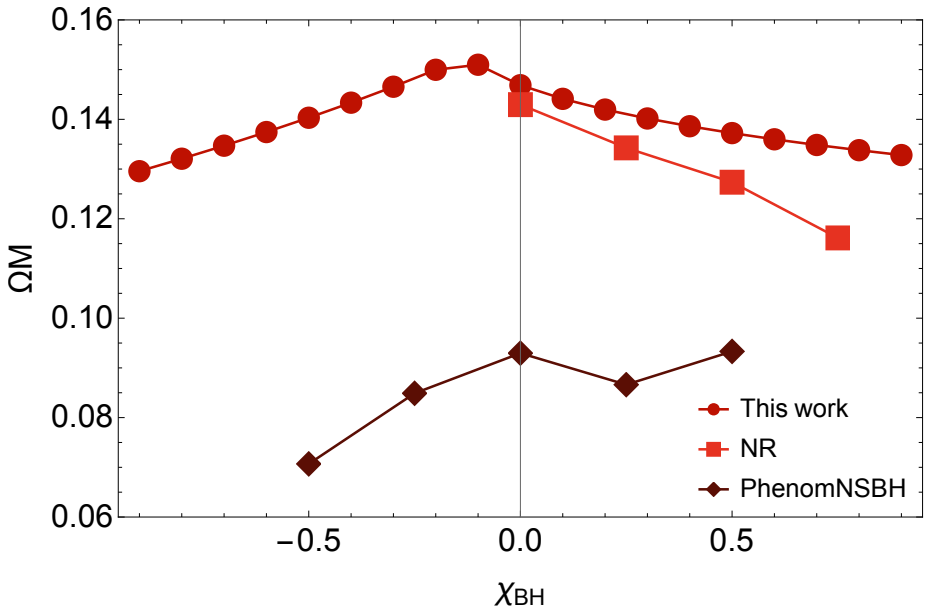

Figure 3.8: NSBH merger frequency (3.6) as a function of $\chi_{\rm BH}$ for fixed $\Lambda_2 = 2324$, $Q = 5$ and a spinless black hole compared to NR simulations and the PhenomNSBH model [7].

model in all aspects. We observe unphysical wiggles in the merger frequency of the PhenomNSBH model in Figures 3.5, 3.6 and 3.8, which could arise from other aspects involved when constructing the waveform than just the calculation of the merger frequency, but this is only speculation. We observe no anomalies in our model for the Λ_2 and Q dependence. The range of validity can therefore be set to $\Lambda_2 \in [1, 5000]$ and $Q \in [1, 10]$ although more NR simulations in the outer regions of the parameter space would be welcome to further validate the model. For the spin dependencies we will restrict the models regime of validity to $\chi_{\rm NS}$ and $\chi_{\rm BH} \in [-0.5, 0.5]$. The expansions up to linear order in the spin parameters restrict us from allowing higher spins. The observation that for $\chi_{\rm BH} > 0.5$ we see the NR data deviating from our model enforces this restriction. For this parameter region, the average absolute relative error can be calculated, both for our model and the PhenomNSBH model compared to the NR data. We will use all the NR data that fits in the above-mentioned region of validity. The $\chi_{\rm NS} = -0.2$ SXS data will be excluded since the PhenomNSNH model does not allow for neutron star spin. We report an average absolute relative error of 4.8% of our model. The PhenomNSBH exhibits an average absolute relative error of 46%. In conclusion, our model significantly increases the accuracy of predicting the merger frequency compared to the PhenomNSBH model.

From the Figures 3.5, 3.6 and 3.8, we also observe that the PhenomNSBH model generally underreports the merger frequency, i.e. the merger frequency is always below the frequency from the NR data. The merger frequencies from the PhenomNSBH model and the NR simulations are obtained in exactly the same way, so errors in comparing the two are not able to enter here. The PhenomNSBH model can be however, subject to all kinds of other systematic errors. We can correct for systematic errors by shifting the relative errors by their mean value. These shifted relative errors give an average absolute relative error 11% for the PhenomNSBH model. The relative errors and their shifted counterparts are shown in Figure 3.9. For our model we also observe a slight shift to the negative side in the relative errors. One explanation could be that our hypothesis of the tidal disruption frequency corresponding one to one to the merger frequency is not entirely correct. This deviation is small however, and only decreases the average absolute relative error down to 4.0%. This small systematic offset leaves us to

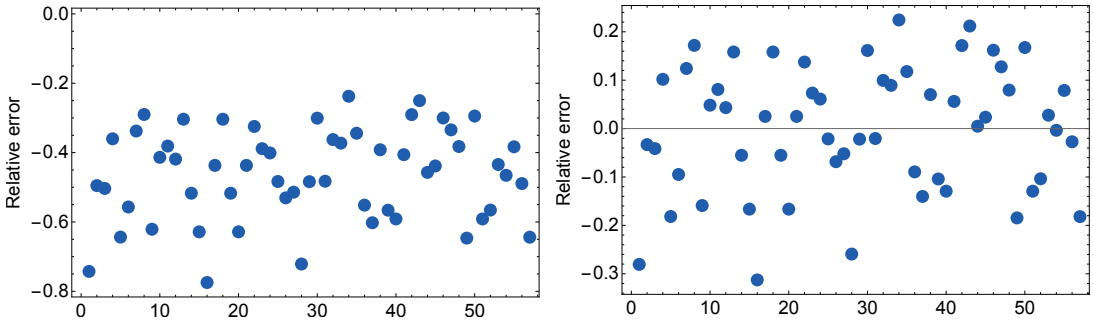

(a) **(b)**

Figure 3.9: The relative errors from the PhenomNSBH model compared to 57 NR simulations from Table F.1 with $\chi_{\rm BH} = 0.75$ excluded: (a) not corrected (b) shifted to a zero mean value.

conclude that our hypothesis that the tidal disruption frequency coincides with the frequency at which the gravitational wave amplitude is at a maximum seems reasonable. The relative errors and the shifted zero mean value relative errors are shown in Figure 3.10. Even with the corrections for systematic errors our model has a better accuracy of almost a factor of three. This means that in any case it captures the dependence of the parameters better.

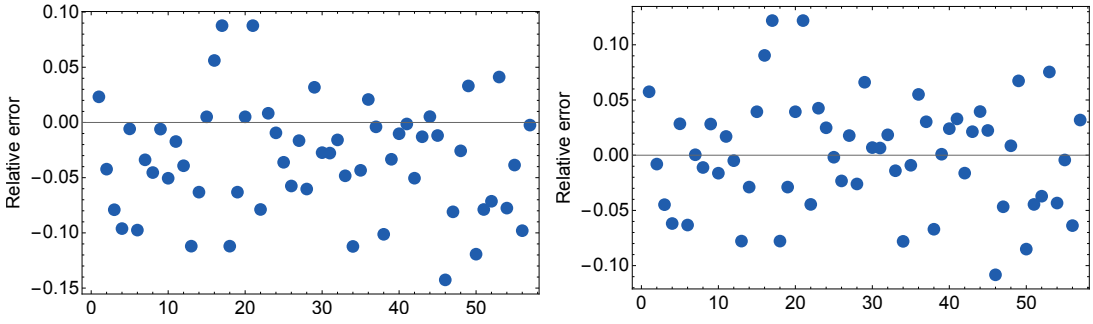

(a) **(b)**

Figure 3.10: The relative errors from our model compared to 57 NR simulations from Table F.1 with $\chi_{\rm BH} = 0.75$ excluded: (a) not corrected (b) shifted to a zero mean value.

3.3 Fitting Procedure

To explicitly find a functional form of $\Omega_{\rm tidal}$ as a function of the four model parameters Λ_2, Q, $\chi_{\rm NS}$ and $\chi_{\rm BH}$ we can fit a model to data generated from (3.5). We will not fit (3.6), since it will be harder to fit to such a composite function. Once we have an explicit function for $\Omega_{\rm tidal}$ we can use the explicit version of $\Omega_{\rm BBH}$ to calculate the merger frequency according to (3.6). We will generate a table that spans the following parameter space: $\Lambda_2 \in \{1, 101, ..., 5001\}$, $Q \in \{1, 2, ..., 10\}$, $\chi_{\rm NS} \in \{-0.5, -0.4, ..., 0.5\}$ and $\chi_{\rm BH} \in \{-0.9, -0.8, ..., 0.9\}$. Subsequently, we can fit a model to the table $\{\Lambda_2^i, Q^i, \chi_{\rm NS}^i, \chi_{\rm BH}^i, \Omega_{\rm tidal}^i\}$ using the `NonLinearModelFit` function from Wolfram Mathematica. Finding a model that fits the data however, is very challenging. The Wolfram documentation [50] states the following on the subject:

One of the most difficult topics in all of data analysis in the physical sciences is fitting data

to nonlinear models. Often such fits require large computational resources and great skill, patience, and intuition on the part of the analyst. These difficulties are one of the reasons that, as we shall see, the whole topic of spectral line shapes is still a very active subject of research spanning the fields of chemistry, physics, astronomy, and more. In addition, computational methods of nonlinear fitting are still a current research topic in computer science.

With this in mind, we do not claim to find the optimal fitting formula here. We merely present an approach in which the fitting procedure can be done. The approach is inspired by [51]. The fitting models are mostly just based on intuition gained from the sensitivity of Ω on the different parameters.

3.3.1 One and Two-Dimensional Fits

We will start with one-dimensional subspace fits to find a good model for the four possible subspaces and to generate good initial conditions for the full final fit. Figure 3.5 inspires the following model for the Ω-Λ subspace:

$$\exp\{\alpha + \beta \ln \Lambda_2 + \gamma(\ln \Lambda_2)^2\}, \tag{3.8}$$

which represents a polynomial on a log-log scale. The other variables do not operate on these larger scales and can therefore independently be modelled by polynomials. The trend of the Ω-Q subspace plots appears to depend heavily on the choice of fixed $\chi_{\rm BH}$. The Ω-Q subspace is therefore modelled by polynomials with coefficients that depend on $\chi_{\rm BH}$ which therefore also models the Ω-Q-$\chi_{\rm BH}$ subspace. Instead of a pure polynomial, we will use the following rational function:

$$\frac{\sum_{i=0}^{3} a_i \chi_{\rm BH}^i Q + \sum_{i=0}^{3} b_i \chi_{\rm BH}^i Q^2 + \sum_{i=0}^{3} c_i \chi_{\rm BH}^i Q^3}{1 + \sum_{i=0}^{3} d_i \chi_{\rm BH}^i Q}, \tag{3.9}$$

where a rational function of polynomials of lower order can approximate a polynomial of higher order, or any other function, according to the Padé approximant [52]. The neutron star spin parameter $\chi_{\rm NS}$ has a much smaller impact on the trend of the other subspace plots. The polynomial in $\chi_{\rm NS}$ will therefore be just added to the model. Also, the Λ_2 parameter is most sensitive to changes in $\chi_{\rm BH}$ and Q, (3.8) will therefore be multiplied with the polynomial that is a function of Q and χ_{BH}. We first fit (3.8) to the data $\{\Lambda_2^i, \Omega_{\rm tidal}^i\}$. We will use the limit of high mass ratio ($Q = 10$) and black hole spin $\chi_{\rm BH} = 0.5$ as fixed values. The reason is that in the final model, the Ω-Λ subspace model (3.8) will be multiplied with the Ω-Q-$\chi_{\rm BH}$ subspace model (3.9) and it is the most important to find initial parameters for when the sensitivities of these subspace functions are the greatest. The best fit parameters which will serve as initial conditions for the final fit are shown in Table 3.2. Subsequently, we fit (3.9) to the data $\{Q^i, \chi_{\rm BH}^i, \Omega_{\rm tidal}^i\}$ with intermediate fixed values for the tidal deformability parameter ($\Lambda_2 = 1001$) and the neutron star's spin ($\chi_{\rm NS} = 0$). The best fit parameters which will serve as initial conditions for the final fit are shown in the left column of Table 3.2.

3.3.2 Full-Dimensional Fit

The final fitting model for the tidal disruption frequency consists of (3.8) multiplied with (3.9) and a polynomial in $\chi_{\rm NS}$ added:

$$\Omega = \exp\{\alpha + \beta \ln \Lambda_2 + \gamma(\ln \Lambda_2)^2\} \frac{\sum_{i=0}^{3} a_i \chi_{\rm BH}^i Q + \sum_{i=0}^{3} b_i \chi_{\rm BH}^i Q^2 + \sum_{i=0}^{3} c_i \chi_{\rm BH}^i Q^3}{1 + \sum_{i=0}^{3} d_i \chi_{\rm BH}^i Q} + \sum_{i=1}^{3} e_i \chi_{\rm NS}^i. \tag{3.10}$$

The model with the initial conditions from Table 3.2 can be fit to the data $\{\Lambda_2^i, Q^i, \chi_{\rm NS}^i, \chi_{\rm BH}^i, \Omega_{\rm tidal}^i\}$ using `NonLinearModelFit`. We included the constraint $|\alpha| < 1$ to ensure the fitting formula is well behaved. The final fit parameters are shown in the middle column of Table 3.2. The merger frequency is again given by the minimum of the frequency obtained from the fit and the BBH merger frequency.

a_0	2.88589	a_0	6910.96	a_0	37030.2
a_1	25.004	a_1	167606.	a_1	$-267867.$
a_2	77.4691	a_2	555439.	a_2	664730.
a_3	33.9088	a_3	274936.	a_3	$-477051.$
b_0	2.73311	b_0	7026.48	b_0	78145.5
b_1	24.6834	b_1	178265.	b_1	-9023.64
b_2	74.4328	b_2	517780.	b_2	$-273972.$
b_3	20.0229	b_3	60698.	b_3	223018.
c_0	-0.000772169	c_0	-10.2872	c_0	-7269.02
c_1	-0.309261	c_1	-4154.87	c_1	1735.72
c_2	-1.18553	c_2	-13337.1	c_2	29650.4
c_3	-0.913701	c_3	-2163.82	c_3	-26887.2
d_0	205197.	d_0	70515.3	d_0	1.91904×10^8
d_1	1.79948×10^6	d_1	1.70683×10^6	d_1	-2.59297×10^8
d_2	5.48092×10^6	d_2	5.32785×10^6	d_2	1.19994×10^8
d_3	1.92115×10^6	d_3	1.81105×10^6	d_3	-6.49771×10^7
α	$-8.99429317474172 \times 10^{-8}$	α	0.00111765	α	5.68328
β	-1.24268×10^{-4}	β	-0.0840207	β	0.0840207
γ	-8.19994×10^{-3}	γ	-0.0112478	γ	-0.00818597
		e_1	0.243007	e_1	0.113971
		e_2	0.0503988	e_2	0.0503988
		e_3	-0.191301	e_3	0.191301

Table 3.2: Left column: initial conditions for the fitting model (3.10). Middle column: best fit parameters for (3.10) fitted to the data from our tidal disruption frequency model $\{\Lambda_2^i, Q^i, \chi_{\rm NS}^i, \chi_{\rm BH}^i, \Omega_{\rm tidal}^i\}$. Right column: best fit parameters for (3.10) fitted to the NR data with the middle column as initial parameters.

3.3.3 Fit Including Numerical Relativity Data

The fitting formula (3.10) can also be fitted again to the NR data by using the same model with the best fit parameters found in the middle column of Table 3.2 as initial parameter values. The final fitting model is (3.10) with the best fit parameters given by the right column of Table 3.2.

The hope is that the normal merger frequency model (3.6) captures the dependence on the parameters and that a fitting procedure against the NR simulations will only just alter the coefficients such that better agreement with the NR data is reached. A closed-form expression, which can be reached using a fitting procedure, is computationally more efficient to include in a model than having to solve the energy balance every time one wants to generate a waveform. However, as stated at the beginning of this section 3.3, finding an excellent fit is an art. Especially with a function dependent on four variables. The fits produced here are therefore not of great quality, and the relative errors supersede the relative errors of our normal merger frequency model (3.6). One two-dimensional subspace plot is shown in Figure 3.11. An interesting feature that can be observed is that the model fitted to the NR data behaves similar to the PhenomNSBH model. The model fitted to NR trends downward for higher Q because in other regions of the parameter space, namely that of higher $\chi_{\rm BH}$, this feature is present. The fitting formula is unable to have the correct sensitivity to all the parameters in the entire regime. This could be a reason for the behaviour of the PhenomNSBH model, because this model is calibrated to NR data. This is just speculation however.

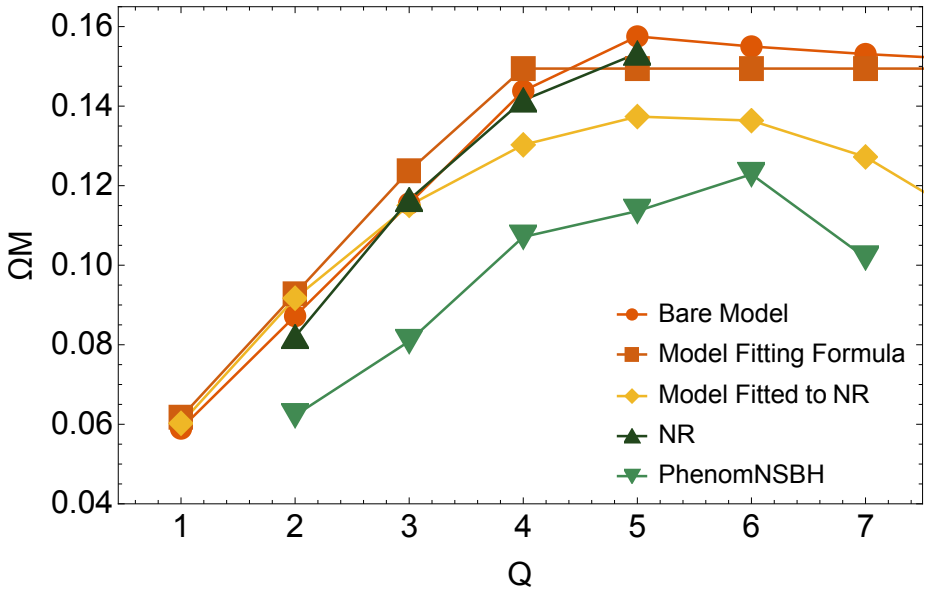

Figure 3.11: NSBH merger frequency (3.6) as a function of Q for fixed $\Lambda_2 = 1211$ and a spinless neutron star and black hole compared to NR simulations, the PhenomNSBH model [7] and the two fitting functions to the merger frequency (3.6) and the NR data.

Chapter 4

Discussion

With the first observations of BBHs, BNs and NSBHs with the LIGO and VIRGO detectors, the need for accurate waveform models came along. While BBHs and BNSs have been the subject of many studies over the past years, NSBHs have been left behind a little bit. NSBHs can give us yet still unknown information about the EOS of the NS. NSBHs are especially interesting to achieve this goal because in an NSBH system, all matter effects can be attributed to the single neutron star, as opposed to a BNS system where matter from the different stars interacts in all sorts of ways. Accurate NSBH waveform models are therefore called for. We are not yet at the point where NR simulations can cover the entire parameter space with waveform templates. The need for computational light, easy-to-use waveform models thus remains.

A unique feature of NSBHs compared to BBHs is that tidal disruption can occur before the neutron star merges with the black hole. The key input parameter for an NSBH waveform model is therefore the tidal disruption frequency. In this thesis, we presented a novel way of calculating the tidal disruption frequency. We calculated the tidal disruption frequency by considering an energy balance that is constructed from setting up a classical action of the NSBH system. This action included first PN order spin-coupling terms coming from an effective field theory description to incorporate the different angular momenta of the system. The action thus also includes general relativistic effects and can therefore be viewed as an effective action. We showed that the model presented in this thesis greatly outperforms the PhenomNSBH model [7] when comparing our merger frequency with theirs.

The parameter region of validity is given by $\Lambda_2 \in [1, 5000]$, $Q \in [1, 10]$, $\chi_{\rm NS}$ and $\chi_{\rm BH} \in [-0.5, 0.5]$. The model is valid for aligned spins. The tidal disruption model depends on empirical fits for $M_{\rm bar}$ (3.1), I, ω_{02} and $M_{\rm NS}/R_{\rm NS}$ (3.2). The final merger frequency also depends on the BBH frequency fit (3.7). These quantities all come with uncertainties of less than a few percent [44, 45, 46, 47, 48]. Furthermore, several approximations have been made: we worked to linear order in the tidal effects and with it to linear order in the tidal deformability parameter λ_2; we worked to linear order in the NS and BH spin; we included only the first multipole moment Q_{ij} and with it only the fundamental-mode frequency ω_{02} of the neutron star. With these approximations in place, we still managed to predict the merger frequency of an NSBH system with an average absolute relative error of 4.8% compared to 57 NR simulations. We view the inevitable conclusion therefore as that the presented approach in this thesis is a success worth pursuing till the end.

The tidal disruption frequency presented in this thesis can also be used as a tool to find regimes where NR simulations can be worth the computation power. The disruptive regime, which we predict as the regime where $\Omega_{\rm tidal} < \Omega_{\rm BBH}$, is the regime where NSBH NR simulations can be worth it. Simulating an NSBH that behaves exactly like a BBH is considered a waste of resources. We can prevent this by using the condition presented in this thesis.

Naturally, the first extensions of the model consist of including higher orders. For now, the black hole spin parameter region is a regime where profit can be made. Thus, adding terms to the Lagrangian with higher order spin can make a positive contribution. These higher order spin terms are already given in [41]. The neutron star spin parameter cannot be discussed because there are no NR simulations in the regime sensitive to $\chi_{\rm NS}$ spin variation. Pure from a model validation standpoint, we therefore recommend more simulations with non-zero neutron star spin to be done. The preferred region is the negative neutron star spin region, since this corresponds to the most disruptive regime.

Another viable extension of the model includes a smooth transition between the $\Omega_{\rm tidal}$ and $\Omega_{\rm BBH}$, i.e. between the disruptive and the non-disruptive regime. This makes the model accurate in the regime where the tidal disruption frequency does not fully yield the merger frequency but where the BBH merger frequency also does not fully yield the merger frequency of the NSBH.

A big strength of our model is that it does not require the introduction of free fit parameters. Current waveform models highly depend on these free fit parameters and overfitting therefore always lurks around the corner. Our model merger frequency model could be part of a much more independent waveform model that does not rely on these fit parameters. In section 3.3 we outlined a procedure to find an explicit formula for the tidal disruption frequency, but such a fitting function would only be a viable option to use when it is more accurate. Even though the NR data was used in constructing the fitting formula, the predictive power of the model decreased compared to our normal frequency model (3.5). A closed-form expression is the most efficient way of computing a merger frequency, which is advantageous to generate waveforms fast, but improvements on the accuracy of the fit have to be made for it to qualify as a contender to use in waveform models. We therefore recommend to use (3.6) together with the energy balance (3.5) in a waveform model to model the merger frequency of an NSBH. The energy balance can be solved as soon as the other parameters are known.

Apart from more sophisticated methods for the fitting formula, it can also be improved by ensuring that it goes to the BBH merger frequency in the appropriate limits. The nature of the fitting formula allows it to stay under the BBH merger frequency for parameter values which are in the non-disruptive regime. In Figure 3.11 it can be seen that the fitting function trends down again, while it has reached the non-disruptive regime. If the fitting formula reaches values above the BBH merger frequency, the BBH merger frequency would automatically take on the NSBH merger frequency for the fitting model according to $\Omega = \min(\Omega_{\rm tidal}, \Omega_{\rm BBH})$. Incorporating these appropriate constraints into the fitting procedure could therefore also improve its accuracy.

Finally, we want to devote some words to the big difference in the average absolute relative error of our model compared to the PhenomNSBH model. It has to be noted that the PhenomNSBH model, as well as other waveform models in the literature, e.g. [8], do not use the distinct peak in the waveform amplitude as a benchmark to model the waveform, i.e. it was not their main goal to get the best merger frequency when constructing their model. This does not mean however, that it has no meaning to compare to these models. On the contrary, the peak amplitude of a gravitational waveform is one of a GWs most clearly visible features and therefore also the most clearly visible in the GW signals measured by the detectors. In our eyes, this should therefore also be the most important aspect of a waveform model. We therefore conclude that the approach to construct waveforms for NSBHs can be improved by adopting this new point of view: constructing the waveforms using the merger frequency as a diagnostic for the peak amplitude of the waveform. This work has presented exactly how this merger frequency can be calculated, which is ready to be used in future NSBH waveform models.

As an outlook, the first immediate steps are to finish this work by realising an actual waveform

model using the merger frequency presented in this thesis. This will not be done however, before we attempt to include higher order black hole spin interactions, since we think that this is where we can make the most profit in the accuracy of the model. To achieve this goal, existing BBH and NSBH waveform models can be modified using their publicly available codes from the LALsuite library [49]. Once it is possible to generate waveforms, it is also possible to statistically analyse the waveforms in depth. A usual method is to calculate the overlap integral of the two waveforms to test their agreement.

Bibliography

[1] B. P. Abbott et al. "Observation of Gravitational Waves from a Binary Black Hole Merger". In: *Physical Review Letters* 116.6 (Feb. 2016).

[2] B. P. Abbott et al. "GW170817: Observation of Gravitational Waves from a Binary Neutron Star Inspiral". In: *Phys. Rev. Lett.* 119.16 (2017), p. 161101. arXiv: 1710.05832 [gr-qc].

[3] R. A. et al. "Observation of Gravitational Waves from Two Neutron Star–Black Hole Coalescences". In: *The Astrophysical Journal Letters* 915.1 (June 2021), p. L5.

[4] *SXS Gravitational Waveform Database*. https://data.black-holes.org/waveforms/index.

[5] K. Kyutoku, M. Shibata, and K. Taniguchi. "Gravitational waves from nonspinning black hole-neutron star binaries: dependence on equations of state". In: *Phys. Rev. D* 82 (2010). [Erratum: Phys.Rev.D 84, 049902 (2011)], p. 044049. arXiv: 1008.1460 [astro-ph.HE].

[6] K. Kyutoku et al. "Gravitational waves from spinning black hole-neutron star binaries: dependence on black hole spins and on neutron star equations of state". In: *Phys. Rev. D* 84 (2011), p. 064018. arXiv: 1108.1189 [astro-ph.HE].

[7] J. E. Thompson et al. "Modeling the gravitational wave signature of neutron star black hole coalescences". In: *Phys. Rev. D* 101.12 (2020), p. 124059. arXiv: 2002.08383 [gr-qc].

[8] A. Matas et al. "Aligned-spin neutron-star–black-hole waveform model based on the effective-one-body approach and numerical-relativity simulations". In: *Phys. Rev. D* 102.4 (2020), p. 043023. arXiv: 2004.10001 [gr-qc].

[9] S. Carroll. *Spacetime and Geometry: An Introduction to General Relativity*. Benjamin Cummings, 2003.

[10] G. Weinstein. *Einstein's Discovery of Gravitational Waves 1916-1918*. 2016. arXiv: 1602.04040 [physics.hist-ph].

[11] A. Einstein. "On gravitational waves Sitzungsber. preuss". In: *Acad. Wiss* 1 (1918), p. 154.

[12] J. M. Bardeen. "Gauge Invariant Cosmological Perturbations". In: *Phys. Rev. D* 22 (1980), pp. 1882–1905.

[13] É. É. Flanagan and S. A. Hughes. "The basics of gravitational wave theory". In: *New Journal of Physics* 7 (Sept. 2005), pp. 204–204.

[14] A. Marunovic and T. Prokopec. "Time transients in the quantum corrected Newtonian potential induced by a massless nonminimally coupled scalar field". In: *Physical Review D* 83.10 (May 2011).

[15] T. Rother. *Green's Functions in Classical Physics*. Vol. 938. Lecture Notes in Physics. Springer International Publishing, Mai 2017, pp. 1–267.

[16] J. W. van Holten. *Dynamical Space-Time and Gravitational Waves*. 2016. arXiv: 1611.01289 [gr-qc].

[17] C. W. Misner, K. S. Thorne, and J. A. Wheeler. *Gravitation*. Macmillan, 1973.

[18] M. Maggiore. *Gravitational Waves: Volume 1: Theory and Experiments*. Gravitational Waves. OUP Oxford, 2008.

[19] T. Hartmann, M. H. Soffel, and T. Kioustelidis. "On the Use of STF-Tensors in Celestial Mechanics". In: *Celestial Mechanics and Dynamical Astronomy* 60.1 (Sept. 1994), pp. 139–159.

[20] R. A. Hulse and J. H. Taylor. "Discovery of a pulsar in a binary system." In: 195 (Jan. 1975), pp. L51–L53.

[21] and J Aasi et al. "Advanced LIGO". In: *Classical and Quantum Gravity* 32.7 (Mar. 2015), p. 074001.

[22] B. P. Abbott et al. "The basic physics of the binary black hole merger GW150914". In: *Annalen Phys.* 529.1-2 (2017), p. 1600209. arXiv: 1608.01940 [gr-qc].

[23] A. et al. "Properties of the Binary Black Hole Merger GW150914". In: *Phys. Rev. Lett.* 116 (24 June 2016), p. 241102.

[24] C. E. Rhoades and R. Ruffini. "Maximum Mass of a Neutron Star". In: *Phys. Rev. Lett.* 32 (6 Feb. 1974), pp. 324–327.

[25] M. Hannam et al. "When can gravitational-wave observations distinguish between black holes and neutron stars?" English. In: *Astrophysical Journal Letters* 766.1 (Mar. 2013). 5 pages, 4 figures. Final version to be published in Ap.J.Lett.

[26] V. Kalogera and G. Baym. "The Maximum Mass of a Neutron Star". In: 470 (Oct. 1996), p. L61. arXiv: astro-ph/9608059 [astro-ph].

[27] M. Boyle et al. "The SXS collaboration catalog of binary black hole simulations". In: *Classical and Quantum Gravity* 36.19 (Sept. 2019), p. 195006.

[28] G. Fragione. "Black-hole–Neutron-star Mergers Are Unlikely Multimessenger Sources". In: *Astrophys. J. Lett.* 923.1 (2021), p. L2. arXiv: 2110.09604 [astro-ph.HE].

[29] P. Amaro-Seoane et al. "Laser Interferometer Space Antenna". In: (Feb. 2017). arXiv: 1702.00786 [astro-ph.IM].

[30] M. Punturo et al. "The Einstein Telescope: A third-generation gravitational wave observatory". In: *Class. Quant. Grav.* 27 (2010). Ed. by F. Ricci, p. 194002.

[31] M. Bulla et al. "Multi-Messenger Constraints on the Hubble Constant through Combination of Gravitational Waves, Gamma-Ray Bursts and Kilonovae from Neutron Star Mergers". In: *Universe* 8.5 (2022), p. 289. arXiv: 2205.09145 [astro-ph.HE].

[32] F. Foucart. "A Brief Overview of Black Hole-Neutron Star Mergers". In: *Frontiers in Astronomy and Space Sciences* 7 (2020), p. 46.

[33] F. Foucart. "Black-hole–neutron-star mergers: Disk mass predictions". In: *Physical Review D* 86.12 (Dec. 2012).

[34] T. Hinderer, L. Rezzolla, and L. Baiotti. "Gravitational Waves from Merging Binary Neutron-Star Systems". In: *Astrophys. Space Sci. Libr.* 457 (2018), pp. 575–635.

[35] K. S. Thorne. "Multipole expansions of gravitational radiation". In: *Rev. Mod. Phys.* 52 (2 Apr. 1980), pp. 299–339.

[36] J. Vines, É. É. Flanagan, and T. Hinderer. "Post-1-Newtonian tidal effects in the gravitational waveform from binary inspirals". In: *Physical Review D* 83.8 (Apr. 2011).

[37] S. Chakrabarti, T. Delsate, and J. Steinhoff. "Effective action and linear response of compact objects in Newtonian gravity". In: *Physical Review D* 88.8 (Oct. 2013).

[38] G. Creci, T. Hinderer, and J. Steinhoff. *Tidal response from scattering and the role of analytic continuation.* 2021. arXiv: 2108.03385 [gr-qc].

[39] J. Steinhoff et al. "Dynamical tides in general relativity: Effective action and effective-one-body Hamiltonian". In: *Physical Review D* 94.10 (Nov. 2016).

[40] E. E. Flanagan and T. Hinderer. "Constraining neutron star tidal Love numbers with gravitational wave detectors". In: *Phys. Rev. D* 77 (2008), p. 021502. arXiv: 0709.1915 [astro-ph].

[41] M. Levi and J. Steinhoff. "Next-to-next-to-leading order gravitational spin-orbit coupling via the effective field theory for spinning objects in the post-Newtonian scheme". In: *Journal of Cosmology and Astroparticle Physics* 2016.01 (Jan. 2016), pp. 011–011.

[42] K.-W. Lo and L.-M. Lin. "The spin parameter of uniformly rotating compact stars". In: *Astrophys. J.* 728 (2011), p. 12. arXiv: 1011.3563 [astro-ph.HE].

[43] J. Steinhoff et al. "Spin effects on neutron star fundamental-mode dynamical tides: Phenomenology and comparison to numerical simulations". In: *Physical Review Research* 3.3 (Aug. 2021).

[44] M. Coughlin et al. "Toward Rapid Transient Identification and Characterization of Kilonovae". In: *Astrophys. J.* 849.1 (2017), p. 12. arXiv: 1708.07714 [astro-ph.HE].

[45] K. Yagi and N. Yunes. "Approximate Universal Relations for Neutron Stars and Quark Stars". In: *Phys. Rept.* 681 (2017), pp. 1–72. arXiv: 1608.02582 [gr-qc].

[46] T. K. Chan et al. "Multipolar universal relations between f-mode frequency and tidal deformability of compact stars". In: *Phys. Rev. D* 90.12 (2014), p. 124023. arXiv: 1408.3789 [gr-qc].

[47] K. Yagi and N. Yunes. "I-Love-Q". In: *Science* 341 (2013), pp. 365–368. arXiv: 1302.4499 [gr-qc].

[48] A. Bohé et al. "Improved effective-one-body model of spinning, nonprecessing binary black holes for the era of gravitational-wave astrophysics with advanced detectors". In: *Phys. Rev. D* 95.4 (2017), p. 044028. arXiv: 1611.03703 [gr-qc].

[49] LIGO Scientific Collaboration. *LALSuite: LIGO Scientific Collaboration Algorithm Library Suite*. Astrophysics Source Code Library, record ascl:2012.021. Dec. 2020. ascl: 2012.021.

[50] *Wolfram* `NonLinearModelFit` *documentation*. https://reference.wolfram.com/applications/eda/Fittin Accessed: 25-06-2022.

[51] X. Jiménez-Forteza et al. "Hierarchical data-driven approach to fitting numerical relativity data for nonprecessing binary black holes with an application to final spin and radiated energy". In: *Phys. Rev. D* 95.6 (2017), p. 064024. arXiv: 1611.00332 [gr-qc].

[52] P. Wynn. "On the Convergence and Stability of the Epsilon Algorithm". In: *SIAM Journal on Numerical Analysis* 3.1 (1966), pp. 91–122. eprint: https://doi.org/10.1137/0703007.

[53] G. Schafer. "Gravitational quadrupole radiation-reaction force and the canonical formalism of ADM". In: *Ann. Phys. (N.Y.); (United States)* 161:1 (Apr. 1985).

[54] G. Schäfer and P. Jaranowski. "Hamiltonian formulation of general relativity and post-Newtonian dynamics of compact binaries". In: *Living Rev. Rel.* 21.1 (2018), p. 7. arXiv: 1805.07240 [gr-qc].

Appendix A

Decomposition of the Metric Perturbation into Gauge Invariant Quantities

We assume that the metric is given by the Minkowski metric with small perturbations. To decompose this metric perturbation into gauge invariant quantities we will first consider the behaviour of the metric perturbation when subject to rotations.

The metric perturbation $h_{\mu\nu}(x)$, which is a second rank tensor, transforms as:

$$\widetilde{h}_{\mu\nu}(\tilde{x}) = \frac{\partial x^\alpha}{\partial \tilde{x}^\mu}\frac{\partial x^\beta}{\partial \tilde{x}^\nu} h_{\alpha\beta}(x). \tag{A.1}$$

Under spatial rotations our coordinates transform as:

$$t \to \tilde{t} = t, \quad x^i \to \tilde{x}^i = \frac{\partial \tilde{x}^i}{\partial x^j} x^j = R^i_j x^j. \tag{A.2}$$

The 00-component of the metric perturbation therefore transforms as:

$$\widetilde{h}_{00}(\tilde{x}) = \frac{\partial x^\alpha}{\partial t}\frac{\partial x^\beta}{\partial t} h_{\alpha\beta}(x) = h_{00}(x), \tag{A.3}$$

and thus transforms as a scalar. The 0i-component transforms as

$$\widetilde{h}_{0i}(\tilde{x}) = \frac{\partial x^\alpha}{\partial t}\frac{\partial x^\beta}{\partial \tilde{x}^i} h_{\alpha\beta}(x) = \frac{\partial x^\beta}{\partial \tilde{x}^i} h_{0\beta}(x) = R^\beta_i h_{0\beta}(x), \tag{A.4}$$

and thus transforms as a spatial three-vector. Finally we have

$$\widetilde{h}_{ij}(\tilde{x}) = \frac{\partial x^\alpha}{\partial \tilde{x}^i}\frac{\partial x^\beta}{\partial \tilde{x}^j} h_{\alpha\beta}(x) = R^\alpha_i R^\beta_j h_{\alpha\beta}(x), \tag{A.5}$$

such that $h_{ij}(x)$ transforms as a symmetric spatial tensor of rank two. We will now relabel the scalar as:

$$h_{00} = 2\phi. \tag{A.6}$$

The spatial three-vector under spatial rotations can be further decomposed as:

$$h_{0i} = B_i + \partial_i S \tag{A.7}$$

where B_i is the transverse (divergence-free) part that obeys $\partial^i B_i = 0$ and $\partial_i S$ is the longitudinal (curl-free) part of h_{0i}, since indeed $\nabla \times (\nabla S) = 0$ holds for any scalar function. The symmetric spatial tensor under spatial rotations can be decomposed as:

$$h_{ij} = 2\delta_{ij}\psi + 2\partial_i\partial_j E + \partial_i F_j + \partial_j F_i + h^{\mathrm{TT}}_{ij}. \tag{A.8}$$

Here ψ and E are scalar functions, F_j is a transverse vector that obeys $\partial^j F_j = 0$ and $h_{ij}^{\rm TT}$ is a transverse traceless tensor that obeys $\partial^i h_{ij}^{\rm TT} = 0$ and $(h^{\rm TT})_i^i = 0$. The transverse traceless tensor is known as the strain and will turn out to contain GWs. We will examine how the introduced quantities behave under infinitesimal coordinate transformations. Consider the infinitesimal coordinate transformation:

$$x^\mu \to \widetilde{x}^\mu = x^\mu + \xi^\mu(x), \quad |\xi| \ll 1. \tag{A.9}$$

The metric (1.1) transforms according to the same transformation law as the metric perturbation (A.1). Using the above coordinate transformation law, both the l.h.s. and the r.h.s. of the transformed metric can be Taylor expanded as:

$$\begin{aligned} \widetilde{g}_{\mu\nu}(x) + \xi^\alpha \partial_\alpha g_{\mu\nu}(x) &= (\delta_\mu^\alpha - \partial_\mu \xi^\alpha(x))(\delta_\nu^\beta - \partial_\nu \xi^\beta(x)) g_{\alpha\beta}(x) \\ &= g_{\mu\nu}(x) - g_{\alpha\nu}\partial_\mu \xi^\alpha(x) - g_{\mu\beta}\partial_\nu \xi^\beta(x), \end{aligned} \tag{A.10}$$

up to first order in ξ. Using the definitions of the covariant derivative $\nabla_\mu \xi_\nu = \partial_\mu \xi_\nu - \Gamma^\alpha_{\mu\nu}\xi_\alpha$ and the connection $\Gamma^\alpha_{\mu\nu} = \frac{1}{2} g^{\alpha\rho}\left(\partial_\mu g_{\nu\rho} + \partial_\nu g_{\rho\mu} - \partial_\rho g_{\mu\nu}\right)$ we can write the above expression as:

$$\widetilde{g}_{\mu\nu}(x) = g_{\mu\nu}(x) - \nabla_\mu \xi_\nu(x) - \nabla_\mu \xi_\nu(x). \tag{A.11}$$

Using (1.1) we can immediately see that $h_{\mu\nu}$ transforms under infinitesimal coordinate transformations as:

$$\widetilde{h}_{\mu\nu}(x) = h_{\mu\nu}(x) - \partial_\mu \xi_\nu(x) - \partial_\mu \xi_\nu(x). \tag{A.12}$$

We have seen that under spatial rotations ξ_μ can be decomposed into a scalar ξ_0 and a vector $\xi_i = \xi_i^T + \partial_i \xi^S$. We can therefore derive the transformation rules for ϕ, B_i, S, ψ, E, F_i and h_{ij}^T by first evaluating how $h_{00}(x)$, $h_{0i}(x)$ and $h_{ij}(x)$ transform:

$$\begin{aligned} h_{00} \to \tilde{h}_{00} &= h_{00} - 2\partial_0 \xi_0 \\ &= 2\widetilde{\phi} = 2\phi - 2\partial_0 \xi_0 \\ h_{0i} \to \tilde{h}_{0i} &= h_{0i} - \partial_0(\xi_i^T + \partial_i \xi^S) - \partial_i \xi_0 \\ &= \tilde{B}_i + \partial_i \tilde{S} = B_i + \partial_i S - \partial_0(\xi_i^T + \partial_i \xi^S) - \partial_i \xi_0 \\ h_{ij} \to \tilde{h}_{ij} &= h_{ij} - \partial_i(\xi_j^T + \partial_j \xi^S) - \partial_j(\xi_i^T + \partial_i \xi^S) = h_{ij} - \partial_i \xi_j^T - \partial_j \xi_i^T - 2\partial_i \partial_j \xi^S \\ &= 2\delta_{ij}\widetilde{\psi} + 2\partial_i \partial_j \widetilde{E} + \partial_i \widetilde{F}_j + \partial_j \widetilde{F}_i + \widetilde{h}_{ij}^{\rm TT} \\ &= 2\delta_{ij}\psi + 2\partial_i \partial_j E + \partial_i F_j + \partial_j F_i + h_{ij}^{\rm TT} - \partial_i \xi_j^T - \partial_j \xi_i^T - 2\partial_i \partial_j \xi^S. \end{aligned} \tag{A.13}$$

By comparing the scalar, transverse, longitudinal and transverse traceless parts we then have:

$$\begin{aligned} \phi(x) &\to \widetilde{\phi}(x) = \phi(x) - \partial_0 \xi_0(x) \\ S(x) &\to \widetilde{S}(x) = S(x) - \xi_0(x) - \partial_0 \xi^S(x) \\ \psi(x) &\to \widetilde{\psi}(x) = \psi(x) \\ E(x) &\to \widetilde{E}(x) = E(x) - \xi^S(x) \\ B_i(x) &\to \widetilde{B}_i(x) = B_i(x) - \partial_0 \xi_i^T(x) \\ F_i(x) &\to \widetilde{F}_i(x) = F_i(x) - \xi_i^T(x) \\ h_{ij}^{\rm TT}(x) &\to \widetilde{h}_{ij}^{\rm TT}(x) = h_{ij}^{\rm TT}(x) \end{aligned} \quad . \tag{A.14}$$

We can immediately see that $\psi(x)$ and $h_{ij}^{\rm TT}(x)$ are invariant under the considered linear coordinate transformation, i.e. they are gauge invariant. We can construct even more gauge invariant quantities by taking the appropriate combinations of the transformation laws above. This gives us the gauge invariant scalar $\Phi(x) = \phi(x) - \partial_0 S(x) + \partial_0^2 E(x)$ and the gauge invariant transverse vector $\overline{B}_i(x) = B_i(x) - \partial_0 F_i(x)$. The two gauge invariant potentials $\Phi(x)$ and

$\psi(x) = \Psi(x)$ are known as the Bardeen potentials.

We are now ready to look at Einstein's equation, we will need expressions for the Ricci tensor and scalar, for which we will first evaluate the Riemann tensor (0.4). The Riemann tensor for the metric (1.1) up to first order in the metric perturbation $h_{\mu\nu}$ is given by:

$$\begin{aligned} R^{\rho}_{\sigma\mu\nu} &= \partial_\mu \Gamma^{\rho}_{\nu\sigma} - \partial_\nu \Gamma^{\rho}_{\mu\sigma} + \Gamma^{\rho}_{\mu\lambda}\Gamma^{\lambda}_{\nu\sigma} - \Gamma^{\rho}_{\nu\lambda}\Gamma^{\lambda}_{\mu\sigma} \\ &= \tfrac{1}{2}\partial_\eta(\eta^{\rho\lambda}(\partial_\nu h_{\sigma\lambda} + \partial_\sigma h_{\lambda\nu} - \partial_\lambda h_{\nu\sigma})) - \tfrac{1}{2}\partial_\nu(\eta^{\rho\lambda}(\partial_\mu h_{\sigma\lambda} + \partial_\sigma h_{\lambda\mu} - \partial_\lambda h_{\mu\sigma})) \\ &= \tfrac{1}{2}\eta^{\rho\lambda}(\partial_\mu\partial_\sigma h_{\lambda\nu} + \partial_\nu\partial_\lambda h_{\mu\sigma} - \partial_\mu\partial_\lambda h_{\nu\sigma} - \partial_\nu\partial_\sigma h_{\lambda\mu}). \end{aligned} \tag{A.15}$$

Because we have a flat metric background indices can be lowered and raised by the Minkowski metric to obtain:

$$R_{\rho\sigma\mu\nu} = \tfrac{1}{2}(\partial_\mu\partial_\sigma h_{\rho\nu} + \partial_\nu\partial_\rho h_{\mu\sigma} - \partial_\mu\partial_\rho h_{\nu\sigma} - \partial_\nu\partial_\sigma h_{\rho\mu}). \tag{A.16}$$

The Ricci tensor is given by:

$$\eta^{\rho\mu}R_{\rho\sigma\mu\nu} = R_{\sigma\nu} = \tfrac{1}{2}(\partial_\sigma\partial^\alpha h_{\alpha\nu} + \partial_\nu\partial^\alpha h_{\alpha\sigma} - \Box h_{\nu\sigma} - \partial_\nu\partial_\sigma h), \tag{A.17}$$

where $h = h^\alpha_\alpha$ is the trace of $h_{\nu\sigma}$. Let us now calculate the different components of the Ricci tensor in terms of the decomposition variables. For R_{00} we have:

$$\begin{aligned} R_{00} &= \tfrac{1}{2}(2\partial_0\partial^i h_{0i00} - \partial_0^2 h^i_i) \\ &= -\nabla^2(\phi - \partial_0 S + \partial_0^2 E) - 3\partial_0^2\psi \\ &= -\nabla^2\Phi - 3\partial_0^2\Psi, \end{aligned} \tag{A.18}$$

where we used that B_i and F_i are divergence-free and $\nabla^2 = \partial_i^2$ denotes the flat space Laplacian. For R_{0i} we have:

$$\begin{aligned} R_{0i} &= \tfrac{1}{2}(\partial_0\partial^j h_{ij} - \partial_i^2 h_{0i} + \partial_i\partial^j h_{j0} - \partial_0\partial_i h^i_i) \\ &= \tfrac{1}{2}(-\nabla^2(B_i + \partial_i S) + \partial_i\partial^j(B_j + \partial_j S) - 6\partial_0\partial_i\psi + 2\partial_0\partial_j\delta^j_i\psi + \partial_0\partial^j\partial_j F_i) \\ &= -\tfrac{1}{2}\nabla^2(B_i - \partial_0 F_i) - 2\partial_0\partial_i\psi \\ &= -\tfrac{1}{2}\nabla^2\overline{B}_i - 2\partial_0\partial_i\Psi, \end{aligned} \tag{A.19}$$

and finally for R_{ij}

$$\begin{aligned} R_{ij} &= -\tfrac{1}{2}\partial_i\partial^0 h_{0j} + \tfrac{1}{2}\partial_i\partial^k h_{ki} - \tfrac{1}{2}\partial_j\partial^0 h_{0i} + \tfrac{1}{2}\partial_j\partial^k h_{ki} + \tfrac{1}{2}\left(\partial_0^2 - \nabla^2\right)h_{ij} - \tfrac{1}{2}\partial_i\partial_j\left(-h^0_0 + h^k_k\right) \\ &= \partial_i\partial_j\left[\phi - \partial_0 S + \partial_0^2 E\right] - \tfrac{1}{2}\partial_0\left[\partial_i B_j - \partial_0\partial_i F_j + \partial_j B_i - \partial_0\partial_j F_i\right] - \partial_i\partial_j\psi - \delta_{ij}\Box\psi - \tfrac{1}{2}\Box h^{\mathrm{TT}}_{ij} \\ &= \partial_i\partial_j\left[\Phi - \Psi\right] - \tfrac{1}{2}\partial_0\partial_i\overline{B}_j - \tfrac{1}{2}\partial_0\partial_j\overline{B}_i - \delta_{ij}\Box\Psi - \tfrac{1}{2}\Box h^{\mathrm{TT}}_{ij}. \end{aligned} \tag{A.20}$$

The Ricci scalar can now also be calculated and is given by:

$$\begin{aligned} R &= \eta^{\mu\nu}R_{\mu\nu} = -R_{00} + \delta_{ij}R_{ij} \\ &= 2\nabla^2\Phi + 2\left(3\partial_0^2 - 2\nabla^2\right)\Psi. \end{aligned} \tag{A.21}$$

We can now see that the Ricci tensor as well as the Ricci scalar can be expressed in terms of gauge independent quantities. Thus, for linear coordinate transformations around Minkowski background all components of the Ricci tensor as well as the Ricci scalar are gauge independent. From the Einstein equation (0.3) we can conclude that if the components of $T_{\mu\nu}$ are gauge invariant, then the Einstein equation is also gauge invariant. The different components of the Einstein tensor become:

$$\begin{aligned} G_{00} &= R_{00} + \frac{1}{2}R = -2\nabla^2\Psi \\ G_{0i} &= R_{0i} = -\frac{1}{2}\nabla^2\overline{B}_i - 2\partial_0\partial_i\Psi \\ G_{ij} &= R_{ij} + \frac{1}{2}\delta_{ij}R = \partial_i\partial_j[\Phi - \Psi] - \partial_0\partial_{(i}\overline{B}_{j)} - \frac{1}{2}\Box h^{\mathrm{TT}}_{ij} + \delta_{ij}\nabla^2\Phi + \delta_{ij}\left(4\partial_0^2 - 3\nabla^2\right)\Psi \end{aligned} \tag{A.22}$$

where we only see gauge invariant quantities appear. The brackets in $\partial_{(i}\overline{B}_{j)}$ denote the symmetric combination $\partial_{(i}\overline{B}_{j)} = \frac{1}{2}\partial_i\overline{B}_j + \frac{1}{2}\partial_j\overline{B}_i$. The 00-component in the absence of matter is given by:

$$\nabla^2\Psi = 0, \tag{A.23}$$

which means that with the boundary condition that $\Psi \to 0$ at spatial infinity we have $\Psi = 0$ everywhere. This implies for the $0i$-component:

$$\nabla^2\overline{B}_i = 0, \tag{A.24}$$

which with the boundary conditions that $\Psi \to 0$ at spatial infinity again implies $\overline{B}_i = 0$. The ij-component in the absence of matter can be split up into a longitudinal part:

$$\partial_i\partial_j[\Phi - \Psi] = 0, \tag{A.25}$$

which implies that $\Phi = \Psi = 0$, and into a transverse part:

$$\Box h_{ij}^{\mathrm{TT}} = 0, \tag{A.26}$$

which is the wave equation for GWs in which the GW amplitude h_{ij}^{TT} is a gauge invariant quanity. Note that this applies only to linear perturbations. In anything beyond linear theory, h_{ij}^{TT} is not gauge invariant anymore. We can also remark that we started out with a theory with ten degrees of freedom contained in the metric perturbation $h_{\mu\nu}$. We eliminated four degrees of freedom with the gauge transformation (A.9) to construct a total of six gauge independent degrees of freedom. We have seen that the only freely propagating degrees of freedom are from h_{ij}^{TT} and thus h_{ij}^{TT} represents the two physical degrees of freedom of gravity in the absence of matter.

Appendix B

Decomposition of the Energy-Momentum Tensor into Gauge Invariant Quantities

We will decompose the energy-momentum tensor in a similar manner to that of the decomposition of the metric perturbation:

$$\begin{aligned} T_{00} &= \rho \\ T_{0i} &= K_i + \partial_i L \\ T_{ij} &= 2P\delta_{ij} + \sigma_{ij}^{\mathrm{TT}} + 2\partial_{(i}\sigma_{j)} + 2\partial_i\partial_j\sigma. \end{aligned} \tag{B.1}$$

Where ρ, σ and P are scalar functions, K_i and σ_i are transverse vectors, $\sigma_{ij}^{\mathrm{TT}}$ is a transverse traceless tensor and $\partial_i L$ is the longitudinal part of T_{0i}. Conservation of Energy-momentum

$$\partial^\alpha T_{\alpha\beta} = -\partial^0 T_{0\beta} + \partial^i T_{i\beta} = 0, \tag{B.2}$$

allows us to express L, σ and σ_i in terms of the other variables. The conservation equations are:

$$\begin{aligned} -\dot{\rho} + \nabla^2 L = 0, \quad (\beta = 0) \\ -\dot{K}_j - \partial_j \dot{L} + 2\partial^j P + \nabla^2\sigma_j\partial_j\nabla^2\sigma = 0, \quad (\beta = j). \end{aligned} \tag{B.3}$$

Comparing the scalar, transverse and longitudinal parts yields:

$$\begin{aligned} \nabla^2 L &= \dot{\rho} \\ \nabla^2\sigma &= -P + \tfrac{1}{2}\dot{L} \\ \nabla^2\sigma_i &= \dot{K}_i. \end{aligned} \tag{B.4}$$

The above conservation equations allow us to write the Einstein equation (0.3), using the Einstein tensor (A.22) and the energy-momentum tensor (B.1), in the form:

$$\begin{aligned} G_{00} &= -2\nabla^2\Psi \\ &= 8\pi\rho \\ G_{0i} &= -\frac{1}{2}\nabla^2\overline{B}_i - 2\partial_0\partial_i\Psi \\ &= 8\pi(K_i + \partial_i L) \\ G_{ij} &= \partial_i\partial_j[\Phi - \Psi] - \partial_0\partial_{(i}\overline{B}_{j)} - \frac{1}{2}\Box h_{ij}^{\mathrm{TT}} + \delta_{ij}\nabla^2\Phi + \delta_{ij}\left(4\partial_0^2 - 3\nabla^2\right)\Psi \\ &= 8\pi(2P\delta_{ij} + \sigma_{ij}^{\mathrm{TT}} + 2\partial_{(i}\sigma_{j)} + 2\partial_i\partial_j\sigma), \end{aligned} \tag{B.5}$$

which can be solved by making use of the conservation equations:

$$\begin{aligned}
\nabla^2\Psi &= -4\pi\rho \\
\nabla^2\overline{B}_i &= -16\pi K_i \\
\nabla^2\Phi &= 4\pi(\dot{L} - 2P - \rho) \\
\Box h_{ij}^{\mathrm{TT}} &= -16\pi\sigma_{ij}^{\mathrm{TT}},
\end{aligned} \tag{B.6}$$

where the first equation is obtained from the 00-component of the Einstein equation, the second equation from the $0i$-component and the third and fourth from the ij-component by comparing the scalar, transverse and longitudinal parts. We can see that only h_{ij}^{TT} obeys a wave-like equation. The other variables are given by a Poisson-type equation. We can expand the four gauge-independent variables in powers of $1/r$. At sufficiently large distances only the $1/r$ terms will dominate. Since the variables Ψ, $\overline{B}_i$ and Φ are given by Poisson-type equations, the coefficients will be given by conserved quantities[1] and therefore Ψ, $\overline{B}_i$ and Φ will not be time-dependent. Thus, even with a source, the only freely propagating degrees of freedom are given by the transverse traceless piece of the metric perturbation h_{ij}^{TT}, at sufficiently large distances from the source.

[1] See section 2.3 for a detailed Taylor expansion of the Poisson equation.

Appendix C

Effective Energy-Momentum Tensor in Linearised Gravity

If we define $G^{(2)}_{\mu\nu}[h^{(1)}] = -8\pi t_{\mu\nu}$, where $t_{\mu\nu}$ represents the effective energy-momentum tensor, the Einstein equation up to second order in the metric perturbation can be written as:

$$G^{(1)}_{\mu\nu}[h^{(2)}] = -\tfrac{1}{2}\Box h^{(2)}_{\mu\nu} = 8\pi t_{\mu\nu}. \tag{C.1}$$

A local coordinate-invariant definition of the energy is not possible because of the equivalence principle. We can circumvent this problem by averaging $t_{\mu\nu}$ over several wavelengths. An operation that is denoted by angle brackets $\langle ...\rangle$. If we average over enough wavelengths, enough of the physical curvature should be encapsulated in $t_{\mu\nu}$ to make it a gauge-invariant measure. The limit of a large averaging region compared to the wavelength also has the practical advantage that derivatives vanish:

$$\langle \partial_\mu F(x)\rangle = 0, \tag{C.2}$$

which allows us to integrate by parts under the averaging brackets:

$$\langle F(x)\partial_\mu G(x)\rangle = -\langle G(x)\partial_\mu F(x)\rangle, \tag{C.3}$$

since the boundary term can be neglected in the leading order approximation.

With this machinery, let us try to calculate $t_{\mu\nu}$. We have to consider the Einstein equation up to second order in the metric perturbation. The full Einstein equation in vacuum in terms of the metric using the known expressions for the Riemann tensor and the Ricci scalar in terms of the metric is given by:

$$\begin{aligned}
G_{\mu\nu} &= R_{\mu\nu} - \frac{1}{2}R\eta_{\mu\nu} = 0 \\
&= \tfrac{1}{8}g^{\alpha\beta}\Big(g^{\gamma\zeta}\big(-2\partial_\alpha g_{\mu\nu}\partial_\beta g_{\gamma\zeta} - 4\partial_\beta g_{\nu\zeta}\partial_\gamma g_{\mu\alpha} + 4\partial_\alpha g_{\mu\nu}\partial_\zeta g_{\beta\gamma} \\
&+ g^{\theta\vartheta}g_{\mu u}\partial_\gamma g_{\alpha\beta}\partial_\zeta g_{\theta\vartheta} + 4\partial_\gamma g_{\mu\alpha}\partial_\zeta g_{\nu\beta} - 4g_{\mu\nu}\partial_\zeta\partial_\beta g_{\alpha\gamma} + 4g_{\mu\nu}\partial_\zeta\partial_\gamma g_{\alpha\beta} \\
&+ 2g^{\theta\vartheta}g_{\mu\nu}\partial_\zeta g_{\beta\vartheta}\partial_\theta g_{\alpha\gamma} - 3g^{\theta\vartheta}g_{\mu\nu}\partial_\theta g_{\alpha\gamma}\partial_\vartheta g_{\beta\zeta} + 4g^{\theta\vartheta}g_{\mu\nu}\partial_\beta g_{\alpha\gamma}\partial_\vartheta g_{\zeta\theta} \\
&- 4g^{\theta\vartheta}g_{\mu\nu}\partial_\gamma g_{\alpha\beta}\partial_\vartheta g_{\zeta\theta} + 2(\partial_\beta g_{\gamma\zeta} - 2\partial_\zeta g_{\beta\gamma})\partial_\mu g_{\nu\alpha} + 2\partial_\mu g_{\alpha\gamma}\partial_\nu g_{\beta\zeta} + 2\partial_\beta g_{\gamma\zeta}\partial_\nu g_{\mu\alpha} \\
&- 4\partial_\zeta g_{\beta\gamma}\partial_\nu g_{\mu\alpha}\big) - 4(\partial_\beta\partial_\alpha g_{\mu\nu} - \partial_\beta\partial_\mu g_{\nu\alpha} - \partial_\beta\partial_\nu g_{\mu\alpha} + \partial_\nu\partial_\mu g_{\alpha\beta})\Big).
\end{aligned} \tag{C.4}$$

We know that the only radiating degrees of freedom are the transverse traceless parts of the metric, therefore we can impose the Lorenz gauge without loss of any radiation information. Remember that the Lorenz gauge condition is given by:

$$g^{\nu\alpha}\partial_\alpha g_{\gamma\nu} - \tfrac{1}{2}g^{\nu\alpha}\partial_\gamma g_{\nu\alpha} = 0, \tag{C.5}$$

and its derivative

$$g^{\nu\alpha}\partial_\alpha\partial_\beta g_{\gamma\nu} + \tfrac{1}{2}g^{\zeta\theta}g^{\nu\alpha}\partial_\beta g_{\nu\zeta}\partial_\gamma g_{\alpha\theta} - \tfrac{1}{2}g^{\nu\alpha}\partial_\gamma\partial_\beta g_{\nu\alpha} - g^{\zeta\theta}g^{\nu\alpha}\partial_\beta g_{\alpha\theta}\partial_\zeta g_{\gamma\nu} = 0, \tag{C.6}$$

such that the full Einstein equation in terms of the metric in the Lorenz gauge is given by:

$$\begin{aligned} G_{\mu\nu} = \tfrac{1}{4}\big(&- 2g^{\alpha\beta}\partial_\beta\partial_\alpha g_{\mu\nu} - 2g^{\alpha\beta}g^{\gamma\zeta}\partial_\beta g_{\nu\zeta}\partial_\gamma g_{\mu\alpha} + 2g^{\alpha\beta}g^{\gamma\zeta}\partial_\gamma g_{\mu\alpha}\partial_\zeta g_{\nu\beta} + g^{\alpha\beta}g^{\gamma\zeta}g_{\mu\nu}\partial_\zeta\partial_\gamma g_{\alpha\beta} \\ &- g^{\alpha\beta}g^{\gamma\zeta}g^{\theta\vartheta}g_{\mu\nu}\partial_\zeta g_{\beta\vartheta}\partial_\theta g_{\alpha\gamma} - \tfrac{1}{2}g^{\alpha\beta}g^{\gamma\zeta}g^{\theta\vartheta}g_{\mu\nu}\partial_\theta g_{\alpha\gamma}\partial_\vartheta g_{\beta\zeta} + 2g^{\alpha\beta}g^{\gamma\zeta}\partial_\gamma g_{\nu\alpha}\partial_\mu g_{\beta\zeta} \\ &+ 2g^{\alpha\beta}g^{\gamma\zeta}\partial_\gamma g_{\mu\alpha}\partial_\nu g_{\beta\zeta} - g^{\alpha\beta}g^{\gamma\zeta}\partial_\mu g_{\alpha\gamma}\partial_\nu g_{\beta\zeta}\big) = 0. \end{aligned} \tag{C.7}$$

We know that up to second order in the metric perturbation this is given by $G^{(2)}_{\mu\nu}[h^{(1)}] - \frac{1}{2}\Box h^{(2)}_{\mu\nu} = 0$. Using the metric (1.55), yields for the Einstein equation in vacuum up to second order in the metric perturbation in the Lorenz gauge:

$$\begin{aligned} \Box h^{(2)}_{\mu\nu} = \tfrac{1}{2}\big(&- \eta^{\alpha\beta}\eta_{\mu\nu}h^{(1)\gamma\zeta}\partial_\beta\partial_\alpha h^{(1)}_{\gamma\zeta} + 2h^{(1)\alpha\beta}\partial_\beta\partial_\alpha h^{(1)}_{\mu\nu} - 2\eta^{\alpha\beta}\eta^{\gamma\zeta}\partial_\beta h^{(1)}_{\nu\zeta}\partial_\gamma h^{(1)}_{\mu\alpha} \\ &+ 2\eta^{\alpha\beta}\eta^{\gamma\zeta}\partial_\gamma h^{(1)}_{\mu\alpha}\partial_\zeta h^{(1)}_{\nu\beta} - \eta^{\alpha\beta}\eta_{\mu\nu}h^{(1)\gamma\zeta}\partial_\zeta\partial_\gamma h^{(1)}_{\alpha\beta} - \eta^{\alpha\beta}\eta^{\gamma\zeta}\eta^{\theta\vartheta}\eta_{\mu\nu}\partial_\zeta h^{(1)}_{\beta\vartheta}\partial_\theta h^{(1)}_{\alpha\gamma} \\ &- \tfrac{1}{2}\eta^{\alpha\beta}\eta^{\gamma\zeta}\eta^{\theta\vartheta}\eta_{\mu\nu}\partial_\theta h^{(1)}_{\alpha\gamma}\partial_\vartheta h^{(1)}_{\beta\zeta} + 2\eta^{\alpha\beta}\eta^{\gamma\zeta}\partial_\gamma h^{(1)}_{\nu\alpha}\partial_\mu h^{(1)}_{\beta\zeta} \\ &+ 2\eta^{\alpha\beta}\eta^{\gamma\zeta}\partial_\gamma h^{(1)}_{\mu\alpha}\partial_\nu h^{(1)}_{\beta\zeta} - \eta^{\alpha\beta}\eta^{\gamma\zeta}\partial_\mu h^{(1)}_{\alpha\gamma}\partial_\nu h^{(1)}_{\beta\zeta}\big), \end{aligned} \tag{C.8}$$

where we can see that the first order non-linear metric perturbations act as a source for the second order metric perturbation. We can set the first term on the r.h.s. to zero since it must obey the wave equation for $h^{(1)}_{\mu\nu}$ and we can set the trace of $h^{(1)}_{\mu\nu}$ to zero at no cost to the energy radiation information:

$$\begin{aligned} \Box h^{(2)}_{\mu\nu} = \tfrac{1}{2}\big(&2h^{(1)\alpha\beta}\partial_\beta\partial_\alpha h^{(1)}_{\mu\nu} - 2\eta^{\alpha\beta}\eta^{\gamma\zeta}\partial_\beta h^{(1)}_{\nu\zeta}\partial_\gamma h^{(1)}_{\mu\alpha} \\ &+ 2\eta^{\alpha\beta}\eta^{\gamma\zeta}\partial_\gamma h^{(1)}_{\mu\alpha}\partial_\zeta h^{(1)}_{\nu\beta} - \eta^{\alpha\beta}\eta^{\gamma\zeta}\eta^{\theta\vartheta}\eta_{\mu\nu}\partial_\zeta h^{(1)}_{\beta\vartheta}\partial_\theta h^{(1)}_{\alpha\gamma} \\ &- \tfrac{1}{2}\eta^{\alpha\beta}\eta^{\gamma\zeta}\eta^{\theta\vartheta}\eta_{\mu\nu}\partial_\theta h^{(1)}_{\alpha\gamma}\partial_\vartheta h^{(1)}_{\beta\zeta} + 2\eta^{\alpha\beta}\eta^{\gamma\zeta}\partial_\gamma h^{(1)}_{\nu\alpha}\partial_\mu h^{(1)}_{\beta\zeta} \\ &+ 2\eta^{\alpha\beta}\eta^{\gamma\zeta}\partial_\gamma h^{(1)}_{\mu\alpha}\partial_\nu h^{(1)}_{\beta\zeta} - \eta^{\alpha\beta}\eta^{\gamma\zeta}\partial_\mu h^{(1)}_{\alpha\gamma}\partial_\nu h^{(1)}_{\beta\zeta}\big). \end{aligned} \tag{C.9}$$

The effective energy-momentum tensor averaged over several wavelengths is thus given by:

$$\begin{aligned} \langle t_{\mu\nu}\rangle = -\tfrac{1}{16\pi}\langle\Box h^{(2)}_{\mu\nu}\rangle = -\tfrac{1}{32\pi}\big\langle &2h^{(1)\alpha\beta}\partial_\beta\partial_\alpha h^{(1)}_{\mu\nu} - 2\eta^{\alpha\beta}\eta^{\gamma\zeta}\partial_\beta h^{(1)}_{\nu\zeta}\partial_\gamma h^{(1)}_{\mu\alpha} \\ &+ 2\eta^{\alpha\beta}\eta^{\gamma\zeta}\partial_\gamma h^{(1)}_{\mu\alpha}\partial_\zeta h^{(1)}_{\nu\beta} - \eta^{\alpha\beta}\eta^{\gamma\zeta}\eta^{\theta\vartheta}\eta_{\mu\nu}\partial_\zeta h^{(1)}_{\beta\vartheta}\partial_\theta h^{(1)}_{\alpha\gamma} \\ &- \tfrac{1}{2}\eta^{\alpha\beta}\eta^{\gamma\zeta}\eta^{\theta\vartheta}\eta_{\mu\nu}\partial_\theta h^{(1)}_{\alpha\gamma}\partial_\vartheta h^{(1)}_{\beta\zeta} + 2\eta^{\alpha\beta}\eta^{\gamma\zeta}\partial_\gamma h^{(1)}_{\nu\alpha}\partial_\mu h^{(1)}_{\beta\zeta} \\ &+ 2\eta^{\alpha\beta}\eta^{\gamma\zeta}\partial_\gamma h^{(1)}_{\mu\alpha}\partial_\nu h^{(1)}_{\beta\zeta} - \eta^{\alpha\beta}\eta^{\gamma\zeta}\partial_\mu h^{(1)}_{\alpha\gamma}\partial_\nu h^{(1)}_{\beta\zeta}\big\rangle. \end{aligned} \tag{C.10}$$

Let us investigate the above expression term by term, for the first term we have:

$$\begin{aligned} \langle h^{(1)\alpha\beta}\partial_\beta\partial_\alpha h^{(1)}_{\mu\nu}\rangle &= -\langle\partial_\beta h^{(1)\alpha\beta}\partial_\alpha h^{(1)}_{\mu\nu}\rangle \\ &= -\tfrac{1}{2}\langle h^{(1)}_{\rho\sigma}\partial^\alpha h^{(1)\rho\sigma}\partial_\alpha h^{(1)}_{\mu\nu}\rangle \\ &= \tfrac{1}{2}\langle h^{(1)}_{\rho\sigma}\partial^2 h^{(1)\rho\sigma}h^{(1)}_{\mu\nu}\rangle = 0, \end{aligned} \tag{C.11}$$

where in the first line we used integration by parts, in the second line we used the Lorenz gauge condition and in the third line we used the wave equation for $h^{(1)}_{\mu\nu}$. Note that going from the second to the third line we could have also used integration by parts again with the first derivative such that the expression vanishes because of the traceless condition. This can always be done when a term of the Lorenz gauge condition can be identified. For the second term we have:

$$\langle\eta^{\alpha\beta}\eta^{\gamma\zeta}\partial_\beta h^{(1)}_{\nu\zeta}\partial_\gamma h^{(1)}_{\mu\alpha}\rangle = \langle\partial^\zeta h^{(1)}_{\nu\zeta}\partial^\alpha h^{(1)}_{\mu\alpha}\rangle = 0 \tag{C.12}$$

where we used integration by parts repeatedly after which the Lorenz gauge condition allows us to conclude that the term must vanish. The third term yields:

$$\langle \eta^{\alpha\beta}\eta^{\gamma\zeta}\partial_\gamma h^{(1)}_{\mu\alpha}\partial_\zeta h^{(1)}_{\nu\beta}\rangle = -\langle \eta^{\alpha\beta}\partial^2 h^{(1)}_{\mu\alpha}h^{(1)}_{\nu\beta}\rangle = 0, \tag{C.13}$$

where single use of integration by parts yields the wave equation for $h^{(1)}$, which vanishes. We can make similar arguments - using integration by parts and either the Lorenz gauge condition or the wave equation for $h^{(1)}$ - to conclude that all the subsequent terms except the last one vanish. The effective energy-momentum tensor is therefore given by:

$$\langle t_{\mu\nu}\rangle = \tfrac{1}{32\pi}\langle \eta^{\alpha\beta}\eta^{\gamma\zeta}\partial_\mu h^{(1)}_{\alpha\gamma}\partial_\nu h^{(1)}_{\beta\zeta}\rangle. \tag{C.14}$$

Appendix D

Hamiltonian Approach to Calculating the Energy of Gravitational Waves

This is a relatively new approach in the literature. If we choose a given Hamiltonian as our starting point the approach has the advantage of being much less involved in considering the energy dissipated by GWs and is therefore the approach which we will follow here. The most common Hamiltonian perspective of GR is the formalism developed by Arnowitt, Deser, and Misner which is called the ADM formalism. In [53] energy considerations of GWs in the ADM formalism can be found and in [54] a general review of the Hamiltonian formulation of GR can be found. The advantage of a Hamiltonian formalism is that once the Hamiltonian of a closed system is found, it is easy to consider its energy. The drawback is that usually it is not easy to set up the Hamiltonian of the system. We will 'cheat' a bit here by immediately posing the Hamiltonian of the system. However, once the correct Hamiltonian is found, it should not be hard to convince the reader that it produces the right equations of motions and therefore this approach should not take away anything of the rigour of the story posed here. When considering an isolated body, whose geometry becomes flat far away, where a perturbation is introduced that can be treated as a wave, the Hamiltonian can be used for energy considerations of the system. We will work in the Lorenz gauge introduced in Box 1. The linearised Einstein equation for the trace reversed metric perturbation is given by:

$$\Box\bar{h}_{\mu\nu} = \Box h_{\mu\nu} - \tfrac{1}{2}\Box h\eta_{\mu\nu} = -16\pi T_{\mu\nu}. \tag{D.1}$$

We will now show that this equation of motion can be derived from the following Hamiltonian for the metric perturbation $h_{\mu\nu}$ and its conjugate momentum $\pi_{\mu\nu}$ [53, 16]:

$$\mathcal{H} = \frac{1}{32\pi}\int d^3x \left[\frac{1}{2}\pi_{\mu\nu}^2 - \frac{1}{4}\pi_\lambda^{\lambda 2} + \frac{1}{2}\left(\nabla h_{\mu\nu}\right)^2 - \frac{1}{4}\left(\nabla h_\lambda^\lambda\right)^2 - 16\pi h^{\mu\nu}T_{\mu\nu}\right]. \tag{D.2}$$

Following [54], the Hamilton equations for the Hamiltonian $\mathcal{H}$ are given by:

$$\dot{h}_{\mu\nu} = 32\pi\frac{\delta H}{\delta\pi^{\mu\nu}} = \pi_{\mu\nu} - \frac{1}{2}\eta_{\mu\nu}\pi_\lambda^\lambda \tag{D.3}$$

$$\dot{\pi}_{\mu\nu} = -32\pi\frac{\delta H}{\delta h^{\mu\nu}} = \nabla^2 h_{\mu\nu} - \frac{1}{2}\eta_{\mu\nu}\nabla^2 h_\lambda^\lambda + 16\pi T_{\mu\nu}. \tag{D.4}$$

We can use the $\dot{h}_{\mu\nu}$ equation (D.3) to write $\pi_{\mu\nu}$ as:

$$\dot{\pi}_{\mu\nu} = \ddot{h}_{\mu\nu} + \frac{1}{2}\eta_{\mu\nu}\dot{\pi}_\lambda^\lambda. \tag{D.5}$$

The trace of the $\dot{\pi}_{\mu\nu}$ equation (D.4) is given by:

$$\dot{\pi}^{\mu}_{\mu} = \eta^{\mu\nu}\dot{\pi_{\mu\nu}} = \eta^{\mu\nu}\nabla^2 h_{\mu\nu} - 2\nabla^2 h^{\lambda}_{\lambda} + 16\pi\eta^{\mu\nu}T_{\mu\nu}, \tag{D.6}$$

which we can plug into (D.5) to yield:

$$\dot{\pi}_{\mu\nu} = \ddot{h}_{\mu\nu} + 2\nabla^2 h_{\mu\nu} - \eta_{\mu\nu}\nabla^2 h^{\lambda}_{\lambda} + 32\pi T_{\mu\nu}. \tag{D.7}$$

Taking the trace of (D.5) implies $\dot{\pi}^{\lambda}_{\lambda} = -\ddot{h}^{\lambda}_{\lambda}$, combining this with (D.6) and multiplying with $\eta_{\mu\nu}$ yields:

$$\nabla^2 h_{\mu\nu} - \tfrac{1}{2}\eta_{\mu\nu}\nabla^2 h^{\lambda}_{\lambda} + 16\pi T_{\mu\nu} + \tfrac{1}{4}\eta_{\mu\nu}\ddot{h}^{\lambda}_{\lambda} = 0. \tag{D.8}$$

Combining (D.7) with (D.4) also yields:

$$\nabla^2 h_{\mu\nu} - \tfrac{1}{2}\eta_{\mu\nu}\nabla^2 h^{\lambda}_{\lambda} + 16\pi T_{\mu\nu} + \ddot{h}_{\mu\nu} = 0. \tag{D.9}$$

We can conclude from (D.8) and (D.9) that:

$$\begin{aligned} \ddot{h}_{\mu\nu} &= \tfrac{1}{4}\eta_{\mu\nu}\ddot{h}^{\lambda}_{\lambda} \\ \tfrac{1}{2}\ddot{h}_{\mu\nu} + \tfrac{1}{2}\ddot{h}_{\mu\nu} &= \tfrac{1}{4}\eta_{\mu\nu}\ddot{h}^{\lambda}_{\lambda}, \end{aligned} \tag{D.10}$$

which gives us the identity:

$$\ddot{h}_{\mu\nu} = -\ddot{h}_{\mu\nu} + \tfrac{1}{2}\eta_{\mu\nu}\ddot{h}^{\lambda}_{\lambda}. \tag{D.11}$$

Plugging this identity into (D.9) gives us the equation of motion for the metric:

$$\begin{aligned} &\nabla^2 h_{\mu\nu} - \tfrac{1}{2}\eta_{\mu\nu}\nabla^2 h^{\lambda}_{\lambda} + 16\pi T_{\mu\nu} - \ddot{h}_{\mu\nu} + \tfrac{1}{2}\eta_{\mu\nu}\ddot{h}^{\lambda}_{\lambda} = 0 \\ &\Box h_{\mu\nu} - \tfrac{1}{2}\Box h\eta_{\mu\nu} + 16\pi T_{\mu\nu} = 0. \end{aligned} \tag{D.12}$$

We want to use the Hamiltonian to find the energy radiated from GWs for some system. For a source that is isolated in a geometry that becomes flat far away from the source, it is possible to derive an expression of the energy of the field in a certain volume. We want to average this energy over several wavelengths, since we know that locally the spacetime structure does not have any energy at all. Consider some volume V, the integral (D.2) over the volume V at a fixed time t can be considered as the total energy of the field in that volume, the time average of the change of the energy over time is then given by:

$$\begin{aligned} \left\langle \frac{dE_V}{dt} \right\rangle &= \left\langle \frac{1}{32\pi}\frac{d}{dt}\int_V d^3x \left[\frac{1}{2}\pi^2_{\mu\nu} - \frac{1}{4}\pi^{\lambda 2}_{\lambda} + \frac{1}{2}\left(\nabla h_{\mu\nu}\right)^2 - \frac{1}{4}\left(\nabla h^{\lambda}_{\lambda}\right)^2 - 16\pi h^{\mu\nu}T_{\mu\nu}\right]\right\rangle \\ &= \left\langle \frac{1}{32\pi}\int_V d^3x \left[\nabla\cdot\left(\pi^{\mu\nu}\nabla h_{\mu\nu}\right) - 16\pi h^{\mu\nu}\dot{T}_{\mu\nu}\right]\right\rangle \\ &= \left\langle \frac{1}{32\pi}\oint_{\partial V} d^2\sigma\pi^{\mu\nu}\nabla_n h_{\mu\nu} - \frac{1}{2}\int_V d^3x h^{\mu\nu}\dot{T}_{\mu\nu}\right\rangle \end{aligned} \tag{D.13}$$

where ∂V represents the boundary of V and $d^2\sigma$ a boundary surface element, ∇_n is the normal component to the surface element of the gradient and the angle brackets $\langle ... \rangle$ denote the time average of the expression. Going from the second line to the third line we used the divergence theorem. We can see that the energy only changes due to gravitational radiation flux through the boundary apart from variations in the energy-momentum density from the source. We will assume that the time averaged change of the energy-momentum tensor vanishes. For the example of a binary system discussed before this holds. We then have:

$$\left\langle \frac{dE_V}{dt} \right\rangle = \frac{1}{32\pi}\left\langle \oint_{\partial V} d^2\sigma\pi^{\mu\nu}\nabla_n h_{\mu\nu}\right\rangle. \tag{D.14}$$

The GW flux at far distances r from the source is then given by the integral:

$$\left\langle \frac{dE_V}{dt} \right\rangle = \frac{1}{32\pi}\left\langle \int_0^{\pi}\int_0^{2\pi} d\theta d\phi r^2 \sin\theta\pi^{\mu\nu}\nabla_n h_{\mu\nu}\right\rangle. \tag{D.15}$$

Where a spherical surface is chosen with the source in the centre and with radius r large enough such that $T_{\mu\nu}$ vanishes on the surface. Using (D.3), the energy flux is given by:

$$\left\langle \frac{dE_V}{dt} \right\rangle = \left\langle \frac{r^2}{8} \left(\dot{h}^{\mu\nu} \nabla_r h_{\mu v} - \frac{1}{2} \dot{h}^v_v \nabla_r h^\mu_\mu \right) \right\rangle . \tag{D.16}$$

We know that the only propagating degrees of freedom are the spatial transverse traceless degrees of freedom of the metric. Therefore the second term vanishes and we are only left with the spatial parts of the first term. Using (1.28) this then becomes:

$$\begin{aligned} \left\langle \frac{dE_V}{dt} \right\rangle &= \left\langle \frac{r^2}{8} \left(\frac{2}{r} \frac{d^3 I_{ij}\left(t_r\right)}{dt^2} \left(P_{ik} P_{jl} - \tfrac{1}{2} P_{ij} P_{kl} \right) \nabla_r \frac{2}{r} \frac{d^2 I_{ij}\left(t_r\right)}{dt^2} \left(P_{ik} P_{jl} - \tfrac{1}{2} P_{ij} P_{kl} \right) \right) \right\rangle \\ &= - \left\langle \tfrac{1}{2} \left(\dddot{I}_{ij}\left(t_r\right) \left(P_{ik} P_{jl} - \tfrac{1}{2} P_{ij} P_{kl} \right) \dddot{I}_{ij}\left(t_r\right) \left(P_{ik} P_{jl} - \tfrac{1}{2} P_{ij} P_{kl} \right) \right) \right\rangle + \mathcal{O}(\tfrac{1}{r}) \\ &\approx - \frac{r^2}{8} \left\langle \dot{h}^{\mathrm{TT}}_{ij} \dot{h}^{\mathrm{TT}}_{ij} \right\rangle , \end{aligned} \tag{D.17}$$

where going from the second to the third line we used that I_{ij} only depends on $t_r = t - r$ such that $\nabla_r I_{ij} = -\partial_t I_{ij}$. Also, since the above energy considerations are only valid for large r, we can neglect all higher order terms in $1/r$. Using $P_{ij} = \delta_{ij} - n_i n_j$ we can expand the projection operators in the definition of h^{TT}_{ij} as:

$$h^{\mathrm{TT}}_{ij} = \frac{1}{r} \left(2\ddot{I}_{ij} - \ddot{I}_{kk}\delta_{ij} + n_k n_l \ddot{I}_{kl}\delta_{ij} + n_i n_j \ddot{I}_{kk} + n_i n_j n_k n_l \ddot{I}_{kl} - 2 n_j n_k \ddot{I}_{ik} - 2 n_i n_k \ddot{I}_{jk} \right) , \tag{D.18}$$

such that the energy dissipation formula is given by:

$$\begin{aligned} \left\langle \frac{dE_V}{dt} \right\rangle &= -\frac{1}{8} \langle 4\, \dddot{I}_{\,ij}\, \dddot{I}_{\,ij} + 4\, \dddot{I}_{\,ij} n_i n_j\, \dddot{I}_{\,mn} n_m n_n - 16\, \dddot{I}_{\,ij}\, \dddot{I}_{\,im} n_j n_m - 3\, \dddot{I}_{\,ij} n_i n_j\, \dddot{I}_{\,mn} n_m n_n \\ &\quad -7\, \dddot{I}_{\,ij} n_i n_j\, \dddot{I}_{\,mn} n_m n_n + 8\, \dddot{I}_{\,ij}\, \dddot{I}_{\,im} n_j n_m + 8\, \dddot{I}_{\,ij} n_i n_j\, \dddot{I}_{\,mn} n_m n_n \rangle \\ &= -\frac{1}{8} \langle 4\, \dddot{I}_{\,ij}\, \dddot{I}_{\,ij} + 2\, \dddot{I}_{\,ij} n_i n_j\, \dddot{I}_{\,mn} n_m n_n - 8\, \dddot{I}_{\,ij}\, \dddot{I}_{\,im} n_j n_m \rangle . \end{aligned} \tag{D.19}$$

Finally, using the relations:

$$\langle n_i n_j \rangle = \frac{1}{3}\delta_{ij}, \quad \langle n_i n_j n_k n_l \rangle = \frac{1}{15} \left(\delta_{ij}\delta_{kl} + \delta_{ik}\delta_{jl} + \delta_{il}\delta_{jk} \right) , \tag{D.20}$$

we obtain the energy dissipation formula for GWs far away from a slowly moving source that is not dominated by self-gravity:

$$\langle \dot{E} \rangle = -\frac{1}{5} \left\langle \dddot{I}_{\,ij}\, \dddot{I}_{\,ij} \right\rangle , \tag{D.21}$$

which agrees with (1.67).

Appendix E

Frame Dragging Effects

Although the coupling of the tidal spin S^i_Q to the black hole's spin $S^i_{\rm BH}$ and the orbital spin L^i gives rise to small effects, at some point one might decide to include them in the analysis. In this work these effects are left out, but the effect on the dynamics of the system will be outlined here for reference. These spin-couplings represent the so-called frame dragging effects. The spin of the companion black hole as well as the orbital spin of the system cause spacetime to distort and lead to precession of the orbit of the neutron star and thus the neutron star's body frame. The black hole spin coupled to the tidal spin, i.e. the spin-spin coupling, is given by (2.90) and becomes:

$$\mathcal{L}^{SS} = \frac{1}{2\lambda_2\omega_{02}^2 r^3}\left[3\hat{n}_i\epsilon^i_{jk}Q^j_l\dot{Q^{kl}}\hat{n}_iS^i_{\rm BH} - \epsilon_{ijk}Q^j_l\dot{Q^{kl}}S^i_{\rm BH}\right]. \tag{E.1}$$

The tidal spin coupled to the orbital spin, i.e. the spin-orbit coupling, is given by (2.90) and becomes:

$$\mathcal{L}^{SO} = \frac{1}{2\lambda_2\omega_{02}^2 r^3}\epsilon_{ijk}Q^j_l\dot{Q^{kl}}L^i\left[2+\frac{3}{2}\frac{M_{\rm BH}}{M_{\rm NS}}\right]^{1}, \tag{E.2}$$

where L^i represents the orbital angular momentum, which is given by $L^z = \mu r^2\Omega$ for stable circular orbits in the $xy-$plane. The total action, where we have excluded the $S^i_{\rm BH}$-L^i coupling term to keep the expressions below manageable, is now given by:

$$\begin{aligned} S = S_{orbit} + \int dt\Bigg[&-\frac{1}{2}Q_{ij}\mathcal{E}^{ij} + \frac{1}{4\lambda_2\omega_{02}^2}\Bigg[\dot{Q}_{ij}\dot{Q}^{ij} - \omega_{02}^2Q_{ij}Q^{ij} + 2C_{\rm NS}\epsilon_{ijk}S^k_{\rm NS}Q^i_k\dot{Q}^{jk} \\ &- \frac{2}{r^3}\epsilon_{ijk}Q^j_l\dot{Q^{kl}}L^i\left[2+\frac{3}{2}\frac{M_{\rm BH}}{M_{\rm NS}}\right] - \frac{2}{r^3}\left[3\hat{n}_i\epsilon^i_{jk}Q^j_l\dot{Q^{kl}}\hat{n}_iS^i_{\rm BH} - \epsilon_{ijk}Q^j_l\dot{Q^{kl}}S^i_{\rm BH}\right]\Bigg]\Bigg], \end{aligned} \tag{E.3}$$

from which we can calculate all the desired quantities in the same way as above. The quadrupole moment tensor is given by:

$$Q_{ij} = \mathcal{A}\begin{pmatrix} \frac{1}{3}+\frac{M_{\rm NS}\omega_{02}^2\cos(2\phi)}{\mathcal{R}} & \frac{M_{\rm NS}\omega_{02}^2\sin(2\phi)}{\mathcal{R}} & 0 \\ \frac{M_{\rm NS}\omega_{02}^2\sin(2\phi)}{\mathcal{R}} & \frac{1}{3}-\frac{M_{\rm NS}\omega_{02}^2\cos(2\phi)}{\mathcal{R}} & 0 \\ 0 & 0 & \frac{-2}{3} \end{pmatrix}, \tag{E.4}$$

with amplitude $\mathcal{A} = \frac{3\lambda_2 M_{\rm BH}}{2r^3}$ and resonance factor $\mathcal{R}$:

$$\mathcal{R} = \frac{2}{r}\mu\Omega^2\left(4M_{\rm NS}+3M_{\rm BH}\right) - \frac{4}{r^3}\Omega M_{\rm NS}S^z_{\rm BH} - M_{\rm NS}\left(-\omega_{02}^2+4\Omega^2+4\Omega C_N S^z_N\right). \tag{E.5}$$

We can see that all the different mechanisms discussed above, namely the Coriolis effect and the spin-spin and spin-orbit frame dragging effects, together have a complex effect on the

[1] This term is also included in the analysis in [39]. Note that equation (3.17) in [39] should be proportional to $1/r^3$.

frequency at which resonance occurs. The spin-orbit coupling, represented by the first term seems to increase the resonance frequency, i.e. resonance occurs for higher orbital frequency or later in the inspiral. The spin-spin coupling, represented by the second term, seems to decrease (increase) the resonance frequency for counter-clockwise (clockwise) spin of the black hole. It can also be seen that the influence of the spin of the black hole term decreases quickly as the orbital separation increases while spin-orbit coupling term effect decreases only as $1/r$ with the increase of the orbital separation. Furthermore, the stable circular orbit radius as a function of the orbital frequency is given by:

$$\begin{aligned} r(\Omega) = \frac{M_{\rm NS}}{\tilde{\mathcal{R}}}\Bigg(2M_{\rm NS}\Bigg(&-2\mu M^{8/3}\left(\omega^2-4\Omega^2\right)\left(8\Omega^3 S^z_{\rm BH}+8M\Omega C_{\rm NS}S^z_N - M\left(\omega^2-4\Omega^2\right)\right) \\ &+3\lambda_2\Omega^{10/3}M^2_{\rm BH}\left(\Omega^3\left(16\Omega^2-7\omega^2\right)S^z_{\rm BH}+2M\left(\Omega C_{\rm NS}\left(8\Omega^2-5\omega^2\right)S^z_N+\omega^4-5\omega^2\Omega^2+4\Omega^4\right)\right)\Bigg) \\ &+\mu M^{2/3}\Omega^{8/3}\left(3M_{\rm BH}+4M_{\rm NS}\right)\left(3\lambda_2\Omega^{10/3}M^2_{\rm BH}\left(7\omega^2-16\Omega^2\right)+16\mu M^{8/3}\left(\omega^2-4\Omega^2\right)\right)\Bigg), \end{aligned} \tag{E.6}$$

where $\tilde{\mathcal{R}}$ is given by:

$$\begin{aligned} \tilde{\mathcal{R}} = 4\mu M^{4/3}\Omega^{2/3}\Big(&M_{\rm NS}\left(-4\left(\Omega^3 S^z_{\rm BH}+M\Omega C_{\rm NS}S^z_{\rm NS}\right)\right. \\ &\left.+8\mu M^{2/3}\Omega^{8/3}+M\left(\omega^2-4\Omega^2\right)\right)+6\mu M^{2/3}\Omega^{8/3}M_{\rm BH}\Big)^2. \end{aligned} \tag{E.7}$$

Finally, the energy as a function of the orbital frequency is given by:

$$\begin{aligned} E(\Omega) = -\frac{1}{2}M^{2/3}\mu\Omega^{2/3}+\frac{9}{8}\lambda_2\Omega^4 M^2_{\rm BH}\Bigg(&\frac{1}{M^2} \\ &+\frac{\omega^2 M M_{\rm NS}\left(6M^{2/3}\mu\Omega^{8/3}M_{\rm BH}+M_{\rm NS}\left(8M^{2/3}\mu\Omega^{8/3}-4\Omega^3 S^z_{\rm BH}+M\left(3\omega^2-4\Omega^2-12\Omega C_N S^z_N\right)\right)\right)}{\left(6M^{2/3}\mu\Omega^{8/3}M_{\rm BH}+M_{\rm NS}\left(8M^{2/3}\mu\Omega^{8/3}-4\Omega^3 S^z_{\rm BH}+M\left(\omega^2-4\Omega^2-4\Omega C_N S^z_N\right)\right)\right)^2}. \end{aligned} \tag{E.8}$$

To explicitly compute energies from the waveforms of explicit binary systems we need expressions in physical units. From [43] we deduce that $C_{\rm NS} = -3/4I$, where I is the moment of inertia of the Neutron star. Recovering units by dimensional analysis allows us to express the distance $r(\Omega)$ and the energy $E(\Omega)$ in dimensionless variables:

$$\begin{aligned} \tilde{r}(x) = \frac{X_{\rm NS}}{\tilde{\mathcal{R}}}\Big(&12\Lambda x^{13/2}\tilde{\rm I}X^8_{\rm NS}X^2_{\rm BH}\chi_{\rm NS}\left(8x^3-5y^3\right)+32\nu x^{3/2}\tilde{\rm I}X^3_{\rm NS}\chi_{\rm NS}\left(4x^3-y^3\right) \\ &+9\Lambda\nu x^9 X^5_{\rm NS}X^3_{\rm BH}\left(7y^3-16x^3\right)+4\nu X_{\rm NS}\left(4x^3-y^3\right)\left(8x^{9/2}\chi_{\rm BH}X^2_{\rm BH}-16\nu x^4+4x^3-y^3\right) \\ &+6\Lambda x^5 X^6_{\rm NS}X^2_{\rm BH}\left(x^4\left(16x^3-7y^3\right)\left(\sqrt{x}\chi_{\rm BH}X^2_{\rm BH}-2\nu\right)+2\left(4x^6-5x^3y^3+y^6\right)\right) \\ &+48\nu^2x^4X_{\rm BH}\left(y^3-4x^3\right)\Big), \end{aligned} \tag{E.9}$$

where $\tilde{\mathcal{R}}$ is now given by:

$$\tilde{\mathcal{R}} = 4\nu x\left(-4x^{3/2}\tilde{\rm I}X^3_{\rm NS}\chi_{\rm NS}+X_{\rm NS}\left(-4x^{9/2}\chi_{\rm BH}X^2_{\rm BH}+8\nu x^4-4x^3+y^3\right)+6\nu x^4 X_{\rm BH}\right)^2, \tag{E.10}$$

and

$$\begin{aligned} \tilde{E}(x) = -\frac{1}{2}\nu x+\frac{9}{8}\Lambda_2 x^6 X^5_{\rm NS}X^2_{\rm BH}\,(1 \\ +\frac{y^3 X_{\rm NS}\left(-12x^{3/2}\tilde{\rm I}X^3_{\rm NS}\chi_{\rm NS}+X_{\rm NS}\left(-4x^{9/2}\chi_{\rm BH}X^2_{\rm BH}+8\nu x^4-4x^3+3y^3\right)+6\nu x^4X_{\rm BH}\right)}{\left(-4x^{3/2}\tilde{\rm I}X^3_{\rm NS}\chi_{\rm NS}+X_{\rm NS}\left(-4x^{9/2}\chi_{\rm BH}X^2_{\rm BH}+8\nu x^4-4x^3+y^3\right)+6\nu x^4X_{\rm BH}\right)^2}. \end{aligned} \tag{E.11}$$

Where we defined the following dimensionless quantities:

$$x = \left(\frac{GM\Omega}{c^3}\right)^{2/3}, \quad y = \left(\frac{GM\omega}{c^3}\right)^{2/3}, \quad X_{\rm NS} = \frac{M_{\rm NS}}{M}, \quad X_{\rm BH} = \frac{M_{\rm BH}}{M}, \quad \tilde{\rm I} = -\frac{3}{4I}\frac{G^2 M_{\rm NS}^3}{c^4}$$
$$\chi_{\rm NS} = \frac{cS_{\rm NS}^z}{GM_{\rm NS}^2}, \quad \chi_{\rm BH} = \frac{cS_{\rm BH}^z}{GM_{\rm BH}^2}, \quad \Lambda_2 = G\lambda_2\left(\frac{c^2}{GM_{\rm NS}}\right)^5, \quad \nu = \frac{\mu}{M}, \quad \tilde{r} = \frac{rc^2}{GM}, \quad \tilde{E} = \frac{E}{Mc^2} \tag{E.12}$$

Appendix F

Numerical Relativity Parameter Settings

Λ_2	Q	χ_{NS}	χ_{BH}	Ω
791	3	0	0.9	0.0982903
791	4	0	0.9	0.121301
791	1	-0.2	0	0.052097525906917879 8
791	2	-0.2	0	0.0746469

Table F.1: NR simulations parameter settings generated from the SXS code [4] together with the dimensionless merger frequency calculated as the frequency at the point of maximum amplitude of the gravitational waveform. The neutron star mass is 1.4 solar masses.

Λ_2	Q	χ_{NS}	χ_{BH}	$\bar{\Omega}$	Λ_2	Q	χ_{NS}	χ_{BH}	$\bar{\Omega}$
323	3	0	0.5	0.155299	607	4	0	0	0.151837
734	3	0	0.5	0.12092	288	4	0	0	0.166286
1110	3	0	0.5	0.106031	2324	5	0	0	0.142958
1740	3	0	0.5	0.0937559	1211	5	0	0	0.153271
323	5	0	0.5	0.182615	607	5	0	0	0.155074
734	5	0	0.5	0.164517	288	5	0	0	0.150265
1110	5	0	0.5	0.158517	2324	3	0	0.25	0.0872545
1740	5	0	0.5	0.140808	1211	3	0	0.25	0.108859
323	7	0	0.5	0.179823	607	3	0	0.25	0.136309
734	7	0	0.5	0.172205	288	3	0	0.25	0.157062
1110	7	0	0.5	0.177835	2324	4	0	0.25	0.108432
1740	7	0	0.5	0.174083	1211	4	0	0.25	0.135237
323	3	0	0.75	0.145979	607	4	0	0.25	0.16258
734	3	0	0.75	0.118379	288	4	0	0.25	0.171547
1110	3	0	0.75	0.100803	2324	5	0	0.25	0.134259
1740	3	0	0.75	0.0887119	1211	5	0	0.25	0.162933
323	5	0	0.75	0.182588	607	5	0	0.25	0.169767
734	5	0	0.75	0.158277	288	5	0	0.25	0.166894
1110	5	0	0.75	0.149742	2324	3	0	0.5	0.0838467
1740	5	0	0.75	0.131007	1211	3	0	0.5	0.103683
323	7	0	0.75	0.178638	607	3	0	0.5	0.12836
734	7	0	0.75	0.212258	288	3	0	0.5	0.160862
1110	7	0	0.75	0.15913	2324	4	0	0.5	0.104552
1740	7	0	0.75	0.161974	1211	4	0	0.5	0.126888
2324	2	0	0.75	0.0626452	607	4	0	0.5	0.150138
1211	2	0	0.75	0.0772153	288	4	0	0.5	0.193606
607	2	0	0.75	0.095872	2324	5	0	0.5	0.127353
422	2	0	0.75	0.105355	1211	5	0	0.5	0.154565
288	2	0	0.75	0.116268	607	5	0	0.5	0.167278
2324	2	0	0	0.0669978	288	5	0	0.5	0.183236
1211	2	0	0	0.0820339	2324	3	0	0.75	0.0817907
607	2	0	0	0.103022	1211	3	0	0.75	0.097785
422	2	0	0	0.117908	607	3	0	0.75	0.12334
288	2	0	0	0.132699	288	3	0	0.75	0.155966
2324	2	0	0	0.0669978	2324	4	0	0.75	0.0984636
1211	2	0	0	0.0820339	1211	4	0	0.75	0.12227
607	2	0	0	0.103022	607	4	0	0.75	0.14332
288	2	0	0	0.132699	288	4	0	0.75	0.158725
2324	3	0	0	0.0914112	2324	5	0	0.75	0.116144
1211	3	0	0	0.11648	1211	5	0	0.75	0.14434
607	3	0	0	0.134576	607	5	0	0.75	0.164945
288	3	0	0	0.154963	288	5	0	0.75	0.199149
2324	4	0	0	0.116065					
1211	4	0	0	0.14149					

Table F.2: NR simulations parameter settings generated from the SACRA code [6, 5] together with the dimensionless merger frequency calculated as the frequency at the point of maximum amplitude of the gravitational waveform. The neutron star mass is 1.35 solar masses.